Titre: Title:	Rheological effect in film blowing
Auteur: Author:	Yunli Fang
Date:	1999
Type:	Mémoire ou thèse / Dissertation or Thesis
Référence: Citation:	Fang, Y. (1999). Rheological effect in film blowing [Mémoire de maîtrise, École Polytechnique de Montréal]. PolyPublie. https://publications.polymtl.ca/8616/

UNIVERSITÉ DE MONTRÉAL

RHEOLOGICAL EFFECT IN FILM BLOWING

YUNLI FANG
DÉPARTEMENT DE GÉNIE CHIMIQUE
ÉCOLE POLYTECHNIQUE DE MONTRÉAL

MÉMOIRE PRÉSENTÉ EN VUE DE L'OBTENTION
DU DIPLÔME DE MAÎTRISE ÈS SCIENCES APPLIQUÉES
(GÉNIE CHIMIQUE)
AOÛT 1999

UNIVERSITÉ DE MONTRÉAL

ÉCOLE POLYTECHNIQUE DE MONTRÉAL

Ce mémoire intitulé:

RHEOLOGICAL EFFECT IN FILM BLOWING

présenté par : FANG YUNLI

en vue de l'obtention du diplôme de : Maîtrise ès sciences appliquées

a été dûment acceptée par le jury d'examen constitué de :

M. LEGROS Robert, Ph.D., président

M. CARREAU Pierre J., Ph.D., membre et directeur de recherche

M. LAFLEUR Pierre G., Ph.D., membre et codirecteur de recherche

M. GRMELA Miroslav, Ph.D., membre

ACKNOWLEDGEMENTS

I am deeply indebted to my thesis director Professor Pierre Carreau and co-director Professor Pierre G. Lafleur for their patience, encouragement, financial support and supervision in this work. This thesis would not have been possible without their guidance.

I am grateful to all my fellow graduate students and staff of the "Département de génie chimique" for their assistance and friendship. I would like to give my thanks to Mr. Luc Parent, Mr. Frédéric Cotton and Sébastien Tremblay for their considerable and continuous assistance with all aspects of film blowing and rheological experiments carried out. I also would like to acknowledge Ms. Min Wu and Mr. Claude Thibodeay for their experienced advice.

I would like to express my sincere thanks to my parents for their continuous encouragement. Finally, I would like to extend my appreciation to my wife Hui-Min Tian for her love, care, passion and understanding.

RÉSUMÉ

Le soufflage des gaines est un important procédé de transformation des matières plastiques et pourtant, les phénomènes impliqués sont loin d'être compris, surtout au niveau de l'influence des propriétés de rhéologiques des résines. À notre connaissance, aucune équation constitutive connue peut décrire de façon satisfaisante les effets rhéologiques observés dans le soufflage des gaines et la modélisation du procédé reste encore un exercice empirique.

Les effets de la rhéologie sur la cinématique et la dynamique du soufflage de gaines pour cinq résines de polyéthylène différentes, c'est-à-dire, deux polyéthylènes de basse densité (PEBDa, PEBDb), un de haute densité (PEHD), un de basse densité linéaire (PEBDL) et un polyéthylène métallocène (PEm) ont été étudiés en utilisant une unité de laboratoire instrumentée.

En comparant notre travail et les données expérimentales de travaux précédents obtenues dans nos laboratoires, le PEm démontre une stabilité de bulle similaire au PEBDL, qui présente une plage d'opération plus petite et des instabilités de bulle à faible BUR.

Les courbes maîtresses des cinq résines ont été déterminées en utilisant le principe de superposition de temps-température. Les viscosités complexes et en cisaillement pur

de cinq résines de polyéthylène ont été étudiées. La règle de Cox-Merz fonctionne relativement bien avec le PEm et le PEBDL, mais présente quelques déviations pour le PEBDa, le PEBDb et le PEHD.

Dans la plage opératoire pratique de l'extrudeuse, où les taux de cisaillements sont généralement compris entre 10 et 1000 secondes réciproques, les données recueillies démontrent que les viscosités en cisaillement sont un bon indicateur de la stabilité des bulles : plus une résine est visqueuse, plus la bulle formée sera stable.

Le rapport de Trouton biaxial (RTB), qui est le rapport entre la viscosité élongationelle biaxiale et la viscosité en cisaillement (η_{fe}/η), a été également étudié pour cinq polymères en fonction du taux de déformation. Comme le rapport de Trouton, le RTB des cinq polymères dépasse celui des fluides newtoniens égal à 6. Les RTB du PEBDa et du PEBDb dépassent ceux du PELBD et du PEHD, et montrent un comportement rhéoépaississant relativement très prononcé. Nous croyons que plus le polymère fondu est rhéoépaississant et plus son RTB est élevé, plus la bulle sera stable pendant le procédé du soufflage de gaines.

En se basant sur nos données expérimentales et celles d'auteurs précédents (Ghaneh-Fard et al) dans notre laboratoire, les viscosités élongationnales biaxiales apparentes non-uniformes et les taux de déformation des cinq résines de polyéthylène à une température de référence de 170°C ont été calculés. Nous avons observé que le

PEBDb à un comportement rhéoépaississant à des taux d'elongation élevés alors que le mPE, pour sa part, montre un comportement rhéofluidifiant. De plus, nous pouvons voir que le comportement rhéoépaississant est le suivant: PEBDa > PEHD > PELBD, ce qui coïncide avec l'ordre de stabilité des bulle, de stable à instable.

Il n'existe pas encore d'équations constitutives simples permettant de corréler la viscosité élongationelle biaxiale avec la viscosité élongationelle uniaxiale et la viscosité en cisaillement simple.

ABSTRACT

Film blowing is a major plastic transformation process and yet, the phenomena involved are far from being understood, mainly with respect to the influence of the rheological properties of the resins. As far as we are aware, no known constitutive equation can satisfactorily describe the rheological effects observed in film blowing and modeling of the process remains an empirical exercise.

The effects of rheology on the kinematics and dynamics of film blowing for five different polyethylene resins, namely two low density polyethylenes (LDPEa, LDPEb), a high density (HDPE), a linear low density polyethylene (LLDPE), a metallocene-catalyzed polyethylene (mPE), have been extensively studied using a fully equipped laboratory unit.

The bubble stability of mPE have been studied and compared with the data of previous authors (Ghenard-Fard et al., 1996a) in our laboratory. The bubble of mPE is most unstable in the comparison with LDPE and HDPE during film blowing.

Master curves of five resins have been determined using the time-temperature superposition principle. The complex and shear viscosities of five polyethylene resins have been studied. The Cox-Merz rule works fairly well with mPE and LLDPE, but still shows deviation for the LDPEs and HDPE.

In the region of practical extrusion operations, where the shear rates are somewhere between 10-1000 s^{-1}, our data showed that the order of shear viscosities, from high to low, coincides with order of resin bubble stabilities, from unstable to stable.

The uniaxial elongational viscosities of three resins, HDPE, LDPEb and mPE, have been studied using two convergent dies and two techniques, Cogswell and Binding analyses. The uniaxial elongational viscosity can not be correlated to the bubble stability.

The velocity and diameter profiles of LDPEb and mPE along the bubble length, which used to determine the strain rate, were measured using a Laser Doppler Velocimetry (LDV) and S-VHS camera respectively. The technique for the measurement of birefringence has been presented. The data of on-line birefringence were used to obtain the stresses along the length of the bubbles, for mPE and LDPEb. For mPE, the birefringence value is shown to be very small in the molten zone and increases rapidly in the crystallization zone. The stresses in MD (machine direction) and TD (transverse direction) for mPE and LDPEb are similar in necking zone. However, they are quite different in the expanding zone. There is no simple equation relating stresses and strain rates in film blowing.

Based on our experimental data of ours and of previous authors (Ghenard-Fard et al, 1997b) in our laboratory, the apparent non-uniform biaxial elongational viscosities and rates of deformation of the five polyethylene resins at a reference temperature of 170°C have been calculated. Both the Trouton ratio, which is ratio of uniaxial elongational viscosity with shear viscosity, and the biaxial Trouton ratio (BTR), which is the ratio of biaxial elongational viscosity with shear viscosity, η_b / η, have been presented. It appears that the more relative strain-hardening the polymer melt is, the more stable bubble during the film blowing process.

Even though we got some qualitative conclusions of rheological effect in film blowing process, we still can not correlate the rheological effects observed in film blowing and modeling of the process through any constitutive equation.

CONDENSE EN FRANÇAIS

Le soufflage des gaines est un important procédé de transformation des matières plastiques et pourtant, les phénomènes impliqués sont loin d'être compris, surtout au niveau de l'influence des propriétés de rhéologiques des résines. À notre connaissance, aucune équation constitutive connue peut décrire de façon satisfaisante les effets rhéologiques observés dans le soufflage des gaines et la modélisation du procédé reste encore un exercice empirique.

Notre objectif ultime est d'optimiser le procédé de soufflage des gaines en maximisant le taux de production tout en maintenant des propriétés physiques et mécaniques optimales. L'objectif de ce mémoire est d'étudier le rapport entre le comportement rhéologique de divers polyéthylènes et leur facilité de transformation par le procédé de soufflage de gaines.

Les effets de la rhéologie sur la cinématique et la dynamique du soufflage de gaines pour cinq résines de polyéthylène différentes, c'est-à-dire, deux polyéthylènes de basse densité (PEBDa, PEBDb), un de haute densité (PEHD), un de basse densité linéaire (PEBDL) et un polyéthylène métallocène (PEm) ont été étudiés en utilisant une unité de laboratoire instrumentée et un rhéomètre à contraintes imposées pour déterminer la viscosité complexe, les modules élastiques et de perte. L'unité de laboratoire comprend une extrudeuse monovis, un train optique pour la mesure de biréfringence, un vélocimètre

à laser Doppler (VLD) pour mesurer les profils de vitesse des bulles et un appareil vidéo pour mesurer le diamètre des bulles et en examiner la stabilité.

Les courbes maîtresses des cinq résines ont été déterminées en utilisant le principe de superposition de temps-température et l'équation d'Arrhénius. Cette équation est généralement valide lorsque la température est au moins 100K au-dessus de la température de transition vitreuse, Tg. Nous n'avons pas utilisé l'équation de Williams-Landel- Ferry puisqu'elle est seulement valide pour des températures avoisinant la température de transition vitreuse.

Les viscosités complexes et en cisaillement pur de cinq résines de polyéthylène ont été étudiées. La règle de Cox-Merz fonctionne relativement bien avec le PEm et le PEBDL, mais présente quelques déviations pour le PEBDa, le PEBDb et le PEHD.

Dans la plage opératoire pratique de l'extrudeuse, où les taux de cisaillements sont généralement compris entre 10 et 1000 secondes réciproques, les données recueillies démontrent que les viscosités en cisaillement sont un bon indicateur de la stabilité des bulles : plus une résine est visqueuse, plus la bulle formée sera stable.

Les viscosités élongationnelles uniaxiales de trois résines (PEHD, PEBDb et PEm) ont été déterminées en utilisant deux filières convergentes de concert avec deux techniques différentes, celles de Cogswell et Binding. La contribution du cisaillement

peut être négligée puisqu'elle représente environ 40% de la perte de charge dans la section convergente. La viscosité élongationnelle calculée à partir de la méthode de Binding est inférieure à celle déterminée par la méthode de Cogswell. Les séries de données recueillies à partir des deux filières utilisées présentent de faibles écarts et ne sont pas en parfait accord. Cependant, les écarts sont acceptables en considérant les difficultés d'obtenir des mesures significatives et d'estimer précisément la contribution du cisaillement à la perte de charge (surtout aux faibles débits d'extrusion). Nos données montrent que la viscosité élongationnelle uniaxiale ne peut être corrélée à la stabilité des bulles.

Afin de déterminer le taux de tension, les profils de vitesse et de diamètre du PEBDb et du PEm furent mesurés à l'aide d'un vélocimètre par Laser Doppler (VLD) et d'un appareil vidéo S-VHS.

La vitesse de déformation du PEm dans le sens machine est toujours plus élevée que celle dans le sens transverse dans la région comprise entre la sortie de la filière et la hauteur de solidification. Pour le PEBDL, la vitesse de déformation dans le sens transverse n'était pas toujours plus basse que celle dans la direction machine, sauf à proximité de la hauteur de solidification.

La technique de mesure par biréfringence a déjà été présentée. Les données de la biréfringence en ligne ont été utilisées pour obtenir les contraintes le long des bulles pour

le PEm et le PEBDb dans la direction transversale. En-dessous de la hauteur de solidification, les valeurs de biréfringence du PEm et du PEBDb représentent une même tendance. Elles augmentent légèrement avec la bulle. Ceci indique que l'orientation dans la direction machine augmente avec la déformation axiale. À proximité de la hauteur de solidification, la biréfringence diminue légèrement et semble indiquer que l'orientation dans la direction machine augmente plus lentement que celle dans la direction tranverse. Ceci peut être dû à la relaxation de l'orientation des molécules. Cependant, le comportement est tout-à-fait différent au-dessus de la hauteur de solidification. Pour le PEm, la valeur de biréfringence augmente radicalement indiquant une grande augmentation de l'orientation pendant la cristallisation. Ceci peut être dû à la nucléation orientée et au procédé de croissance. Pour le PEBDb, la biréfringence diminue. Ce qui peut être dû à la bulle devenant translucide au-dessus de la hauteur de solidification et rend la mesure de biréfringence inexacte. Nos données de biréfringence montrent un bon accord avec celles obtenues par Ghaneh-Fard et al. pour le PEBDa.

Pour le PEm et le PEBDb, la contrainte dans la direction de la machine est toujours supérieure à celle de la direction transversale et les différences augmentent avec la distance axiale. Par rapport au PEBDb, la PEm montre des contraintes d'extension plus basses dans la bulle fondue soufflée et ceci rend la bulle du PEm plus sensible aux instabilités.

Une nouvelle méthode relativement simple est introduite pour mesurer la densité des polymères fondus.

En comparant notre travail et les données expérimentales de travaux précédents obtenues dans nos laboratoires, le PEm démontre une stabilité de bulle similaire au PEBDL, qui présente une plage d'opération plus petite et des instabilités de bulle à faible BUR. L'ordre relatif de la stabilité des polymères étudiés est :

PEBDa> PEHD> PEBDL ou PEm

Le courbe de $LogG'$ en fonction du $LogG''$ est à toutes fins pratiques indépendante de la température pour tous les polymères examinées. Plus le G' est élevé, plus stable est la bulle pendant le soufflage des gaines.

En se basant sur nos données expérimentales et celles d'auteurs précédents (Ghaneh-Fard et al) dans notre laboratoire, les viscosités élongationnales biaxiales apparentes non-uniformes et les taux de déformation des cinq résines de polyéthylène à une température de référence de 170°C ont été calculés. Nous avons observé que le PEBDb a un comportement rhéoépaississant à des taux d'elongation élevés alors que le mPE, pour sa part, montre un comportement rhéofluidifiant. De plus, nous pouvons voir que le comportement rhéoépaississant est le suivant: PEBDa > PEHD > PELBD, ce qui coïncide avec l'ordre de stabilité des bulle, de stable à instable.

Le rapport de Trouton, qui est le rapport de la viscosité élongationelle uniaxiale et la viscosité en cisaillement(η_e / η), a été étudié en fonction du taux de déformation, pour le PEHD, le PEBDb et le PEm. Dans tous les cas, ce rapport dépasse celui des fluides newtoniens égal à 3. Le rapport de Trouton du PEBDb est beaucoup plus grand que celui du PEHD et du PEm et augmente avec le taux d'élongation (comportement rhéoépaississant). Ceci est une propriété qui détermine surtout la stabilité de bulle (et facilité la mise en œuvre).

Le rapport de Trouton biaxial (RTB), qui est le rapport entre la viscosité élongationelle biaxiale et la viscosité en cisaillement (η_{fe} / η), a été également étudié pour cinq polymères en fonction du taux de déformation. Comme le rapport de Trouton, le RTB des cinq polymères dépasse celui des fluides newtoniens égal à 6. Les RTB du PEBDa et du PEBDb dépassent ceux du PELBD et du PEHD, et montrent un comportement rhéoépaississant relativement très prononcé. Nous croyons que plus le polymère fondu est rhéoépaississant et plus son RTB est élevé, plus la bulle sera stable pendant le procédé du soufflage de gaines.

Il n'existe pas encore d'équations constitutives simples permettant de corréler la viscosité élongationelle biaxiale avec la viscosité élongationelle uniaxiale et la viscosité en cisaillement simple.

Les résultats de l'étude actuelle sont très encourageants, mais plusieurs questions devront être répondues dans l'avenir. Nous recommandons les thèmes suivants pour les travaux futurs:

- Compléter les données de viscosité élongationelle uniaxiale en améliorant l'équipement, afin d'obtenir des taux d'élongation plus bas et plus fiables;

- La technique de mesure de biréfringence utilisée dans cette étude est la retardation de la lumière polarisée monochromatique. Cette technique est convenable pour les mesures de l'orientation biaxiale dans les polymères avec un bas degré d'orientation (Takahashi et Fuller). Dans le procédé du soufflage de gaines, il est recommandé de développer un appareil amélioré qui se prête mieux à l'étude des films très orientés.

- Afin d'améliorer la mise en forme du PEm, il est conseillé de le mélanger avec du PEBD et d'ensuite examiner la dynamique de bulles par rapport aux données de rhéologiques de différents mélanges.

- Les propriétés rhéologiques du polymère fondu devraient être corrélées aux propriétés mécaniques et optiques du film final.

TABLE OF CONTENTS

LIST OF TABLES

LIST OF FIGURES

NOMENCLATURE

a_T	Temperature shift factor
C	Stress-optical coefficient (m^2 / N)
c_0	End correction factor
d	Bubble diameter (mm)
h	Film thickness (mm)
h_0	Die gap (mm)
D_0	Outer diameter of the die (mm)
E_a	Activation energy for flow (J)
F_z	Bubble drawdown force at frost line (N)
G'	Storage modulus (Pa)
G''	Loss modulus (Pa)
I	Light intensity
I_0	Incident light intensity
l_d	Length of convergent die (mm)
k	Boltzmann constant ($1.381 \times 10^{-23}\ J / K$)
L	Parameter of elongational viscosity ($Pa \cdot s^t$)
m	Power-law parameter of shear viscosity ($Pa \cdot s^n$)
n	Power-law index of shear viscosity
Δn	Birefringence
P	Degree of polymerization
ΔP	Pressure difference across the bubble (Pa)
ΔP_{ent}	Entry Pressure drop (Pa)
$\Delta P_{elongational}$	Entry pressure drop due to elongation (Pa)
ΔP_{shear}	Entry pressure drop due to shear (Pa)

Q_f	Volumetric flow rate (m^3 / s)
r	Bubble radius (m)
R_0	Outlet radius of nozzle die (m)
R_1	Inlet radius of nozzle die (m)
R_L	Radius of curvature in machine direction (m)
R_H	Radius of curvature in transverse direction (m)
T_0	Reference temperature (K)
t	Power-law index of elongational viscosity
$<V_z>$	Average velocity (m / s)
w	Mass flow rate of molten polymer (kg^3 / s)
$\dot{W}$	Energy dissipation (W)
z	Axial distance (m)

Abbreviation

BI	Bubble instability
BTR	Biaxial Trouton ratio (η_{fb} / η)
BUR	Blow –up-ratio
DHI	Degree of helical instability
FI	Freeze line height instability
FLH	Frost line height
HDPE	High density polyethylene
LCB	Long chain branching
LDPE	Low density polyethylene
LLDPE	Linear low density polyethylene
MD	Machine direction
MDW	Molecular weight distribution
MI	Melt index

mPE	Metallocene-catalyzed polyethylene
MS	Melt strength
MW	Molecular weight
PE	Polyethylene
PH	Partially helical
PS	Polystyrene
SAXS	Small angle X-ray scattering
SCB	Short chain branching
SEM	Scanning electron microscopy
TD	Transverse direction
TEM	Transmission electron microscopy
TUR	Take-up ratio
WAXS	Wide angle X-ray scattering
XRS	X-ray scattering

Greek Letters

β	Inverse of the contraction ratio
$\eta, \eta(\dot{\gamma})$	Shear Viscosity ($Pa \cdot s$)
η^*	Complex viscosity ($Pa \cdot s$)
η_e	Uniaxial elongational viscosity ($Pa \cdot s$)
η_{be}	Apparent biaxial elongational viscosity ($Pa \cdot s$)
η_{fb}	Apparent non-uniform elongational viscosity ($Pa \cdot s$)
λ	Relaxation time (s)
λ	Wavelength (m)
ζ	Translational friction coefficient per monomer unit
a	Length characteristic of the chemical structure of the molecule
σ	Shear stress tensor (Pa)

$\dot{\varepsilon}$	Uniaxial elongational strain rate (s^{-1})
$\dot{\varepsilon}_B$	Rate of deformation (s^{-1})
ρ	Density (kg/m^3)
$\dot{\gamma}$	Shear rate tensor (s^{-1})
$\bar{\dot{\gamma}}$	Effective rate of deformation (s^{-1})
ω	Frequency (s^{-1})
θ	Bubble inflation angle
δ	Retardation

CHAPTER I INTRODUCTION

1.1. Generalities

There is no polymer processing operation more important than tubular film extrusion. This technology, which can be dated back to 1915 (Kang et al, 1915), was first applied to cellulosic derivatives. Now, tubular film production is the most important application area to produce bags for conventional low density polyethylenes (LDPEs), linear low density polyethylenes (LLDPEs), high density polyethylenes (HDPEs), and likewise is the major outlet for the new families of metallocene-catalyzed polyethylenes (mPEs).

1.1.1. The Process Description

A schematic diagram of tubular film extrusion is shown in figure 1.1. A thin film is produced by means of the extrusion of a polymer melt through an annular die. The molten polymer, in the form of a tube, exiting from the die is drawn upward by a take-up device. When the process starts up, air is introduced at the bottom of the die to inflate the tube and form a bubble. An air ring is also used to rapidly cool the hot bubble and solidify it at some distance above the die exit. This distance is usually called Frost Line Height (FLH). The inflated, solidified bubble is then flattened as it passes through the nip rolls. The nip rolls, driven by a variable-speed motor, provided the axial tension needed to pull the film upward, and they form an airtight seal to keep a constant pressure inside the bubble. The pressure is controlled by the air supply to the bottom of the die. The bubble is then wound onto cylindrical cores and sold or used as 'lay-flat' tubing; alternatively, the edges can be trimmed off after passing through the nip rolls and two rolls of flat sheet can be wound from the lay-flat tube. This process is usually carried out vertically upward, sometimes vertically downward, and occasionally horizontally.

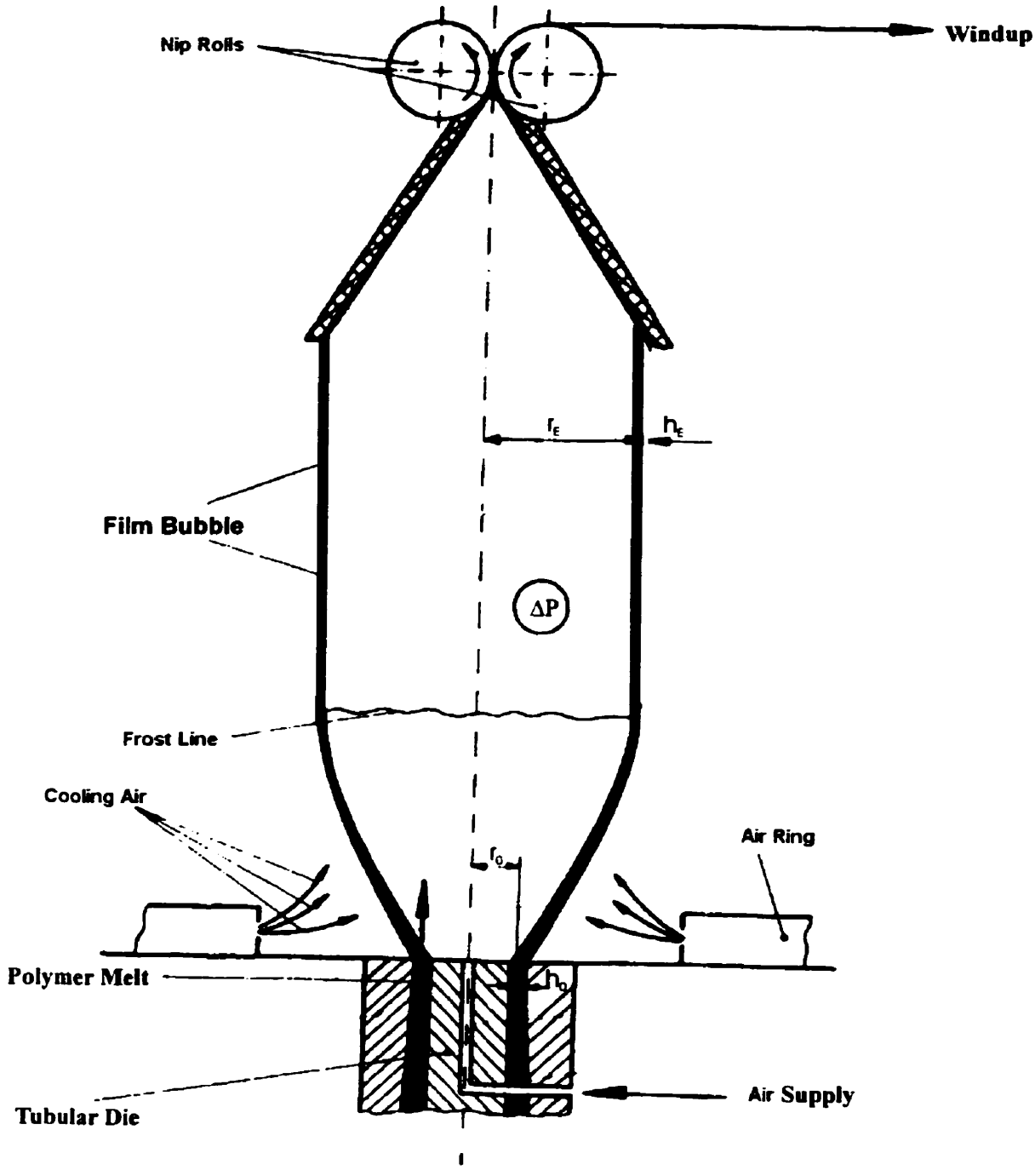

Figure 1.1. Schematic Diagram of the film blowing process.

As the polymer film moves towards the nip rolls, it is being drawn longitudinally by the nip rolls and stretched transversely by the internal pressure. Therefore, the thickness of the molten polymer tube will decrease progressively as the polymer is drawn away from the die. At some distance from the die, a point will be reached whereby the pressure inside the bubble will exceed the melt strength of the thin walled tube and this will cause the tube to expand radically. The transition of the molten polymer to a solid film is accelerated and localized by a jet of cold air directed onto the outer surface of the film from an annular ring just above the die. The height above the die at which solidification occurs can be controlled through the airflow rate and negligible deformation of the bubble occurs beyond the frost line in most processes. The film dimensions are determined by the blow-up ratio (BUR), which is the ratio of the bubble radius at the freeze line to the die radius, and the take-up ratio (TUR), which is the ratio of the take-up velocity to the extrudate velocity at the die exit.

1.1.2. Rheological View of the Process

The film blowing process is a complex manufacturing process involving interactions between melt rheology, heat transfer, and free surface kinematics.

The film blowing process is kinematically similar to film casting and fiber spinning. The flow in all three processes is primarily elongational and under free surfaces. The major difference is that the processes of casting and spinning result in a uniaxially oriented product and therefore increased strength in one direction whereas film blowing provides biaxial orientation and therefore increased strength in two directions. This two-directional orientation is one of the primary attractions of the film blowing process, since it allows for precise control of the mechanical properties of the product sheet by variation of the axial draw velocity and blow-up pressure.

During the film blowing process, the molten polymer is subjected to different stress fields that develop at various stages of the process. First, as the melt flows through the annular die, it is subjected to shearing stresses, resulting in a partial molecular orientation in the machine direction (MD). Upon leaving the die, where the melt is suddenly free of the constrains imposed by the contact with the die wall, this orientation may be partially relaxed but further orientation of the macromolecules will occur as a result of biaxial stretching. The level of extensional stresses will then increase with increasing viscosity due to cooling. Depending on the cooling rate of the melt a second relaxation process may also take place, causing reorientation macromolecules. In the vicinity of the frost line height the melt under stress starts to crystallize (Ghaneh-Fard et al., 1997c; Maddams and Preddy, 1978a).

The film processability of a polymer is intimately related to its rheological behavior, which in turn, depends on the molecular parameters, namely, molecular weight and its distribution, and the degree of long chain branching. What makes the matter more complicated is that, whereas the rheological behavior of a polymer is a direct response to molecular parameters, it also depends on many other factors, which including: 1) the types of flow field (i.e., kinematics); 2) the intensity of the rate of deformation; 3) the deformation and thermal histories.

1.2. Objective

The ultimate objective is to optimize the film blowing process, that is say, to obtain a maximum production rate with optimal physical and mechanical properties. Ultimate film properties are controlled by molecular orientation and stress-induced crystallization. Many parameters influence the morphology development of blown films in a very complex way. These parameters include the polymer characteristics (molecular weight, molecular weight distribution, and branching) and the equipment characteristics (such as die size, die gap, and cooling system) as well as processing variables (such as

polymer flow rate, extrusion temperature, FLH, BUR and TUR). The influence of each of these parameters on film properties is found to be highly interactive with the others. Melt elongational rheology should also play an important role on the final film properties (Ghaneh-Fard, 1997c).

From the practical point of view, it is highly desirable to have a criterion (or criteria) for the choice of resins that will give good tubular film proccessability, without having to perform a time-consuming tubular film blowing operation. Such a criterion, once established, will help the resin producers to tailor-make specific resins for certain applications and, also, will help the tubular film producers to conduct routine test of quality of the resin that they receive from the resin producers. So, our second objective is to establish such a criterion.

CHAPTER II LITERATURE REVIEW

2.1. Modeling Film Blowing Process

The analysis of tubular film blowing was first proposed by Alfrey (1965). Based on his analysis, Pearson and Petrie (1970a, 1970b) gave a detailed description of modeling the flow of the molten polymer between the die exit and the frost line, even though they assumed the flow to be isothermal, and the polymer to be an incompressible Newtonian fluid with constant viscosity. A thin-shell theory, which could use local rectangular Cartesian coordinates, was also employed. Their analysis of the film kinematics and dynamics provided a theoretical framework for most subsequent studies and has been universally recognized and extensively utilized in all succeeding investigation. Most subsequent literatures can be characterized as an evaluation of the incorporation of rheological models into Pearson and Petrie's kinematic and dynamic analysis.

Petrie (1973b) numerically showed the bubble for different Maxwell-type models. He predicted that the radius and thickness of the bubble decrease with increasing the elasticity of the polymer. Later (1975), he extended the calculation to a non-isothermal Newtonian fluid. Agreement between theoretical predictions and experimental measurement was sought by Wagner (1976), but he assumed an average Newtonian viscosity for the process, which due to viscoelastic effects, was of course found to depend strongly on the TUR.

Han and Park (1975) employed a power–law model dependent melt viscosity without taking the temperature effects into consideration to successfully predict stresses and the shape of the bubble. However, it was of less value as a fully predictive model.

Petrie (1974) was the first one who considered the heat transfer during the film blowing process in his analysis. Kanai and White (1985) have also used the Newtonian model in the non-isothermal simulation of film blowing.

Gupta (1982) et al. considered the general non-isothermal process and reported measurements of PS bubble shapes, velocities, stretch rates, stresses and temperatures in the melt region. The viscoelastic nature of the melt was described by the White-Metzner equation.

Kanai and White (1984) presented a basic study of the kinematics, dynamics, and heat transfer occurring during tubular film extrusion of three kind of polyethylenes – LDPE, HDPE and LLDPE by using crystallization model. The bubble stabilities were investigated over a wide range of blow up ratios, take up ratios and frost line heights. They also measured the strain rates, temperature profiles, tensions and inflation pressures and compared the characteristics of the three resins.

Luo and Tanner (1985) extended Petrie's work on film blowing to cover viscoelastic isothermal and non-isothermal flow for both the convected Maxwell and the Leonov models. They showed that the Levonov model had poor agreement with experimental data since it did not stiffen enough with increasing elongational rate to model the bubble well. Owing to numerical instability, they did not get any results for cases in which BUR < 1. However, for BUR > 1, they obtained a good agreement between the predictions of the Maxwell model and Gupta's data on PS by modifying the relevant mean relaxation time. It is worth mentioning variation of properties due to temperature was seen as dominant effect.

Cain and Denn (1988) considered the Newtonian and two viscoelastic models: the upper convected Maxwell model and Marrucci model and compared their predictions to the data of Gupta (1981). Moreover, they assumed the convective heat transfer

coefficients were constant along the bubble length. They predicted that multiple solutions for the bubble were possible and it was impossible to determine the bubble profile by simply defining pressure difference and take-up force.

Seo and Wissler (1989) considered the extrudate swell effect in modeling the film blowing process in addition to Pearson and petrie's work. Their prediction made good agreement with the experimental data of Wagner for TUR. For high TUR values, the die swelling effect is not significant. They did not attempt non-Newtonian due to the high Weisenberg problem difficulty.

Alaie and Papanastasiou (1993) analyzed the melt film-blowing by means of a nonlinear integral constitutive equation that incorporates shear history effects, spectrum of relation times, shear thinning and extension thinning or thickening. The temperature history, as predicted by the simultaneously solved energy equation, was introduced into the constitute equation by means of the appropriate shift factor incorporated in the linear modulus of the constitutive equation. The resulting system of integrodifferential equations is solved by finute element discretization and Newton iteration. The model predicts that with increasing elasticity, both the bubble radius and film thickness decrease but the velocity of film increases. Moreover, the thickness, radius, temperature, and MD stress profiles show a good agreement with experimental data of Gupta (1981). However, the stresses in TD is slightly overestimated near at die exit and underestimate in the vicinity of FLH. It is worth noting they mistakenly reported that the stress in TD is greater than that in MD for a Gupta's experiment due to an error in unit conversion.

In above analyses, computations were primarily based on trial and error and proceed up to the freeze line. Two-phase model, which is the combination of modified Maxwell model and modified Hookean model, was first introduced by Campbell and Cao (1987) who proposed that the film, in the tube forming area, was composed of two layers. This idea was supported by the experimental evidence that the surface temperature of the

film differs from the bulk average (through thickness) by as much as 15 to 20°C in the tube foaming area. (Cao et al., 1990). In another publication, Cao and Campbell (1990) introduced yield stress as a criterion for the cessation of radial deformation beyond the freeze-line, leading to a plastic-elastic transition and thus successfully extended the model above this line. They have predicted blown film process from die exit to nip roll and compared their predictions to the experimental data of Gupta. Their model is the first to yield qualitatively correct predictions of all process variables, even though it slightly overestimates the film thickness above the FLH. Later, Ashok and Campbell (1992) have used an upper convected Maxwell equation of state with a single relaxation time and the Oldroyd and applied derivative to the amorphous or liquid-like phase while a perfect plastic model with yield was used to describe the deformation of crystallized phase. The model is in qualitative agreement for the bubble radius and axial velocity profiles. However, contradictory results, as in the Pearson and Petrie model, are predicted. This may be due to assumptions – there is no extrudate swell and no temperature gradient across the film, which have been demonstrated by Cao et al. (1990) to be substantial.

Liu et al. (1995a) reported the detailed experimental data on film blowing process. Most are in contradiction to the modeling results on tubular film blowing that appeared in the literature. Later (1995b), they used a "quasi-cylindrical" model for the tubular film blowing geometry, combined with a deformation-thinning viscosity equation, and satisfactorily explains the essential features of the experimental data. However, the assumptions are only satisfactory for a solid mechanics problem but not for a fluid mechanics problem.

All the experiments mentioned above have been performed on a small scale machine and a small amount of resin. Kanai et al. (1986) have presented a study on scale-up of the tubular film process and suggested that the melt behavior in tubular film process, the orientation factors of film, and physical properties of film were independent on film width and thickness under the scale-up conditions. They concluded that one can

predict the film processability and film physical properties for the large scale tubular film process, once the tubular film extrusion is carried out by using the small scale machine and a small amount of resin.

In summary, only limited success has been so far achieved, even though there are a lot of efforts in the literature to simulate film blowing using various models. One major problem in validating the film blowing models is the lack of sufficient and reliable kinematic and dynamic data due to experimental difficulties.

2.2. Rheological Properties and Their Effects of on Film Process and Film Properties

2.2.1. Strain, Strain Rates and Stress

Huang and Campbell (1985, 1986) have measured the strain rates and bubble temperature in blown film of LLDPE and LDPE and found that the peak strain rates occur closer to the die exit. The strain rates of LDPE are higher than those of LLDPE. Moreover, they also found that the addition of a small amount of LDPE to LLDPE could cause a significant increase in the strain rates at lower axial positions.

Farber and Dealy (1974) were the first to postulate that the orientation in the film in the immediate vicinity of the FLH and they concluded that melt rheology did not play an improtant role in the generation of the orientation which was observed in blown films. However, Babel and Campbell (1993a) have attempted to correlate the mechanical properties of blown films with the kinematics and dynamics of the process. They suggested that the plastic strain, defined as the strain put in the film after the onset of crystallization, could be a correlating variable, even though their experimental data were too scattered to claim any clear correlation. Later, Babel and Campbell (1993a, 1995) have attempted to correlate the film properties with both plastic strain and strain rates

based on a limited set of experimental data. Since the quatitative determination of velocity and diameter profiles still remain a very difficult task, their results are easily questionable. Tas (1994) calculated the machine direction (MD) stress of blown film at the freezed line using the PTT model and correlated MD stress with the mechanical properties. He concluded that the equal MD stresses at the freeze line resulted in the same mechanical properties, regardless of the type of LDPE, equipment and processing conditions as well. However, he was not successful in correlating the TD stresses with film properties due to the fact that the PTT model did not predict the TD stresses at all well. However, the influence of the TD stresses on final film properties can not be neglected.

Agassant et al. (1991) have analyzed the film blowing process for a Newtonian fluid. They calculated the pulling force and then predicted that the entire stress history in the film, independently of any hypothesis on the material behavior.

More recently, Kuijk et al. (1998) have presented a comprehensive model for film blowing of PE, whereby film properties (optical and mechanical) can be calculated starting from the relevant PE properties (rheological characteristics and density) and the processing conditions (including die geometry). They suggested that the final MD and TD stresses in the bubble during film blowing at the freeze line are important parameters for determining the mechanical end-properties of the resulting blown film.

It should be mentioned that the rate of deformation has been mostly measured by a tacer technique using a video camera. Tas (1994) and Michaeli and Schmitz (1995) have imployed the laser doppler velocimetry to measure the velocity profiles of the blown bubble during the film blowing. The stress field in the bubble has been determined via force balance by measuring the bubble drawing force at the nip rolls using mechanical transducers. However, the bubble force measurement is influenced by different frictional forces during flattening of the film bubble, pinching-off and taking-up. Ghaneh-Fard et

al. (1997b) introduced the flow birefringence technique to measure the stresses indirectly via stress-optical law.

2.2.2. Molecular Structure and Elongational Viscosities

2.2.2.1. Uniaxial Elongational Viscosity

Han et al. (1983), Han and Kwack (1983) and Kwack and Han (1983) found that the blowability is increased as the resin molecular weight distribution (MWD) becomes narrower and the degree of long chain branching (LCB) is less. They also concluded that a resin having lower elongational viscosity tends to give a better blowability. Moreover, they observed that a more uniform tensile strength in the MD and TD was was achievable with a LLDPE resin than with a LDPE resin. This may due to the absence of long side chain branching in LLDPE.

Ghijsels and Ente (1990) used the melt strength as an identifier to assess the bubble stability in film blowing process. A high melt strength is identified with a good bubble stability. He suggested that the molecular weight and the LCB are the two most important molecular structural factors governing the melt strength. The type of short chain branching (SCB) – both in terms of side-chain length and structure – has no significant effect, where the effect of molecular weight distribution is also considered to be small.

Fleissner (1988) suggested that the bubble stability in film blowing is related to rheological properties, from investigation of LDPE, HDPE, LLDPE in film blowing on a commercial production line. They also suggested that shearing of the material in the pelletizing improves its stability. This improvement is partly due to the reduction in elongational viscosity and partly due to degradation of the polymer.

Debbaut et al. (1998) developed high quality LLDPEs based on the idea that LCB affects the rheology while SCB affects the optical properties; a higher molecular weight affects the crystallization, and thus the optical properties : crystallisation is more rapid, leading to increased haze; the lower viscosity at high shear rates reflects the better processability of the resins.

Ramesh and Malwitz (1997) use a simple rheological technique based on the entrance pressure drop method (Cogswell, 1994), which is used to obtain a value for the elongational viscosity, to predict the behavior of new resins under film blowing conditions. They pointed out that an increased slope, followed by a flat elongational rheology curve is best for achieving stable bubble.

Micic et al. (1998) investigated the transient elongational viscosity of LLDPE and its blends with 10% and 20% of LDPE at two temperatures. They suggested that the bubble behavior is mostly determined by the strain hardening characteristics of the polymer. Increasing strain-hardening characteristics could improve the bubble stability. Shear curves seem to be of limited use in predicting the bubble stability as a function of temperature in film blowing.

Beagan et al. (1999) suggested that shear viscosity of blends of mPE and LDPE increases with increasing mPE content and 100% mPE was shown to be less shear thinning than LDPE.

Bin Wadud and Baird (1999) have investigated three mPEs – One of the PE's is linear i.e. no LCB, while the other two have different amounts of LCB and suggested that the shear viscosity of the linear PE is reflective of the narrow molecular weight distribution of mPEs while the apparently branched PE's exhibit a higher viscosity and an

earlier onset of shear thinning. The linear polymer exhibited lower activation energy than the branched PE with similar molecular weight.

More recently, Chai (1999) defined two new parameters: δ(MS)/δP, the melt strength pressure derivative and $\delta(MS)/\delta(\log \dot{\gamma})$, the melt strength shear derivative to study the effects of molecular structure on melt rheology of different types of LLDPEs (one Zieler and three metallocenes) and their processabilities by using an improved Rheotens. Under the same processing conditions, the higher values the two parameters are, the more processable the resins will be.

2.2.2.2. Biaxial Elongational Viscosity

It was Han and Park (1975a) who first have attempted to determine the elongational viscosity in film blowing, namely, biaxial elongational viscosities. They suggested that the non-uniform biaxial elongational viscosity, η_{be}, may be represented as:

$$\eta_{be} = \frac{\sigma_{11}}{\dot{\gamma}_{11} - \dot{\gamma}_{22}} \tag{2.1}$$

or

$$\eta_{be} = \frac{\sigma_{33}}{\dot{\gamma}_{33} - \dot{\gamma}_{22}} \tag{2.2}$$

where $\dot{\gamma}_{11}, \bar{\dot{\gamma}}_{22}, \dot{\gamma}_{33}$ are strain rates in machine, normal and transverse directions respectively. σ_{11} and σ_{33} are stresses in machine and transverse directions resepctively.

In order to avoid the influence of the non-isothermal bubble along the length, they used a special isothermal chamber with a glass window. However, their results are easily questionable since the following reasons: (1) it is very difficult to avoid the influence of the non-isothermal bubble due to the existence of cooling effects. (2) the quantitative determination of stress via classical mechanical method is a very difficult task, since the impact of the energy loss by frictional forces during flattening, pinching-off and taking-up of the film bubble on the drawing forces is difficult to evaluate. Han and Park suggested that the results calculated from equations (2.1) and (2.2) were acceptable, even though they are not identical. Ghaneh-Fard et al. (1997) have shown that the disagreement became worse for LDPE.

Kanai and White (1984) used only equation (2.1) to examine the apparent elongational viscosity in film blowing. Agassant et al. (1991) have suggested that η_{be} can be obtained by adding the two components of the stress tensor:

$$\eta_{be} = \frac{\sigma_{11} + \sigma_{33}}{\dot{\gamma}_{11} + \dot{\gamma}_{33}} \tag{2.3}$$

This suggestion has been adopted by Ghaneh-Fard et al. (1997) to calculated the non-uniform biaxial elongational viscosity. Moreover, Ghaneh-Fard et al. (1997) improved the technique, using birefringence measurement instead of the classical mechanical method, to determine the stress.

2.2.3. Bubble Stability

The problem of bubble stability was first described by Ast (1974) and Han and Park (1975c) and later expanded by Han and Shetty (1977). They presented detailed description of the instability and compared it to the so-called "draw resonance" phenomenon observed in film casting from silt dies. They concluded that lowering the

extrusion temperature improved the blown stability for HDPE and LDPE. A theoretical stability analysis of instabilities due to axisymmetric disturbances in an isothermal Newtonian fluid has been given by Yeow (1976). Based on his analysis, Cain and Denn (1988) have utilized an upper convected Maxwell model to analysis the bubble stability. The models they have utilized do not show good agreement with experimental data.

The most extensive work was given by Kanai and White (1984), Minoshima and White (1986), White and Yamane (1987) and Ghaneh-Fard et al. (1996). Kanai and White (1984) investigated the kinematics and stability of the tubular film process over a wide range of BURs, TURs and FLHs for LLDPE, LDPE and HDPE and suggested that the stability should be in the following order: LDPE > HDPE > LLDPE. Minoshima and White (1986) have concluded that in tubular film extrusion, the LDPEs are most stable but the narrower distribution HDPEs and LLDPEs are much more unstable than the broader distribution HDPE. They also discussed the results in terms of convected Maxwell model representations. Yamane and White (1987) used a crystallization model to predict that the activation energy has a much greater effect on the bubble shape than variations in non-Newtonian characteristics. Both decreasing activation energy and power law exponent may produce narrow necked bubble.

Following previous authors, Ghaneh-Fard et al. (1996) has extensively studied the bubble stabilities for LDPE, HDPE, LLDPE and PP by giving detailed definition of bubble instabilities and suggest that relative order of stability is: LDPE > HDPE > LLDPE > PP. LDPE is always the most stable in the polymers investigated during film blown, it is due to the strain-hardening behavior of LDPE in elongational flow. This conclusion has also been shown by Fleissner (1988).

Ghijsels et al. (1990) suggested that a small axial take-up force is needed to stretch the low melt strength film in absence of strain-hardening for LLDPE, so a low-

tension bubble becomes sensitive to surrounding air flows and gravity forces, leading to bubble instabilities.

Sweeney et al. (1992) have shown that using video analysis system is an effective way to quantify the bubble instabilities.

2.3. Birefringence Measurements

It is well-established that molecular orientation and stress-induced crystallization in a fabricated blown film influence its mechanical and physical properties. For semi-crystalline polymers like polyethylenes, the orientation of both the crystalline and amorphous phases is controlling the film properties.

Several techniques have been used by different researchers for off-line measurement of orientation in polymers. These techniques include birefringence, spectroscopy (FTIR, Raman, fluorescence, NMR, ...), X-ray scattering (XRS) (wide angle X-ray scattering (WAXS), small angle X-ray scattering (SAXS)), transmission electron microscopy (TEM), scanning electron microscopy (SEM), ultrasonic techniques etc. Among these, the birefringence is the simplest and relatively quick. Moreover, it is a measurement of total molecular orientation in the sample and could also be very useful to determinate the stresses occurring in the melt zone during film blowing.

The technique of birefringence measurement most wildly used include refractometry, monochromatic polarized light retardation (Marsh et al. (1995) and Hoppler et al. (1995)), multiwavelength (Abel and Fuller (1990), Hongladarom and Burghardt (1993) and Beedmans and Boer (1996)), some qualitative techniques (fringes and light scattering). Refractometry is limited by several factors : use of contact liquid is not appropriate in many cases, it is tedious and can not be applied for on-line monitoring. Monochromatic polarized light techniques are suitable low orientation (low retardation)

which are encountered in some cases, but are useless for moderately or highly oriented films, sheets or shapes. Takahashi and Fuller (1996) and Hongladarom and Burghardt (1994) have used this technique for biaxial orientation measurements in polymers with low degrees of orientation. The multiwavelength technique on the other hand, has been limited to uniaxial orientation and monolayer materials. More recently, Ajji et al. (1998) and Ajji et al. (1999) have used a technique based on an incident multi-wavelength double beam and a photodiode array assembly, combined with in-house developed software to overcome the problems mentioned above.

Redner (1999) suggested to use birefringence as an ideal parameter to control the production of clear material. He has the used Spectra Contents Analysis, which is high-speed birefringence based on PC, to measure the biregringence, both ON and OFF lines.

CHARTER III EXPERIMENTAL

3. 1. Apparatus and Materials

A 45mm Killion single screw extruder with two helical blown film dies of different geometry was used in this study. One die (outer diameter D_0 = 50.82 mm and die gap at exit h_0 = 0.68 mm with single lip) was used to study the bubble stabilities and another die (D_0 = 63.5, h_0 = 1.5 mm with double lips) was used to study the rheological properties of the bubbles.

Five different film-grade polyethylenes were used in this study: a high density polyethylene (HDPE), two low density polyethylenes (LDPEa, LDPEb), a linear low density polyethylene (LLDPE), a metallocene catalyzed polyethylene (mPE). The main characteristics of the five resins are summarized in Table 3.1.

Table 3. 1. Materials used in this study and main characteristics.

Polymer	Supplier	MI (dg/min)	Density (kg/m^3)	η_0 $(Pa \cdot s)$
LDPEa*	Novacor LF0219-A	2.0	919	21 800
LDPEb	Dow Chemical 503A	1.9	923	-
HDPE*	Petromont DMDC-6400	0.7	960	136 400
LLDPE*	Union Carbide TUFLIN HS-7028	1.0	924	17,100
MPE**	Dow Affinity® PL1880	1.0	902	10,500

* adopted from Ghaneh-Fard (1997b)

** adopted from Bin Wadud and Baird (1999)

LDPE is a long-chain branched (LCB) resin with the branching being introduced by the free radical mechanism of the polymerization, so it has wider molecular weight distribution (MWD). LLDPE resin is a linear copolymer in which small amounts of the second monopolymer breakup some of the ethylene crystallinity. It contains little or no LCB but has substantial amounts of short-chain branching (SCB) (Wild et al., 1983). Compared to LDPE, LLDPE has relatively narrow MWD. HDPE is primarily a linear homopolymer.

mPEs are new polymers that can be tailored to achieve better physical properties, so they are always reported to have superior properties over conventional polyethylenes, principally due to their narrow molecular weight distribution and more uniform co-monomer distribution. However, due to their special molecular structure, these polymers are more difficult to process because of the higher viscosity encountered during melt processing.

3.2. Rheological Measurements

3.2.1. Viscoelasticity

The samples for rheological measurements have been prepared by compression molding using a CARVER laboratory press at 200°C. The pressure was increased progressively form 200 kPa to 1.1 MPa.

The dynamic rheological properties, storage modulus (G'), loss modulus (G'') and complex viscosity (η^*) were measured by using a controlled stress rheometer (Bohlin CSM) in a concentric disk configuration under a dry nitrogen atmosphere at desired temperature. The stabilities of all resins were verified at a low constant frequency (0.01Hz) for periods of over 1.5 h. The linear viscoelastic properties were measured as a

function of frequency with the frequency range from 0.01 to 30 Hz and the applied stress was adjusted to maintain the experiments in the linear domain. The diameters of the concentric disks are 25mm and the gap about 1.2 mm. Each measurement was repeated at least three times. The final results were obtained from reproducible experiments (the range of error is within $\pm 10\%$).

A most useful empiricism is known as Cox-Merz (1958) relationship which is given by:

$$\eta(\dot{\gamma})|_{\dot{\gamma}=\omega} = |\eta^*(\omega)| = \sqrt{\eta'^2(\omega) + \eta''^2(\omega)} \tag{3.22}$$

For highly elastic fluids and polymer melts, it is very difficult to measure steady viscosity at high shear rates using a rotational device. In this case, the shear viscosity can be estimated from the Cox-Merz relation. This empiricism seems to work well for homogeneous polymer solutions and melts (Kitano et al., 1980).

3.2.2. Determination of Master Curves

The rheological properties are usually highly temperature dependent. This means that to obtain a complete picture of the behavior, even if the behavior is linear, experiments must be carried out at several temperatures. It is often found that data, for example G'(ω) and G"(ω), taken at several temperatures can be brought together on a single master curve by means of "time-temperature superposition." This greatly simplifies the description of the effect of temperature. Furthermore, it makes possible the display on a single curve of material behavior covering a much broader of time or frequency than can ever be measured at a single temperature. Materials whose behavior can be displayed in this way are said to be "thermo-rheologically simple." The principle has been largely verified for amorphous polymers. The principle follows also from molecular theories, such as the Rouse theory (1953) for dilute solution.

In non-isothermal blowing, the effects of the temperature history have to be taken into account. The temperature dependency of a "thermo-rheologically simple" material can be represented by a temperature shift factor, a_T, which relates the stress relaxation time λ at temperature T to that at a reference T_0. The relaxation time λ at temperature T is related to the relaxation time λ_0 at reference temperature T_0, by $\lambda = a_T \lambda_0$. The principle is as following (Dealy, 1990):

Bueche predicts that the relaxation modulus is given by:

$$G(t) = \frac{\rho RT}{M} \sum_{p=1}^{N} e^{-t/\lambda_p} \tag{3.1}$$

$$\lambda_p = \frac{a^2 P^2 \zeta}{6\pi^2 p^2 kT} \tag{3.2}$$

where: ζ is the translational friction coefficient per monomer unit;

a is a length characteristic of the chemical structure of the molecule;

P is the degree of polymerization

The viscosity is given by:

$$\eta_0 = \frac{\zeta \rho a^2 M N_0}{36 M_0^2} \tag{3.3}$$

The Rouse theory predicts that temperature affects the relaxation modulus in two ways. First, it changes all the relaxation times by the same factor. For example, if $\lambda_1(T_0)$, $\lambda_2(T_0)$, $\lambda_3(T_0)$... are relaxation times at a reference temperature, T_0, then the effect of changing the temperature to a different value, T, will be to change these times to $\lambda_1 a_T$, $\lambda_2 a_T$, $\lambda_3 a_T$ ... where a_T is a function of T and is equal to unity at T_0. Thus:

$$\lambda_i(T), = \lambda_i a_T(T_0) \tag{3.4}$$

a_T is a function of both T and T_0. The Rouse theory further indicates that the magnitude of the coefficients, G_i, are altered as follows by a change of temperature:

$$G_i(T) = G_i(T_0)T_0/(T_0\rho_0) \tag{3.5}$$

Using the above two relationships, the relaxation modulus of a generalized Maxwell fluid can be rewritten as:

$$G(t,T) = \frac{T\rho}{T_0\rho_0}\sum_{i=1}^{N} G_i(T_0)\exp\{-t/[\lambda_i(T_0)a_T]\} \tag{3.6}$$

or, letting:

$$G_r(t) \equiv G(t,T)T_0\rho_0/T\rho \tag{3.7}$$

and

$$t_r \equiv t/a_T \tag{3.8}$$

So, we can write:

$$G_r(t_r) = \sum_{i=1}^{N} G_i(T_0)\exp[-t_r/\lambda_i(T_0)] \tag{3.9}$$

This equation implies that if G_r is plotted as a function of t_r, data taken at various temperatures should all fall on the same curve as those taken at the reference temperature, T_0.

In fact, the Rouse theory that leads to the above conclusions about the temperature dependence of linear properties is not quantitatively valid for bulk polymers. However, experience has shown that data for different temperatures can often be superposed as suggested above. In addition, while the a_T function cannot be predicted from first principles it can be determined empirically as a "shift factor". Thus, if one makes a plot of G (or logG) versus logt, a_T is obtained from the horizontal shift necessary to bring the data for any temperature T onto the same curve as data for the temperature T_0.

If the equation (3.9) is assumed to be valid for all values of t_r, it can be used, together with Boltzmann superposition principle, to show that all linear viscoelastic properties obey a time-temperature superposition principle (Graessley, 1984).

We know the relationship between the viscosity and the modulus is as follows (Careau et al., 1997):

$$\eta = \int_0^\infty G(s)ds \tag{3.10}$$

Rewriting equation (3.10), we can get the following equation in terms of G_r and t_r:

$$\eta(T) = \frac{a_T T\rho}{T_0\rho_0}\int_0^\infty G_r(t_r)dt_r \tag{3.11}$$

However, since:

$$\eta(T_0) = \int_0^\infty G(t,T_0)dt = \int_0^\infty G_r(t_r)dt_r \tag{3.12}$$

and

$$a_T(T_0) = 1 \tag{3.13}$$

This implies that:

$$\eta(T) = (a_T T\rho / T_0\rho_0)\eta(T_0) \tag{3.14}$$

or:

$$a_T = \frac{\eta(T)T_0\rho_0}{\eta(T_0)T\rho} \tag{3.15}$$

Thus, the shift factor can be found by measuring the temperature dependence of the viscosity.

Because the ratio $(T_0\rho / T\rho)$ changes relatively little with temperature in the usual range of melt rheology measurements, an effective shift factor is:

$$a_T = \eta(T) / \eta(T_0) \tag{3.16}$$

In this case, the shift factor can be determined by measuring the temperature dependence of the viscosity. An empirical relationship for $\eta(T)$ is the Arrhenius equation:

$$a_T = \frac{\eta(T)}{\eta(T_0)} = \exp\left[\frac{E_a}{R}\left(\frac{1}{T} - \frac{1}{T_0}\right)\right] \tag{3.17}$$

where E_a is an "activation energy for flow" and $R = 8.31\times10^{-3} kJ \cdot mol \cdot K^{-1}$ the gas constant. This equation is often found to be valid as long as the temperature is at least 100K above the glass transition temperature, T_g. Closer to T_g. Williams-Landel-Ferry equation (Williams et al., 1955; Ferry, 1970) is applied:

$$\log(a_T) = \frac{-C_1(T - T_0)}{C_2 + (T - T_0)} \qquad (T_g \le T \le T_g + 100°C) \tag{3.18}$$

For polyethylenes, the glass transition temperature is more than 100 degrees lower than the measuring temperature. In that case, the temperature dependence is of Arrhenius-type and is governed by the flow activation energy E_a.

Turning to the storage and loss moduli, we can rewrite the their definitions in terms of reduced variables.

$$G_r'(a_T\omega) = a_T\omega \int_0^\infty G_r(t_r)\sin[(a_T\omega)(t_r)]dt_r \tag{3.20}$$

$$G_r''(a_T\omega) = a_T\omega \int_0^\infty G_r(t_r)\cos[(a_T\omega)(t_r)]dt_r \tag{3.21}$$

where G_r' and G_r'' have the same relationship to G' and G'' as G_r has to G. These equations imply that if dynamic data are plotted in terms of reduced variables, these taken at various temperatures will all fall on a single master curve, which is the curve $G(\omega, T_0)$.

In a similar way, time-temperature superposition procedures can be derived for any type of strain history. If the ratio $(T_0\rho_0/T\rho)$ varies little with temperature, superposition can often be accomplished by plotting:

$G(t)$ versus t/a_T
$G'(\omega)$ versus ωa_T
$G''(\omega)$ versus ωa_T
$\eta'(\omega)/a_T$ versus ωa_T
$\eta''(\omega)/a_T$ versus ωa_T

We should mention here, that the agreement between shift factors in shear and elongation has been verified by Munstedt et al. in 1979. In addition, it is necessary to note that long-chain branched polyethylenes show a dependence of flow-activation energy on the stress level (Laun et al, 1989). That means their behavior is not thermo-

rheologically simple in a strict sense. Thermo-rheological complexity is also reported by Carella et al (1986) for some branched polymers. Yet, a constant value of the flow-activation energy is a good approximation to the real material behavior in a limited range of stress.

3.2.3. Capillary Rheometry

As it will be shown in next section, shear viscosity data, and more precisely power-law parameters of the resins are needed to determine an apparent extensional viscosity. The capillary rheometer is the simplest and most popular method used to measure the viscosity of fluids and polymer melts. Capillary viscosity measurement is based on the relationships between the pressure drop across the capillary and the flow rate.The capillary rheometers used in our study are piston-driven capillary rheometer and on-line capillary rheometer. The geometries of two kinds of rheometers is listed in Table 3.2 and 3.3 respectively.

Table 3. 2. Geometry of the dies for piston-driven capillary rheometer (mounted on an INSTRON).

L/D = 39.52	Diameter(mm)	1.27
	Length(mm)	50.038
L/D = 24.61	Diameter(mm)	1.27
	Length(mm)	31.2547

Table 3. 3. Geometry of the dies for on-line capillary rheometer (mounted on a Kilion extruder).

L/D = 8	Diameter(mm)	1.6
	Length(mm)	12.8
L/D = 12	Diameter(mm)	1.6
	Length(mm)	19.2
L/D = 16	Diameter(mm)	1.6
	Length(mm)	25.6

In its simplest configuration, the capillary rheometer consists of a small tube through which melt is made to flow, either by means of an imposed pressure from the extruder or a piston moving at a fixed speed. The detailed description of on-line capillary rheometer will be introduced in next section.

Following Rabinowitsch analysis (Careau et al., 1997), by plotting σ_R versus $\frac{4Q_f}{\pi R^3}$, power-law parameters can be obtained and are given by:

$$n = \frac{d \ln \sigma_R}{d \ln\left(\frac{4Q_f}{\pi R^3}\right)} \tag{3.22}$$

and

$$m = K'\left(\frac{4n}{3n+1}\right) \tag{3.23}$$

where $\sigma_R (= \frac{(\Delta p)R}{2L})$ is the shear stress at wall, R and L the diameter and length of the die respectively, Δp the pressure drop, K' the slope of the plot. Q_f the volumetric flow rate.

The end effects is corrected by using Bagley correction, which is given by:

$$\sigma_R = \frac{(\Delta p)R}{2(L + c_0 R)} \tag{3.24}$$

where c_0 is the end correction factor and is independent of the capillary geometry.

3.2.4. Uniaxial Elongational Viscosity

3.2.4.1. Technique

Polymer melt elongation is one of the most important deformations in polymer processing. Determining the elongational viscosity remains a very difficult task for rheologists due to experimental difficulties. Many different and unique techniques have been used for measuring the elongational viscosities, such as jet opposed nozzles, fiber spinning, converging flow. Commercially availabe Meissner extensional rheometers use rotary clamps yields true uniaxial elongational measurements, but it not easily accessible and trivial to use. Moreover, it has only a limited range of operation.

One of the most commonly utilized techniques of determining uniaxial elongational viscosity is converging cone method. As melt flows from the reservoir into a conical shape zero length die or orifice die, the streamlines converge and thus producing a strong extensional flow. The key assumption is that the extensional strain is so large

that the stored elastic energy due to extension is approximately equal everywhere to some maximum value and that the flow is predominantly viscous. The viscous resistance to flow is described by using the power law model. The entry flow through a contraction where the entry pressure drop is recorded as a function of flow rate. Moreover, this technique is particularly adapted to usual processing conditions. In this case, the elongational viscosity can be determined from the flow rate and pressure drop measurements once knowing the die geometry and eventually the shear viscosity. The first to analysis the convergent flow was Cogswell (1972). He divided the fluid deformation into two terms: one is due to shear and the other to elongation. Binding (1988) and Mackay and Astaria (1997) re-examined and improved Cogswell's analysis (1972 and 1978) by using the technique of power consumption minization. In our study, both Cogswell (1972) and Binding (1988) analyses have been employed.

One of the critical requirements in the measurement of melt elongational viscosity is that a controlled and constant elongational strain rate should be applied. This can be achieved by choosing properly the shape of the converging section. Binding and Jones (1989), Kim et al (1994) used a planar hyperbolic die to measure and explained the elongational viscosities of polymer solution. James and Chandler (1990) suggested that if the shape of a cylindrical converging die was given by $R_{(z)}^2 = const$, where R is the die rudius depending on z, a constant elongational strain rate could be reached. The elongational strain rate for an axisymmetric converging die with the shape $R = R_{(z)}$ is given by (Lacroix et al., 1999) :

$$\dot{\varepsilon} = \frac{d < V_z >}{dz} \tag{3.25}$$

where $< V_z >$ is the average velocity at a given z, which can be written as:

$$< V_z >= \int \dot{\varepsilon}(z) dz \tag{3.26}$$

If Q_f denotes the total volumetric flow rate, then:

$$Q_f = \pi R_{(z)}^2 < V_z > \tag{3.27}$$

Therefore,

$$\dot{\varepsilon}(z) = \frac{Q_f}{\pi} \frac{d}{dz}\left(\frac{1}{R_{(z)}^2}\right) \tag{3.28}$$

Integration along the die,

$$\int_0^d \dot{\varepsilon}(z)\pi dz = \int_{R_1}^{R_0} Q_f d(\frac{1}{R_{(z)}^2}) \tag{3.29}$$

Then we can get a constant elongational strain rate as following:

$$\dot{\varepsilon} = \frac{Q_f}{\pi d_d}\left(\frac{1}{R_0^2} - \frac{1}{R_1^2}\right) \tag{3.30}$$

where l_d is the length of the die; R_0, R_1 the entry and exit radii of the die respectively.

By imposing a constant elongational strain, equation (3.28) leads to:

$$R_{(z)} = \left(\frac{\dot{\varepsilon} \pi z}{Q_f} + \frac{1}{R_1^2} \right)^{-\frac{1}{2}} \tag{3.31}$$

A setup, which is also illustrated in Figure 3.1, has been designed to measure capillary as well as extensional properties from a single screw extruder. A by-pass valve was employed in order to change the flow rate through the converging die, while the total extruder flow rate remained constant and thus leaving extruder-operating conditions unchanged. Converging dies can be mounted on the extruder exit reservoir after the section where the pressure and temperature are measured. With this design, the polymer before die extrusion can be controlled by keeping the thermomechanical history unchanged. The melt temperature was kept at 200°C, which is the same as the extrusion temperature during the film blowing process, and the screw rotating speed were 75rpm. In this study, we used two different dies. The geometry of the dies is listed in Table 3.4.

Table 3. 4. Geometry of the converging dies for measuring elongational viscosity.

D_1	Entry Radius (mm)	12.7
	Exit Radius (mm)	1.995
	Length (mm)	10
D_2	Entry Radius (mm)	12.7
	Exit Radius (mm)	2.805
	Length (mm)	20

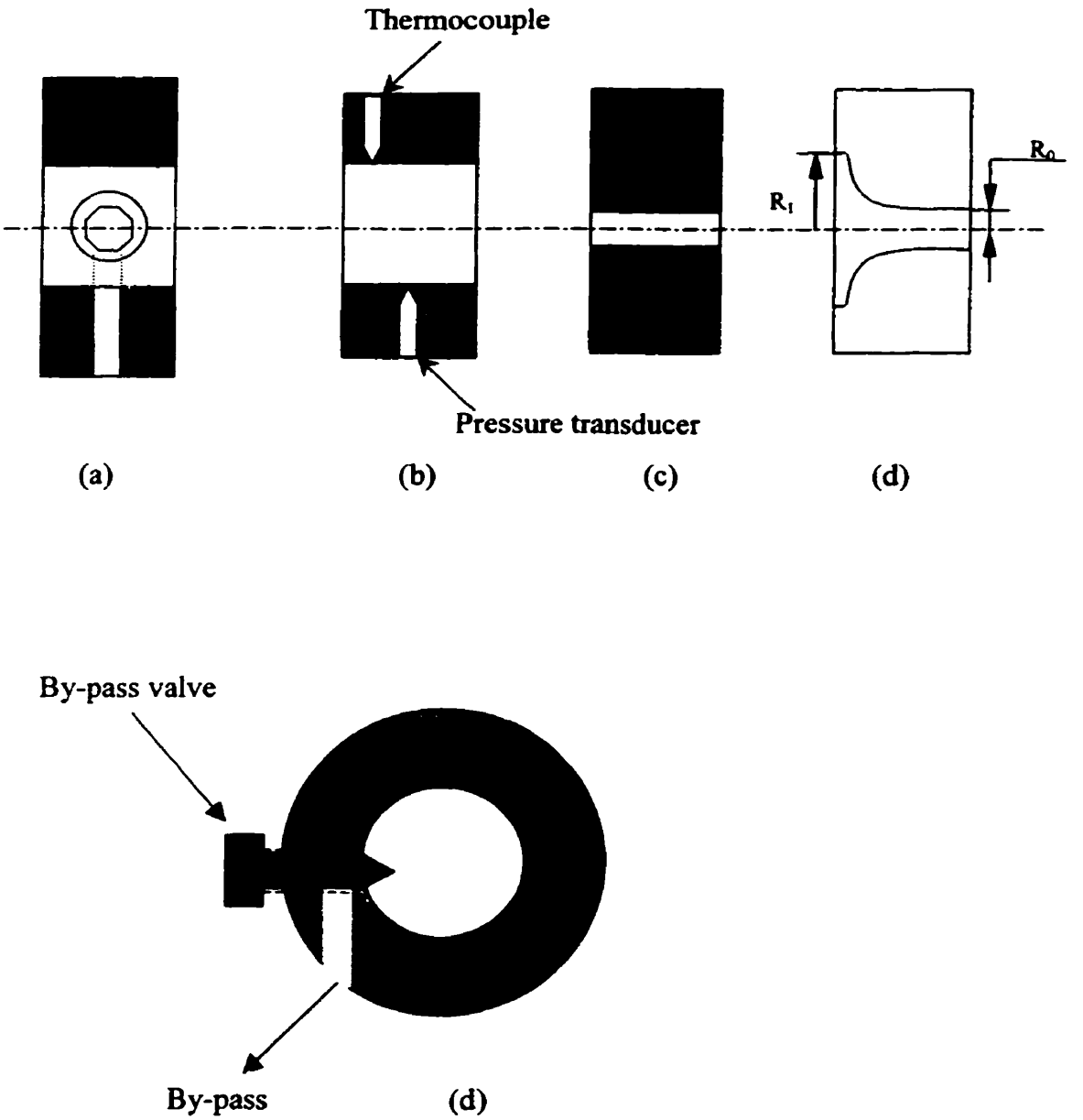

Figure 3. 1. Extrusion setup. (a), (d) by-pass setup. (b) capillary die. (c) convergent die.

3.2.4.2. Cogswell's analysis

Cogswell (1972) provided a basic analysis, which the entry pressure drop can be divided into shear and elongation terms as following:

$$\Delta P_{ent} = \Delta P_{shear} + \Delta P_{elongation} \tag{3.32}$$

Assuming:

(i) Fully developed flow and the inertial effects can be neglected.

(ii) For the shear in an element of length dz, the pressure drop is:

$$dP_{shear} = \frac{2\sigma_R}{R_z} dz \tag{3.33}$$

where σ_R is the shear stress at the wall. For a power law fluid, it can be expressed by:

$$\sigma_R = m\dot{\gamma}_R^n \tag{3.34}$$

where $\dot{\gamma}_R$ is the shear rate evaluated at wall, n and m are the power-law index and parameter of he shear viscosity respectively.

From Rabinowitsch analysis:

$$\dot{\gamma}_R = -\frac{3n+1}{4n}\left(\frac{4Q_f}{\pi R_{(z)}^3}\right) \tag{3.35}$$

where Q_f is the volumetric flow rate.

From equations (3.33), (3.34), and (3.35), integrating along the die length, we can get the pressure drop due to the shear can be expressed as:

$$\Delta P_{shear} = \frac{4}{3}\frac{mQ_f}{(n+1)\dot{\varepsilon}\pi}\left(\frac{(3n+1)Q_f}{n\pi}\right)^n\left[\left(\frac{1}{R_0}\right)^{3(n+1)} - \left(\frac{1}{R_1}\right)^{3(n+1)}\right] \tag{3.36}$$

On the other hand, the elongational contribution to the entrance pressure drop can be derived from energy considerations. If the flow is purely elongational, the pressure difference through a contraction is defined by:

$$\Delta P_{elongation} = \int_d^0 (\sigma_{zz} - \sigma_{rr})\dot{\varepsilon}\frac{\pi R_{(z)}^2}{Q_f}dz \tag{3.37}$$

where $(\sigma_{zz} - \sigma_{rr})$ is the primary normal stress difference. The elongational viscosity is defined by:

$$\eta_e = \frac{\sigma_{zz} - \sigma_{rr}}{\dot{\varepsilon}} \tag{3.38}$$

Assuming that the elongational viscosity is constant through the nozzle and by substituting equations (3.31), (3.38) into (3.37), after integration, we can obtain:

$$\Delta P_{elongation} = 2\eta_e \frac{Q_f}{\pi d_d}\left(\frac{1}{R_0^2}-\frac{1}{R_1^2}\right)\ln\left(\frac{R_1}{R_0}\right) \tag{3.39}$$

Apparently, if the power-law index and shear viscosity data are known, the extensional viscosity can be readily estimated from experimental entrance pressure drop/flow rate data.

3.2.4.3. Binding's analysis

Binding (1988) presented a more rigorous analysis by extending the work of Cogswell. He used an energy balance and variational calculus. In addition, he assumed a power-law form for the extensional viscosity which is then determined form minimization of the power consumption W, which related to the entrance pressure drop by $W = \Delta P_{ent} Q_f$. W is divided into three contribution of shear, elongation and kinetic energy variation; the converging angle is assumed very small, $\frac{d^2 R_{(z)}}{dz^2} \approx 0$, so that the fully developed flow assumption is valid.

In the converging section,

$$V_z = \frac{3n+1}{n+1}\frac{Q_f}{\pi R_{(z)}^2}\left[1-\left(\frac{r}{R_{(z)}}\right)^{1+\frac{1}{n}}\right] \tag{3.40}$$

where n is the power law index and $R_{(z)}$ the distance to the vortex from the center line or the constrained convergence.

Following Binding's analysis the rate of work per unit volume may be expressed by:

$$\dot{W} = \dot{W}_{shear} + \dot{W}_{elongation} + \dot{W}_{kinetic} \tag{3.41}$$

In contrast to Cogswell, Binding assumes power-law behavior for both shear and elongational properties. That is to say:

$$\dot{W}_{shear} = m|\dot{\gamma}|^{n+1} \tag{3.42}$$

$$\dot{W}_{elongation} = L|\dot{\varepsilon}|^{t+1} \tag{3.43}$$

where t and L are power-law index and parameter of elongational viscosity respectively.

In cylindrical coordinates:

$$\dot{\gamma} = \frac{\partial V_z}{\partial r} \tag{3.44}$$

$$\dot{\varepsilon} = \frac{\partial V_z}{\partial z} \tag{3.45}$$

Lacroix et al. (1999) derived the expression for a hyperbolic shaped die with constant elongational rate as:

$$W = \frac{4mQ_f^2}{3(n+1)\dot{\varepsilon}\pi}\left[\frac{(3n+1)}{n\pi}\right]^n\left[\left(\frac{1}{R_0}\right)^{3(n+1)} - \left(\frac{1}{R_1}\right)^{3(n+1)}\right] + I_{nt}Q_f L\left(\frac{3n+1}{n+1}\right)^{t+1}\left(\frac{\dot{\varepsilon}}{2}\right)^t ln\left(\frac{1}{\beta^2}\right) + \frac{3}{2}\rho Q_f^3 \frac{(3n+1)^2}{(2n+1)(5n+3)}\frac{1-\beta^4}{\pi^2 R_0^4} \tag{3.46}$$

where β is the inverse of the contraction ratio ($\beta = \frac{R_0}{R_1}$), and I_{nt} is defined by:

$$I_{nt} = \int_0^1 \left|2 - \frac{3n+1}{n}\phi^{1+\frac{1}{n}}\right|^{t+1} \phi d\phi \tag{3.47}$$

The power-law parameter t of the elongational viscosity can be obtained from pressure drop/flow rate and shear viscosity parameter. Once t is determined, the I_{nt} can be easily evaluated form equation (3.44) and the value of L is then obtained from equation (3.43).

3.3. Measurement of Densities of Molten Polymers

As early as 1964, Terry and Yang (1964) introduced a method for measuring the density of molten polymer using an Instron capillary rheometer by replacing the capillary by a plug. However, the method can be used only to measure the density under a certain pressure. The density at atmosphere pressure can only be obtained extrapolation by using regression. Moreover, the job is tedious.

The method presented here is relatively simple. The densities of the molten polymers were measured by means of compression molding using a CARVER laboratory press. The process, which is schematically illustrated in Figure 4.6, can be described as follows.

First of all, measure the whole height of the reservoir including lid (L_0). Then, put a certain amount (the mass of the polymer is m_0) of polymer into the reservoir. Thirdly, close the lid and press the reservoir under certain pressure and temperature in order to force the air out and make the polymer completely compact. Fourthly, put the reservoir into an oven under desired temperature for one hour and measure the height of the reservoir including the lid again (L_1). The density of the polymer can be easily calculated as following:

$$\rho = \frac{m_0}{\frac{\pi}{4} d^2 (L_1 - L_0)} \tag{3.48}$$

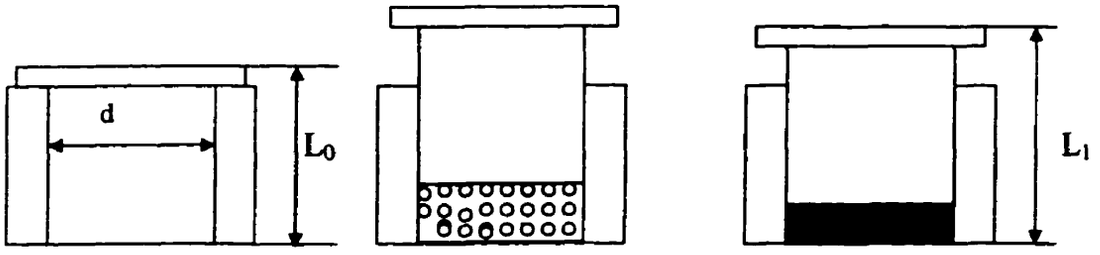

Figure 3. 2. Schematic diagram of measuring the density of molten polymer.

3.4. Measurement of Temperature Profile

The temperature of the bubble as a function of vertical distance from the die (z direction) was measured using an infrared pyrometer (IRCON 3400). This instrument absorbs the infrared radiation in a wavelength of 3.43 micron. Since the transmissivity for polyethylene was found to be very small within this radiation bands, the radiation at these bands can not penetrate into the polymer very far. Therefore, the temperature reading with this wavelength represents the "skin" temperature of the bubble. The measurement

is based on the assumption that the temperature profile in the machine direction is uniform. (Cao et al., 1989).

The instrument was calibrated with the help of a constant temperature paraffin oil bath and a thermometer. During the experiment, the emmittance was set to 0.96 on the front panel. Neglecting the emmittance dependence on the film thickness may cause a maximum error of 2°C within the range of our experimental conditions (See IRCON Operation Manual, 1987).

3.5. Measurement of Strain Rate

In order to obtain the basic kinematic data necessary to calculate the strain rates, it is necessary to measure the velocity and diameter profiles of the bubble as a function of the vertical distance above the die lips.

3.5.1. Measurement of Diameter Profile

Dowd (1972) and soon after Farber (1974) placed a piece of tape onto the molten stalk of the bubble and followed its progress with a movie camera. Kanai and White (1984) used a similar technique in their kinematic study of polyethylene blown films. Huang and Campbell (1985, 1986) placed a mark with a wax pencil on to the stalk of bubble and followed its progress. Based on the technique the previous authors used, Simpson and Harrison (1991) and Ghaneh-Fard et al. (1997) used S-VHS video camera to record the process and deal with the video signal by means of computer.

The technique we used to measure the diameter profile was very similar to above authors. A marker was used to gently mark onto the of the molten stalk surface as it emerged from the air ring and its progress was recorded by a super VHS video camera

system with a shutter speed of 30 frames/second. An electronic timer, accurate to 1/30 of a second, was used as the time reference in the experiment.

After videotaping a run, the recorded type was played back through an S-VHS with frame advance capabilities. The video signal was then channeled through a time base corrector, which digitized the video signal, then to a computer, equipped with image analyzer hardware and software. Distances were measured in pixels, then using correction factors, converted to millimeter.

The diameter (D_z) of solid zone of the bubble is constant when the bubble is stable, so the layflat width of final film can be used as the reference. The diameter can be calculated as following:

$$D_z = \frac{2D_a/\pi}{d_E} \times d_z \tag{3.49}$$

where D_z is the diameter profile along the bubble, D_a the width of the double layer product, d_E the constant bubble diameter above FLH, d_z the diameter profile on screen.

3.5.2. Measurement of Velocity Profile

Many researchers, as mentioned in section 3.5.3, have measured the velocity with the same technique as measuring the diameter profile. In order to calculate the velocity profile, Ghaneh-Fard et al. (1997a) numerically differentiated the collected time-distance data by using a central derivative formula. Obviously, a more accurate and reliable technique is required to obtain the velocity data.

The Laser Doppler Velocimetry (LDV) has been shown to be an extremely accurate, versatile tool for the measurement of velosity field in viscoelastic flow (Lawler et al., 1986) and was chosen for this study. The measuring principle of LDV can be

explained on the so-called interference pattern model (Michaeli and Schmitz, 1995). At the point where two coherent laser beams overlap (measuring volume), interference bands are formed (see Figure 3.3). If a particle passes through this measuring volume, it reflects light when it passes through the interference maxima. These light signals, which are recorded by a detector, contain information on the velocity of the particle. LDV permits direct, contactless measurement of the velocity in fluids and on surface without influencing the flow.

Figure 5 show the measuring setup on the blown film line. The LDV used here consists of three main groups : a laser optical system, which focuses the laser beams at the measuring point and also serves as a detector, a laser from which the laser light is conveyed to the optical system via fiber-optical cable, and an evaluating unit beams is carried out via a tracersing unit. Using this LDV the film velocities were recorded point by point.

The LDV was calibrated with the help of take-up speed. Assuming the velocity of bubble remains constant in the solid zone, we compared the velocity measured by LDV with the take-up speed calculated by measuring the length of collected sample at a give time interval.

3.5.3. Measurement of Thickness Profile

Two methods were employed to measure the thickness of the film along the length of the bubble. Firstly, the whole process, i.e., screw rotation and nip rolls rotation, was stopped simultaneously and the bubble was solidified by blowing the cooling air. The thickness profile of the frozen bubble was then measured by using a micrometer. Secondly, the thickness was calculated from the mass balance equation as following:

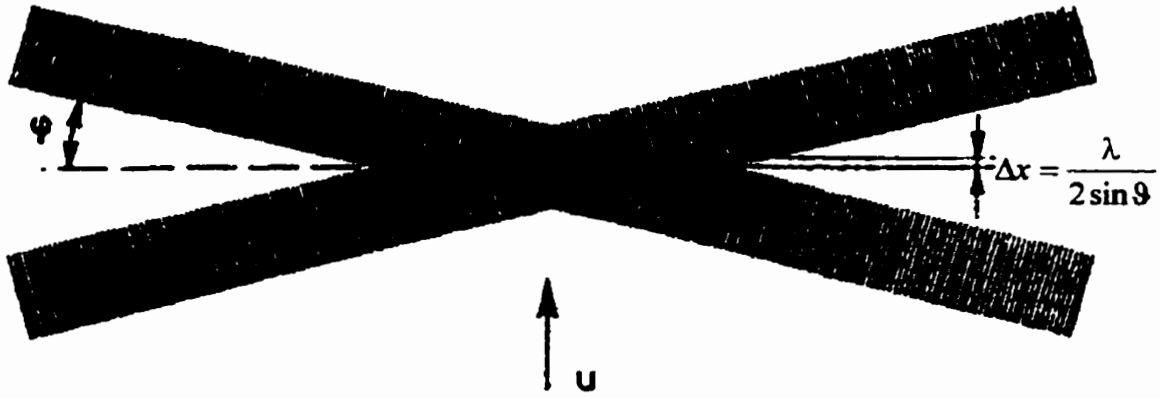

Fringe spacing	Doppler frequency	Velocity
$\Delta x = \frac{\lambda}{2\sin\vartheta}$	$\Delta f = \frac{u}{\Delta x}$	$u = \Delta f \cdot \Delta x$

Figure 3. 3. Interference pattern model in the Laser Doppler Velocimetry (LDV) (adopted from Michaeli and Schmitz, 1995).

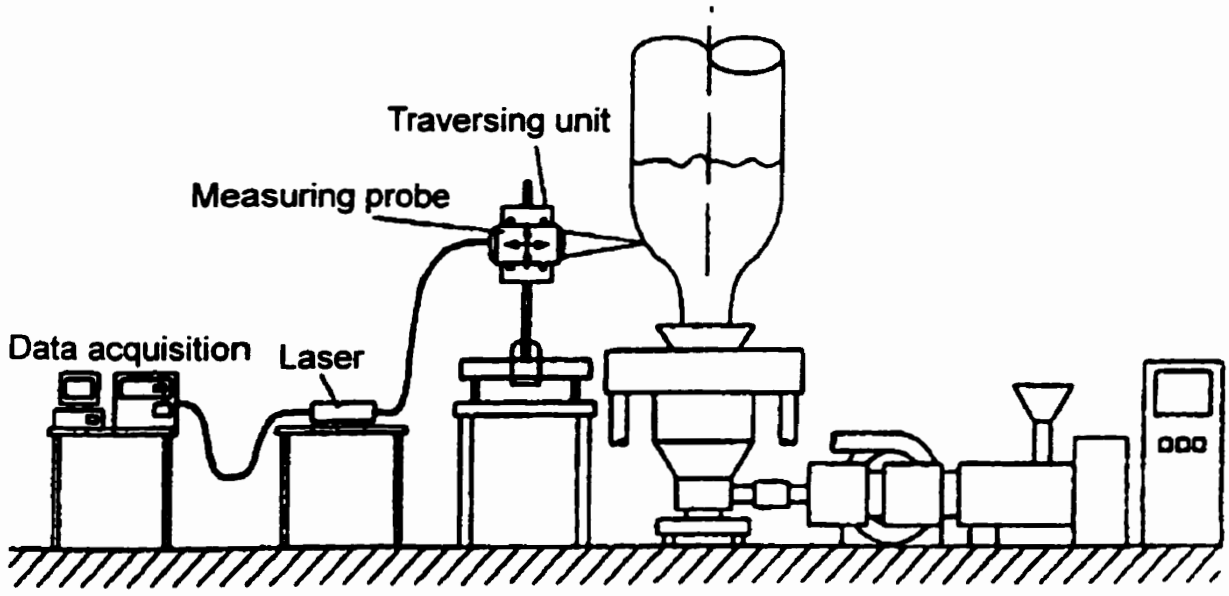

Figure 3. 4. Experimental setup on LDV measurement.

$$h = \frac{w\cos\theta}{2\pi\rho r V_z} \tag{3.50}$$

where h is the thickness profile along the length of the bubble, ρ the density of polymer, r the bubble radius, w the mass flow rate, which was measured by weighing the amount of collected in a known interval of time, and θ the bubble inflation angle, which denotes the angle that the polymer film makes with the vertical direction. θ is given by the relation:

$$\theta = \arctan\left(\frac{dr}{dz}\right) \tag{3.51}$$

3.5.4. Determination of Strain Rate

Pearson and Petrie (1970a, 1970b) were the first to make the thin shell approximation, which assumed that the flow is steady and axisymmetric, and that the film is not only thin compared to the radii of curvature of the bubble but also locally plane. This allows one to use a local rectangular Cartesian coordinate system, as illustrated in Figure 3. In addition, it is also assumed that the shear components of the deformation rate are negligible, and the strain rate tensor may then written as:

$$\dot{\gamma} = \begin{bmatrix} \dot{\gamma}_{11} & 0 & 0 \\ 0 & \dot{\gamma}_{22} & 0 \\ 0 & 0 & \dot{\gamma}_{33} \end{bmatrix} \tag{3.52}$$

The strain rate in the machine direction (MD) is defined as :

$$\dot{\gamma}_{11} = 2\frac{dV_z}{dz} + 2V_z\left(\frac{dr}{dz}\right)\left(\frac{d\theta}{dz}\right) \tag{3.53}$$

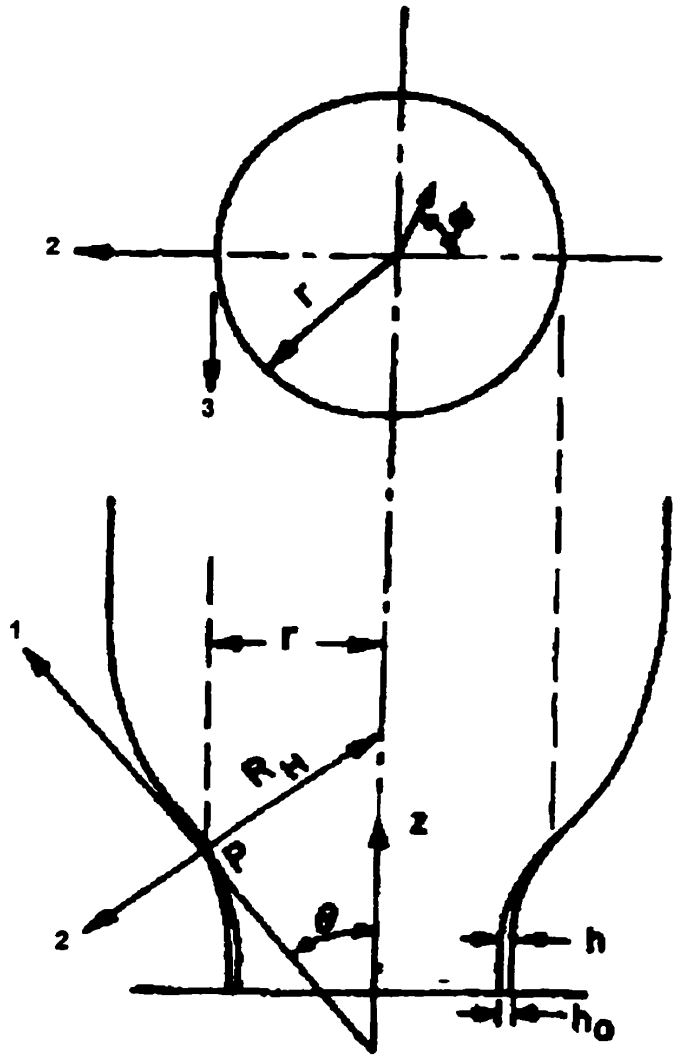

Figure 3. 5. Local rectangular Cartesian coordinate system describing the deformation of a bubble (adopted from Han and Park, 1975).

where V_z is the film velocity in the z-direction, r the bubble radius, and θ the bubble inflation angle. It was found that the second term in equation (3.53) negligible in comparison with the first term as we mentioned before.

The strain rate in the transverse direction (TD) is given by:

$$\dot{\gamma}_{33} = 2\left(\frac{V_z}{r}\right)\frac{dr}{dz} \tag{3.54}$$

Also from continuity for incompressible material:

$$\dot{\gamma}_{22} = -(\dot{\gamma}_{11} + \dot{\gamma}_{33}) \tag{3.55}$$

Thus, once having measured the axial velocity and the radius as functions of the axial distance, one may calculate all the components of the strain rate tensor.

3.6. On-line Birefringence Measurement

3.6.1. Introduction

It is well know that film blowing may induce orientation in polymers, which enhances some properties such as mechanical, optical, barrier, etc.. So it is thus often desirable to induce orientation in the material. In order to evaluate and optimize polymer properties and process conditions, it is thus of great importance to be able to know the orientational states developed in the polymer (Ajji et al., 1999). There are several techniques measure the orientation in polymers. Among these, the the birefringence is the simplest and relatively quick.

If the linear density of the electrically charged particles of matter differs along various directions in a body, the interaction of the light with the body will also differ with direction, and the body will be optically anisotropic. Anisotropy markedly complicates the solutions of the equations of electromagnetism because to any given direction of propagation there correspond two different velocities of propagation of the light. Such material is said to be "birefringent" (Dealy and Wissbrun, 1990).

From birefringence measurement, the biaxial orientation within the material can be described by the refractive index ellipsoid (indicatrix), which is defined by the refractive indices n_1, n_2 and n_3 in the three axial directions (machine, normal and transverse respectively) (Ajji et al, 1999). Birefringence is the difference between the difference refractive indices: $\Delta n_{13} = n_1 - n_3$, $\Delta n_{12} = n_1 - n_2$ and $\Delta n_{23} = n_2 - n_3$.

3.6.2. Optical Train

The optical train, provided by Professor Fuller from Stanford University, is shown in Figure 3.6. The diode laser (Uniphase Corp.) emits a linear polarized light with a wavelength of 632.8 nm. The polarizer and the half-wave plate (Meadowlark Optics) are mounted in front of the diode laser. A saturated waveform could be obtained by rotating the polarizer in its housing relatively to the fixed diode laser which consequently changed the intensity of the laser beam. The rotation of the half-wave plate is driven by using an electromotor at a frequency of about 100 s^{-1}. An encoder mounted externally on the half wave device is used to register the rotation frequency. A hardware unit (Optical Analyzer Controller) transmitted this frequency. The circular polarizer (Meadowlark Optics) is placed in the housing of the detector. The laser diode and the detector are mounted on damped rods (Newport Corp.) to reduce noise in the signal. Data acquisition and control were carried out by the LabVIEW Rheo-Optical Analyzer (ROA) V1.8b (supplied by Professor Fuller), implemented in the LabVIEW (National Instruments), and installed on

a personal computer equipped with a data acquisition board (National Instruments). The optical train was calibrated to correct for imperfections in the half-wave plate by using a polarizer as the sample. The calibration of the optical train was also done to correct the detector offset and phase offset of the waveform as well as non-zero baselines in the values of the coefficients multiplying the sin and cos harmonics of the signal (coefficients A and B in equation 3.56). The birefringence measurement was first tested by using a quarter-wave plate as a standard sample. Very good results were obtained.

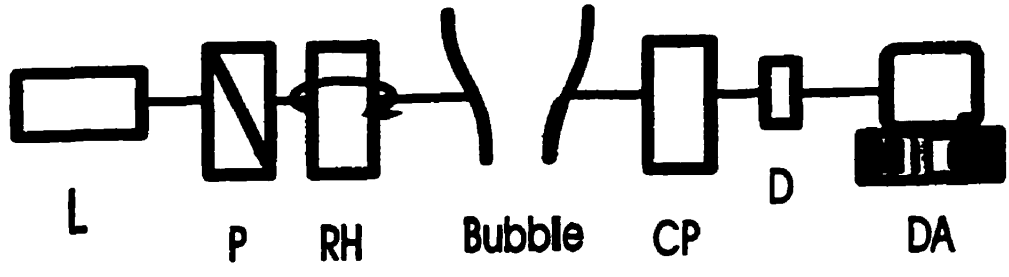

Figure 3. 6. Optical train for birefringence measurement. L-Light source, P-Polarizer, RH-Rotating half-wave plate, CP-circular polarizer, D-Detector, DA-Data acquisition (adopted from Ghaneh-Fard et al., 1996a)

The elements of the apparatus are (1) a light source, which is a He-Ne gas laser beam, (2) a polarization state generator (polarizer and rotating half-wave plate), which defines the polarization of the light prior to transmission through the sample, (3) the blown film, (4) a polarization state analyzer (circular polarizer), (5) a detector and (6) a data acquisition system.

3.6.3. Birefringence Measurement

The equation of light intensity can be expressed as:

$$I = I_0[1 + A\cos(4\omega t) + B\sin(4\omega t)] \tag{3.56}$$

where I_0 is the incident light intensity, ω the rotation frequency of half-wave plate, A and B are related to the retardation and the orientation angle of the film as well as the so-called Fresnel coefficients and can be extracted by performing a fast Fourier transform. The detailed description was given by Ghaneh-Fard et al. (1996a).

The retardation (δ) is related to the birefringence (Δn) according to:

$$\delta = \frac{2\pi\Delta n(\theta_r, \Phi_r)h}{\lambda\cos\theta_r\cos\Phi_r} \tag{3.57}$$

where h is the thickness of the film, λ the wave length, θ_r and Φ_r the components of the refraction angle.

In the case of film blowing where the shear components of the shear tensor are normally assumed to be negligible, the refractive index tensor in the local rectangular Cartesian coordinate system will take the form:

$$n = \begin{bmatrix} n_{11} & 0 & 0 \\ 0 & n_{22} & 0 \\ 0 & 0 & n_{33} \end{bmatrix} \tag{3.58}$$

where subscripts 1, 2, and 3 refer to the machine, normal, and transverse (tangential) directions respectively.

By a suitable coordinate frame rotation of the refractive index tensor, the birefringence and the orientation angle (α) may be calculated, yielding (Ghaneh-Fard et al., 1996a):

$$\Delta n(\theta_r, \Phi_r) = (\cos^2\theta_r \sin^2\Phi_r - \sin^2\theta_r \sin^2\Phi_r)(\Delta_1) + \cos^2\theta_r \cos^2\Phi_r(\Delta_3) + \sin^2\theta_r \cos^2\Phi_r(\Delta_2) \quad (3.59)$$

$$\tan 2\alpha = \frac{2\sin\theta_r \sin\Phi_r \cos\theta_r(\Delta_1)}{\Delta n(\theta_r, \Phi_r)} \quad (3.60)$$

Here, $\Delta_1 = n_{11} - n_{22}$, $\Delta_2 = n_{22} - n_{33}$, and $\Delta_3 = n_{11} - n_{33}$ are the normal optical difference.

For on-center light beam, i.e., $\Phi_r = 0$, equation (3.59) is simplified to:

$$\Delta n(\theta_r) = \cos^2\theta_r \Delta_3 + \sin^2\theta_r \Delta_2 \quad (3.61)$$

From Snell's law:

$$\frac{\sin\theta_r}{\sin\theta_i} = \frac{1}{n} \quad (3.62)$$

where n is the average refractive index of the film and can be taken a value of 1.49 for polyethylene. θ_i is the light incident angle, which is equal to the bubble inflation angle). The maximum value of θ_i, was about 17° within the range of our experimental conditions. The maximum value of θ_r, after calculation, is about 11.3°. Therefore, the contribution of the out-of-plane birefringence (Δ_2) is less than 4% and the on-center light beam is assumed to give in-plane birefringence (Δ_3), which provided information about the difference between the MD and the TD orientation.

3.7. Determination of Stresses

The force balance in the machine direction on a segment of bubble between an axial position z and nip-rolls leads to the relation (Han and Park, 1975a):

$$2\pi rh\sigma_{11}\cos\theta + \pi\Delta P(r_f^2 - r^2) + 2\pi\rho g\int_z^{z_f} rh\sec\theta dz = F_z \tag{3.63}$$

where F_z is the drawdown force; ΔP the bubble pressure; σ_{11} and σ_{33} the stress in machine and transverse direction respectively.

The force equilibrium equation in the normal direction is approximated by the thin membrane equation, neglecting surface tension effects (Han and Park, 1975a):

$$\frac{\Delta P}{h} = \frac{\sigma_{11}}{R_L} + \frac{\sigma_{33}}{R_H} - \rho g\sin\theta \tag{3.64}$$

where R_L and R_H are the radii of curvature in machine and transverse direction, which are given by:

$$R_L = -\frac{\sec^3\theta}{d^2r/dz^2} \tag{3.65}$$

and

$$R_H = r\sec\theta \tag{3.66}$$

The flow birefringence technique is very useful to investigate the stresses occurring in film flow. This technique improved classical mechanical methods in several aspects. Firstly, it does not disturb the flow field (Van Aken and Janeschitz-Kriegl,

1980). Secondly, it responds faster and has higher sensitivity to dilute components. Thirdly, it has the ability to isolate the dynamics of separate constituents in the case of multi-components systems (Dealy and Wissbrun, 1990; Fuller, 1990). However, since the birefringence is only an integrated effect along the direction of light beam, only birefringence data in two-dimensional fields without birefringence gradients in the direction of light beam can be collected. Moreover, optical methods require that the fluid under investigation be transparent (Ghaneh-Fard et al., 1996).

The rheological application of the birefringence method is based on the stress-optical law, which gives a proportionality between the components of the refractive index (polarizability) tensor and the stress tensor. In a wide range of conditions involving not too large stress, the linear stress-optical law is expressed as:

$$\Delta n = C\Delta\sigma \tag{3.67}$$

where C is a material constant known as the stress-optical coefficient, Δn the birefringence, and $\Delta\sigma$ the corresponding difference of the principal stresses. The sign and magnitude of the stress-optical coefficient C depends on the chemical structure of the polymer, which is governed by the polarizability of the bonds between the atoms of the polymer molecule and by the direction of the bond with respect to the polymer backbone Suberammanian and Picot, 1996). According to the rubber-like photoelastic theory (Flory, 1969) for a network of freely jointed Gaussian chain, the stress-optical coefficient is:

$$C = \frac{2\pi}{45kT}\frac{(n^2+2)}{n}(\alpha_1 - \alpha_2) \tag{3.68}$$

where n is the mean refractive index of the material, $(\alpha_1 - \alpha_2)$ the principal polarizability difference of the chain-link parallel and transverse to the link. k is the Boltzmann

constant, and T the absolute temperature. The stress-optical coefficient, C, for PE was taken to be $2.2\times10^{-9}m^2/N$ (Okamoto et al., 1998) in our calculation.

Ghaneh-Fard et al. (1996a) were the first to apply the stress-optical law to calculate the stress during film blow. The stress-optical law,which can translate the birefringence data into stresses, is given by:

$$n_{11}-n_{33}=C(\sigma_{11}-\sigma_{33}) \tag{3.69}$$

The MD and TD stresses $(\sigma_{11},\sigma_{33})$ can be calculated via equation (3.64) and (3.68).

It should be noted that the stress-optical law should be validated for extensional flow. The critical tests of the stress-optical law were rather sparse for elongational flows. Koyama and Ishizuka carried our a poineering work on simultanueously measurements of transient tensile stress and birefringence on a LDPE melt under elongational at constant strain between 120 and 150°C, and reported a value of C equal $1.3\times10^{-9}m^2/N$; independent of strain rate with 0.002 to $0.2s^{-1}$ and only weakly dependent on temperature. Okamoto et al. (1998) have recently found that the stress-optical law is valid for LDPE and C $=2.2\times10^{-9}m^2/N$. It has also been found that the stress-optical law is not valid in some cases (Ryu et al., 1998).

3.8. Biaxial Elongational Viscosity

Film blowing involves biaxial extensional flow, where the blown film is stretched in the MD and TD directions. The stretching or extensional viscosity plays an important role in controlling the bubble during film blowing.

The measurement of biaxial elongational viscosity requires either extensive equipment, great skill, or both. Hence, it is difficult to find any published data on biaxial extension of polyethylenes.

Han and Park (1975a) suggested that the elongational viscosity in non-uniform biaxial stretching biaxial stretching, η_{be}, may be represented as:

$$\eta_{be} = \frac{\sigma_{11}}{2\dot{\gamma}_{11} + \dot{\gamma}_{33}} \tag{3.70}$$

or

$$\eta_{be} = \frac{\sigma_{33}}{2\dot{\gamma}_{33} + \dot{\gamma}_{11}} \tag{3.71}$$

However, the two biaxial elongational viscosity calculated from these equations are not identical (Ghaneh-Fard et al., 1997b). Kanai and White (1984) used only equation (3.70) to examine the apparent elongational viscosity in film blowing. Agassant et al. (1991) suggested that for a non-uniform biaxial elongational, the two components of the stress tensor ca be added:

$$\eta_{be} = \frac{\sigma_{11} + \sigma_{33}}{\dot{\gamma}_{11} + \dot{\gamma}_{33}} \tag{3.72}$$

Ghaneh-Fard et al., (1997) used this equation to investigate the apparent biaxial elongational viscosity.

Note that the definition of elongational viscosity is given by (Carreau et al., 1997):

$$\eta_{fb} = \frac{\sigma_{11} - \sigma_{33}}{\bar{\dot{\gamma}}} \tag{3.73}$$

Here, $\bar{\dot{\gamma}}$, for non-uniform biaxial deformation, is taken as the effective rate of deformation and defined as:

$$\bar{\dot{\gamma}} = \sqrt{\frac{1}{2}\mathrm{II}_{\dot{\gamma}}} = \sqrt{\frac{1}{2}\left(\dot{\gamma}^2{}_{11} + \dot{\gamma}^2{}_{22} + \dot{\gamma}^2{}_{33}\right)} \tag{3.74}$$

and assuming that $\sigma_{11} + \sigma_{22} + \sigma_{33} = 0$, so we can get the biaxial elongational viscosity in film blowing:

$$\eta_{fb} = \frac{(2\sigma_{11} + \sigma_{33})}{\dot{\varepsilon}_B} \tag{3.75}$$

Equations (3.74), (3.75) will be used to represent our experiment data.

3.9. Bubble Stabilities

Bubble stability plays a very important role in evaluating the processability of a polymer. A stable bubble is a requirement not only for the continuous operation of the process but also for the production of an acceptable film.

In order to represent the kinematics of the tubular film process in a global manner, we use three most important kinematic variables, the take-up ratio (TUR), the frost line height (FLH) and the blow-up ratio (BUR), for such a representation. The former two quantities determine the machine direction deformation rates and the latter the transverse direction deformation rates. Increasing values of TUR and BUR is explicitly desirable in

a commercial film production. On the other hand, even though FLH does not control the film geometry, its effect on final film properties cannot be denied as it is a response to cooling conditions.

We followed the criteria reported by previous authors in our laboratory (Ghaneh-Fard et al., 1996b). A video-camera system was used to record the bubble shape and oscillations. The recorded tapes were analyzed by an image analyzer to obtain the bubble diameter and degree of helical instability using the distance of the bubble of the bubble edges from a reference line at a height well above FLH over a period of time (Please refer to Figure 3.10).

$$D_{mean} = P_{l,mean} - P_{r,mean} \tag{3.76}$$

$$D_{\max} = P_{l,\max} - P_{r,\max} \tag{3.77}$$

$$D_{\min} = P_{l,\min} - P_{r,\min} \tag{3.78}$$

$$D_r = D_{\max} - D_{\min} \tag{3.79}$$

$$DHI = \frac{D_r}{D_{mean}} \times 100\% \tag{3.80}$$

Where D_{mean} is the average diameter, P_r is the position of the right bubble edge, P_l is the position of the left bubble edge and DHI is the degree helical instability. Defining:

$$\text{DHI} \begin{cases} < 20\% & \text{stable} \\ \text{between 20\% to 40\%} & \text{partially helical} \\ > 40\% & \text{Helical} \end{cases} \qquad (3.81)$$

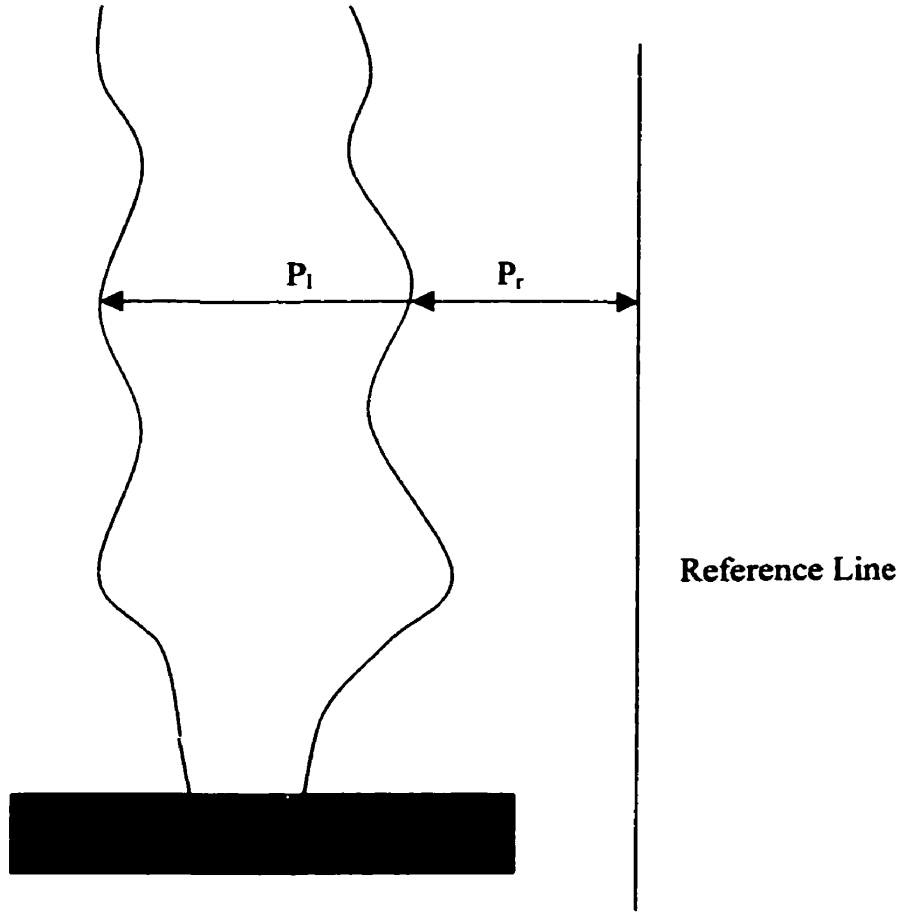

Figure 3. 7. Bubble instability measurement (adopted from Ghaneh-Fard et al., 1996b).

CHARPTER IV RESULTS AND DISCUSSION

4.1. Results of Rheological Behavior

4.1.1. Complex Viscosity

Figure 4.1 shows the complex viscosity of the five resins at the temperature of 200°C. The absolute value of the complex shear viscosity $|\eta^*(\omega)|$, determined by small amplitude oscillatory shear measurements is plotted versus the frequency. Using the Cox-Merz relation (Cox and Merz, 1958), the data of complex viscosity can be used to approximately estimate the steady shear viscosity.

At low frequencies, the order of complex viscosity values, from high to low, is: HDPE, mPE, LLDPE, LDPEa, LDPEb. The HDPE is more shear thinning and does not depict a plateau even in the lowest frequency region. However, at high frequencies, the order changes to: LLDPE, mPE, HDPE, LDPEb, LDPEa.

Figure 4.2 (a) and (b) show the dynamic storage and loss moduli as a function of frequencies for five polyethylene resins respectively. The behaviors described by these two moduli are quite similar — both moduli increase with the frequency. The orders (from high to low) of both moduli values, which are the same, are as following: at low frequencies, HDPE, LDPEa, LDPEb, mPE, LLDPE; at high frequencies, LLDPE, mPE, HDPE, LDPEb, LDPEa.

Using these linear viscoelastic data, we may get the characteristic time, which is defined by:

$$\lambda = \frac{G'}{\omega G''} \tag{4.1}$$

Figure 4.3 shows the relaxation time versus frequency. At high frequencies, the relaxation times of the melts are close to each other. However, at low frequencies, they are quite different. The order of the values of relaxation time at low frequency is the same as that of viscosity. The comparison of rheological behaviors of five polyethylene resins is summarized in Table 4.1.

Table 4. 1. Comparison of rheological behaviors of five polyethylene resins.

Frequency (s^{-1})	Small → Large				
Behavior change with frequency	Slow → Quick				
$\eta^*(Pa \cdot s)$	LLDPE	mPE	LDPEb	LDPEa	HDPE
$G'(Pa)$	HDPE	LDPEa	LDPEb	mPE	LLDPE
$G''(Pa)$	HDPE	LDPEa	LDPEb	mPE	LLDPE
$\lambda(s)$	LLDPE	mPE	LDPEb	LDPEa	HDPE

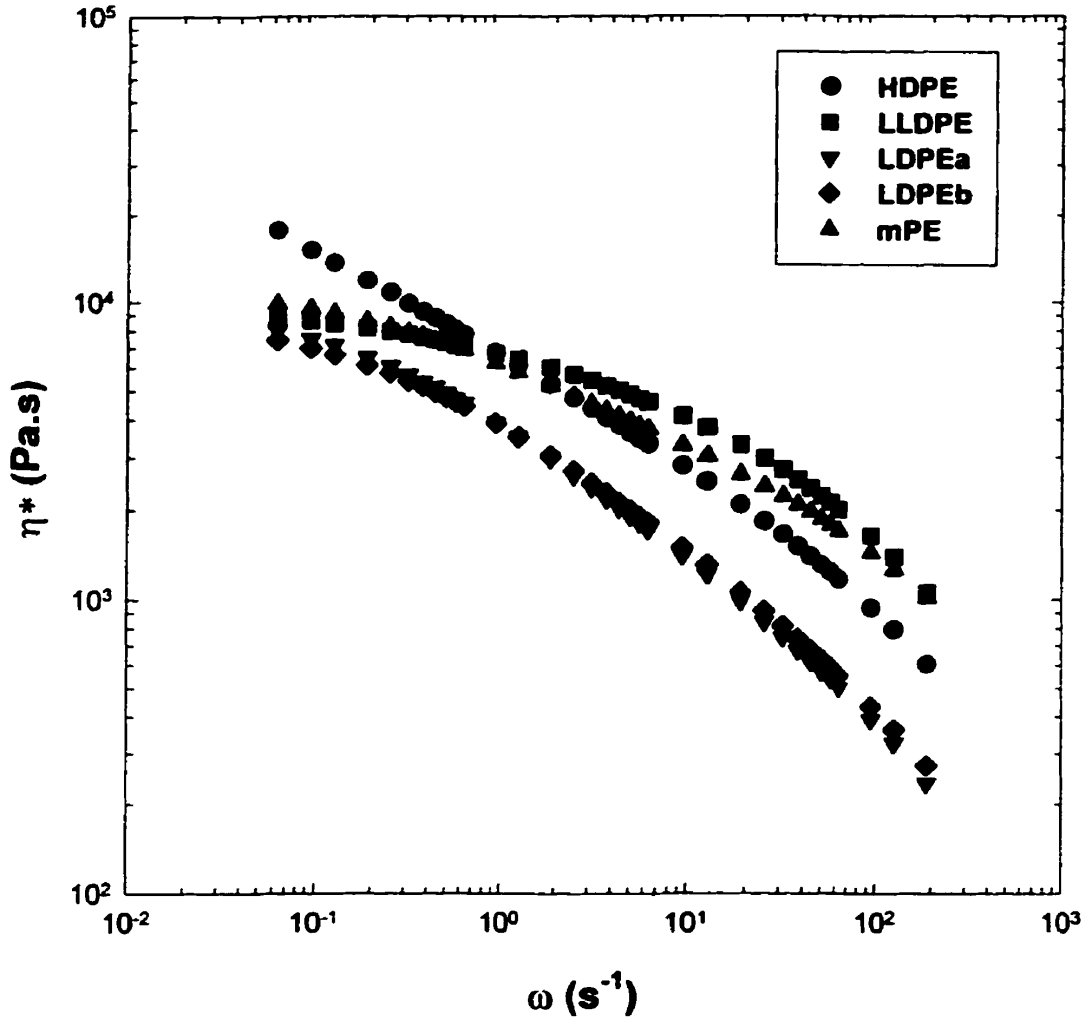

Figure 4. 1. Complex viscosity data versus frequency for five resins at 200°C.

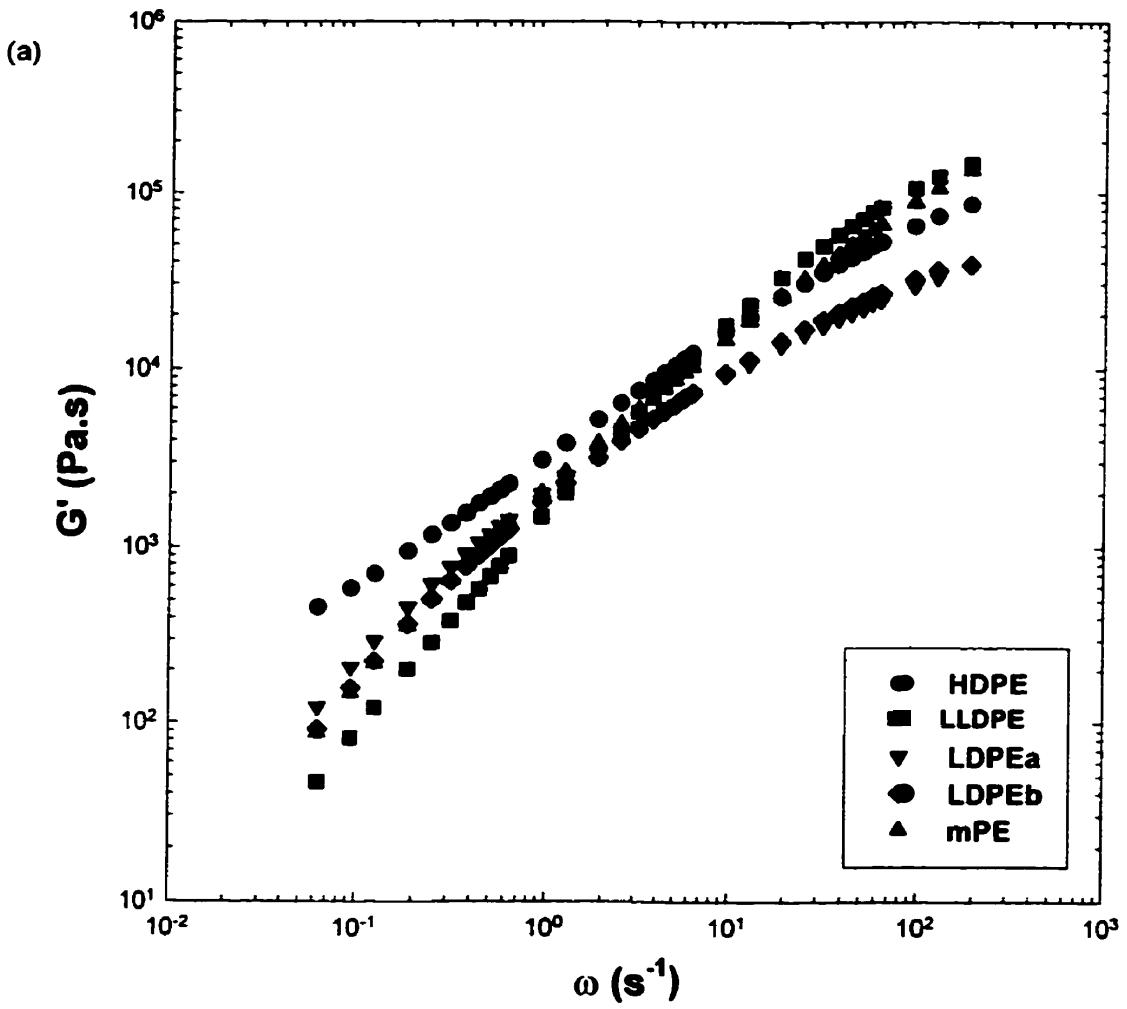

Figure 4. 2. The data of dynamic storage (a) and loss (b) moduli versus frequency for five resins at 200°C.

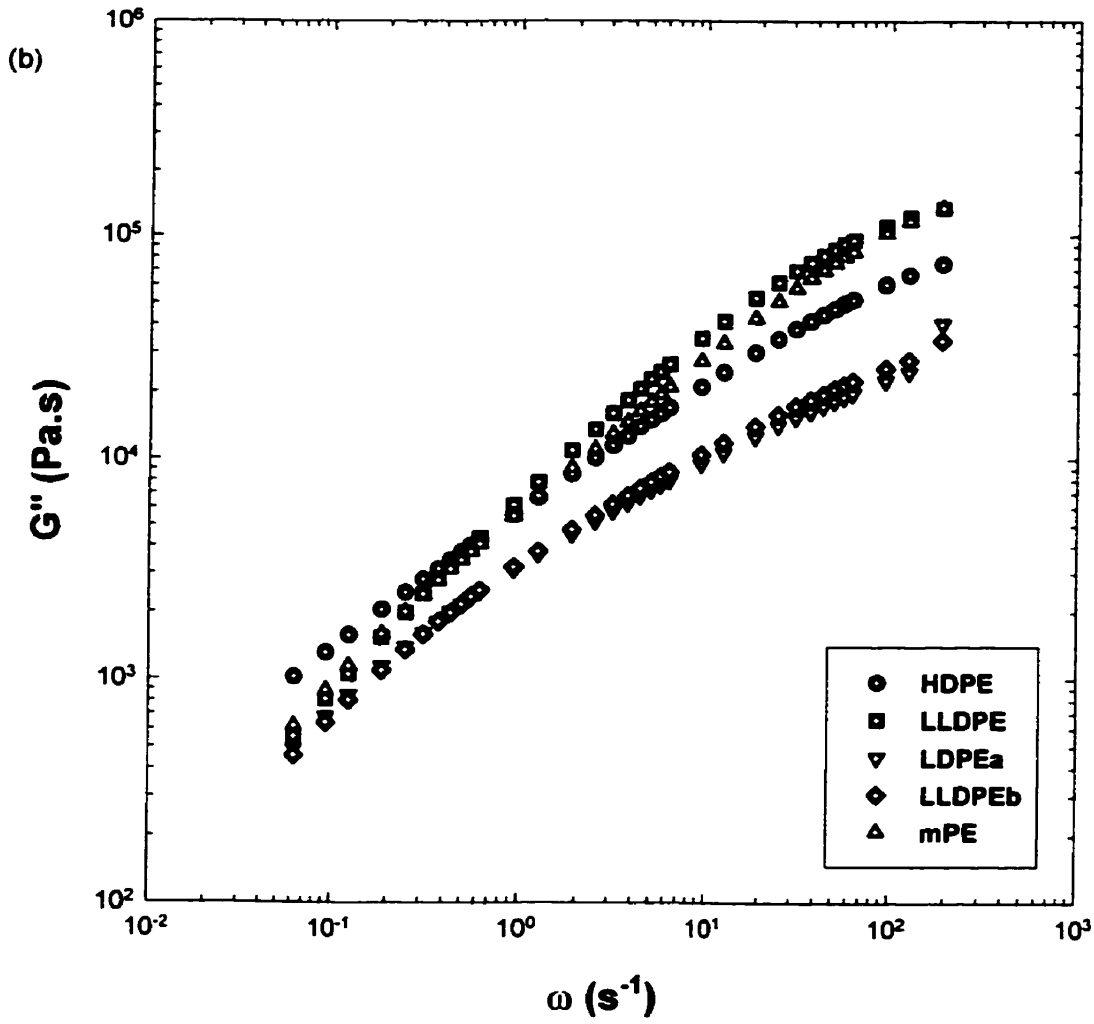

Figure 4.2. (continued)

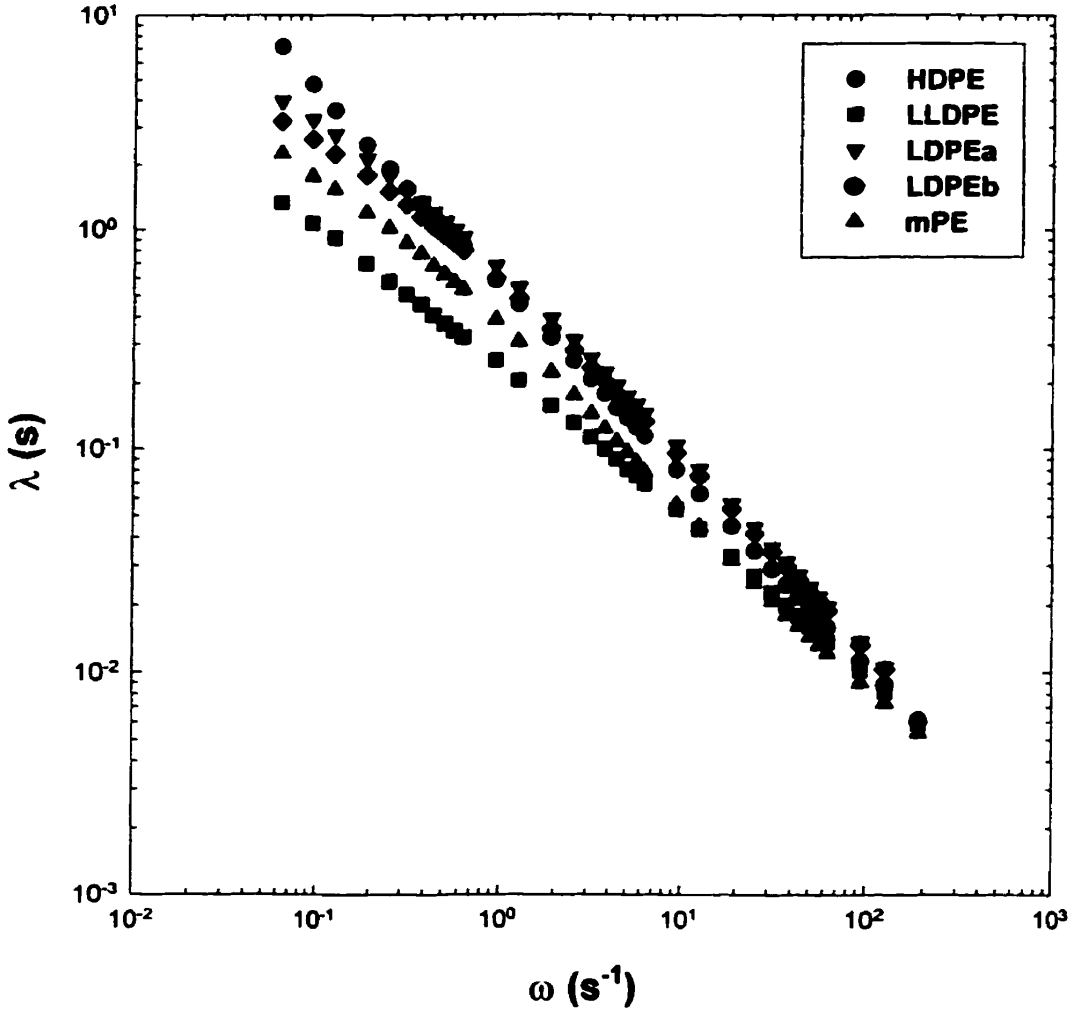

Figure 4. 3. Relaxation time versus frequency for five resins at 200°C.

4.1.2. Master Curve

In order to determine the master curve for all the samples, five different temperatures were employed. Figure 4.4(a, b, c, d, e) shows the G', G'', and η^* versus ω under five temperatures for five resins before using shift factors. Figure 4.5(a, b, c, d, e) shows G', G'', and η^*/a_T versus ωa_T. By shifting the curves, as expected, the curves fall onto a single curve which is so-called master curve.

Figure 4.6(a, b) shows the variation of a_T with temperature, described by the Arrhenius equation:

$$a_T = \frac{\eta(T)}{\eta(T_0)} = \exp\left[\frac{E_a}{R}\left(\frac{1}{T} - \frac{1}{T_0}\right)\right] \tag{4.2}$$

By using linear regression, we can get the parameter $\frac{E_a}{R}$ of Arrhenius equation, and the results were summarized in Table 4.2.

Table 4. 2. Parameters of Arrhenius equation for give resins at a reference temperature of 170°C.

	HDPE	LLDPE	LDPEa	LDPEb	mPE
$\frac{E_a}{R}$(K)	277	503	403	1061	737

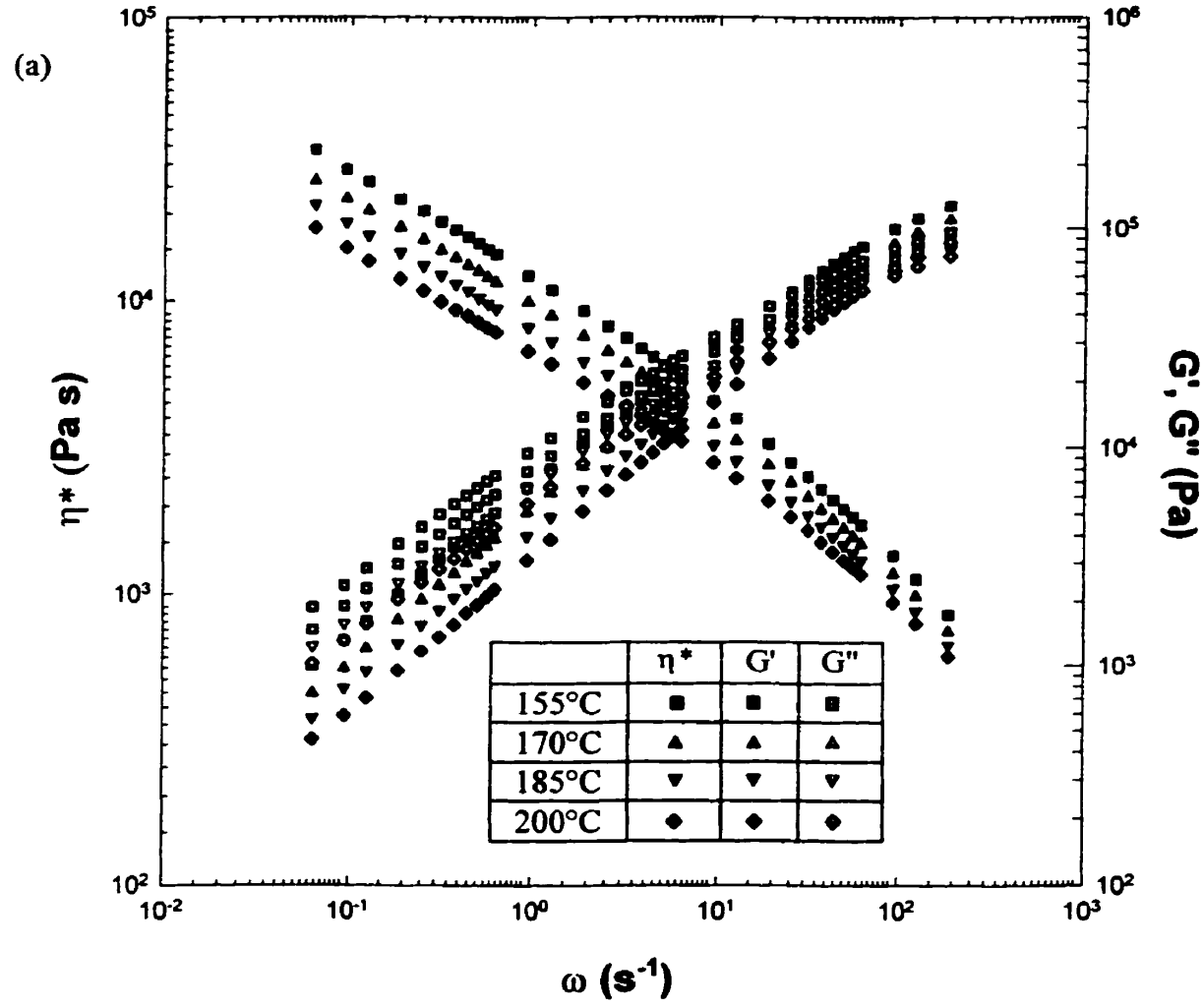

Figure 4. 4. η^*, G', and G" versus ω at five different temperatures for: (a) HDPE, (b) LLDPE, (c) LDPEa, (d) LDPEb, (e) mPE.

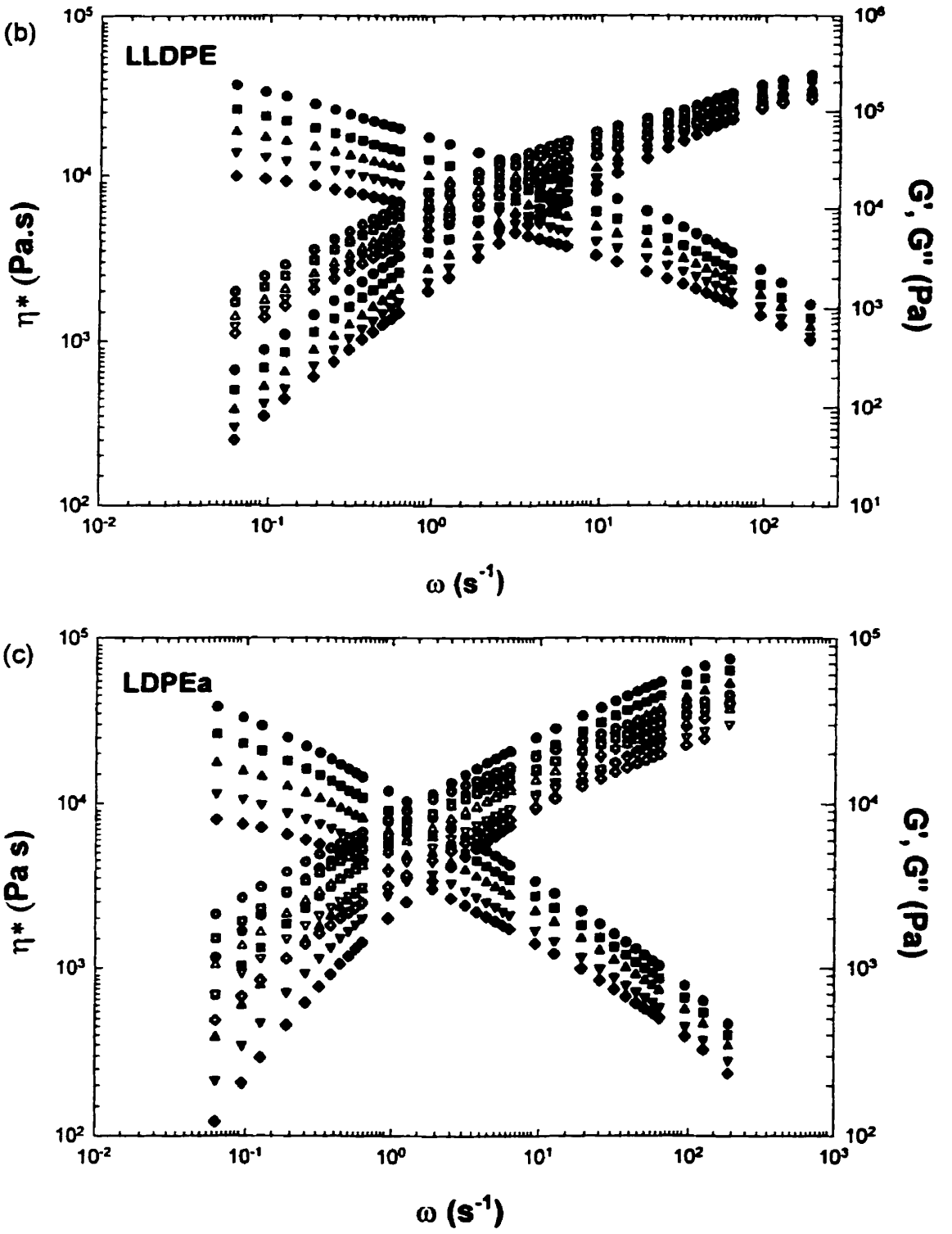

Figure 4.4. (continued)

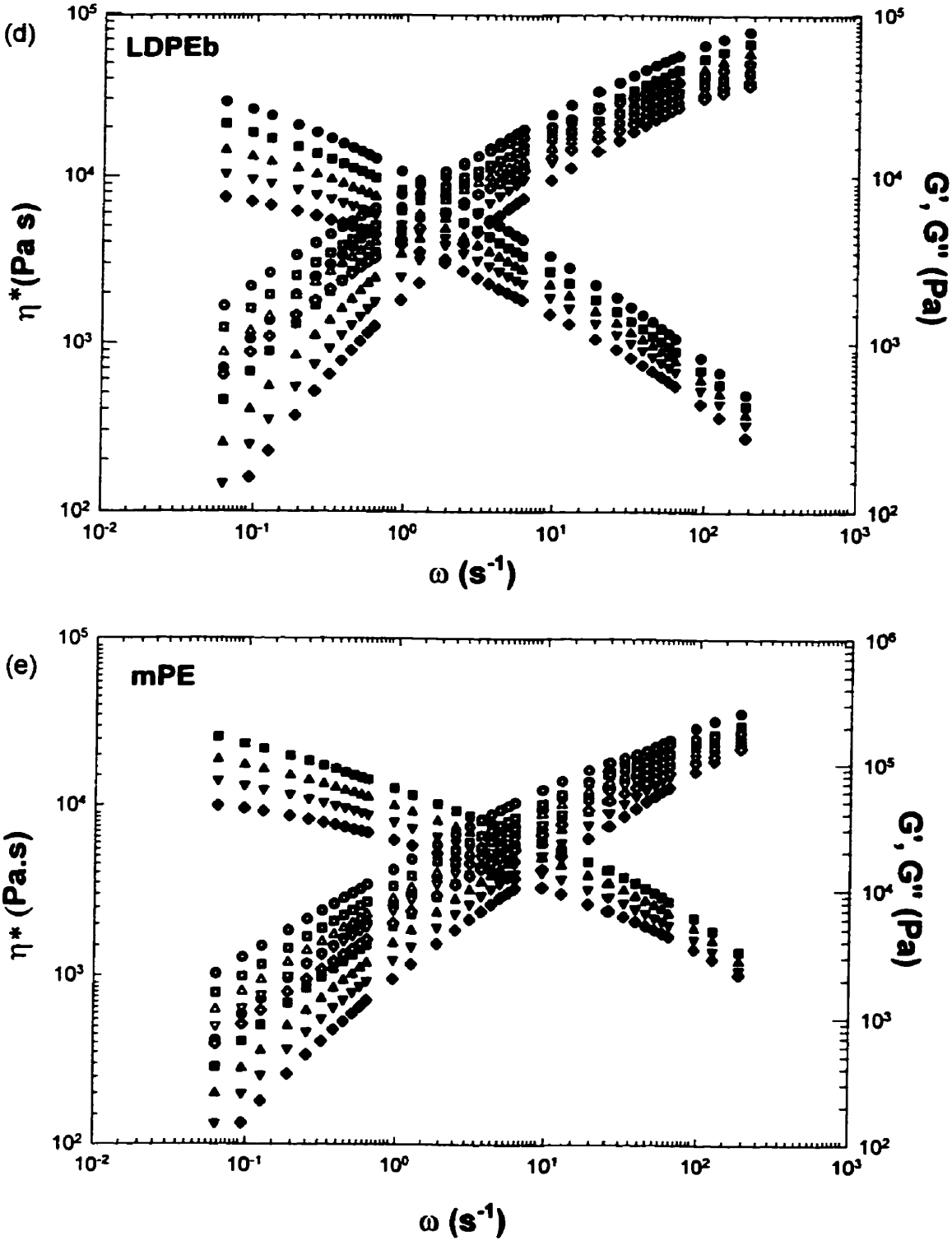

Figure 4.4. (continued)

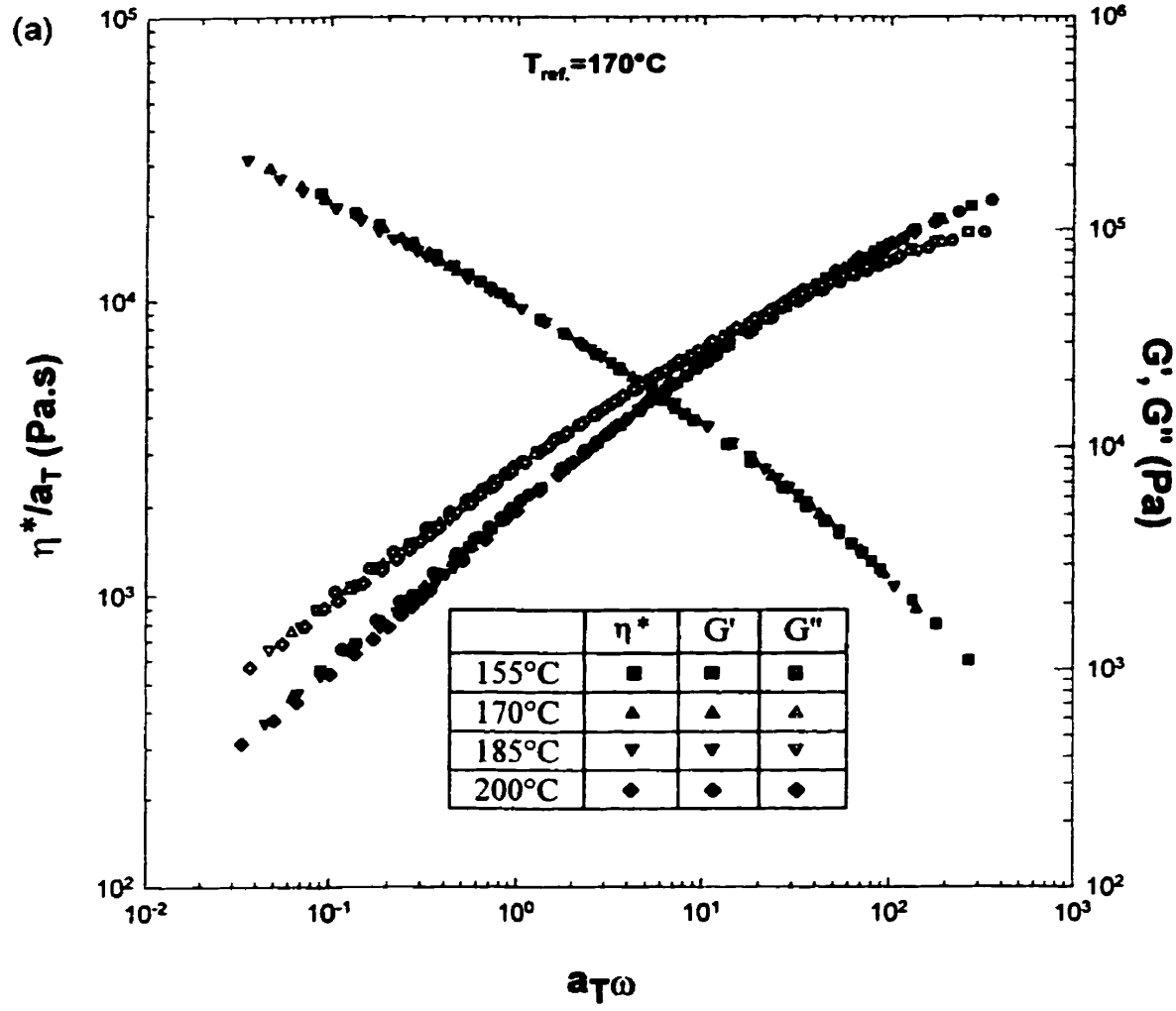

Figure 4. 5. Master curves for η^*, G', and G" at the reference temperature of 170°C for: (a) HDPE, (b) LLDPE, (c) LDPEa, (d) LDPEb, (e) mPE.

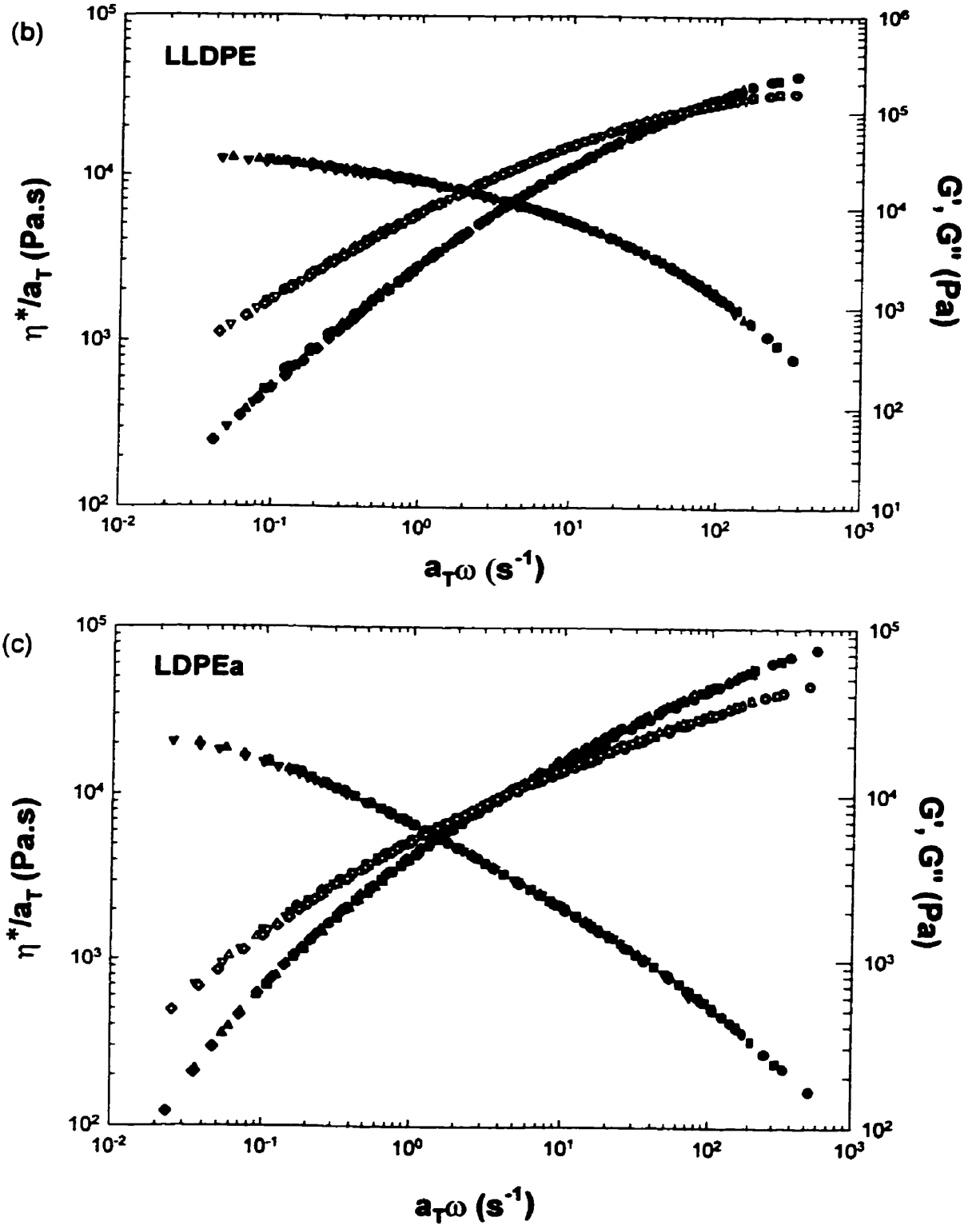

Figure 4.5. (continued)

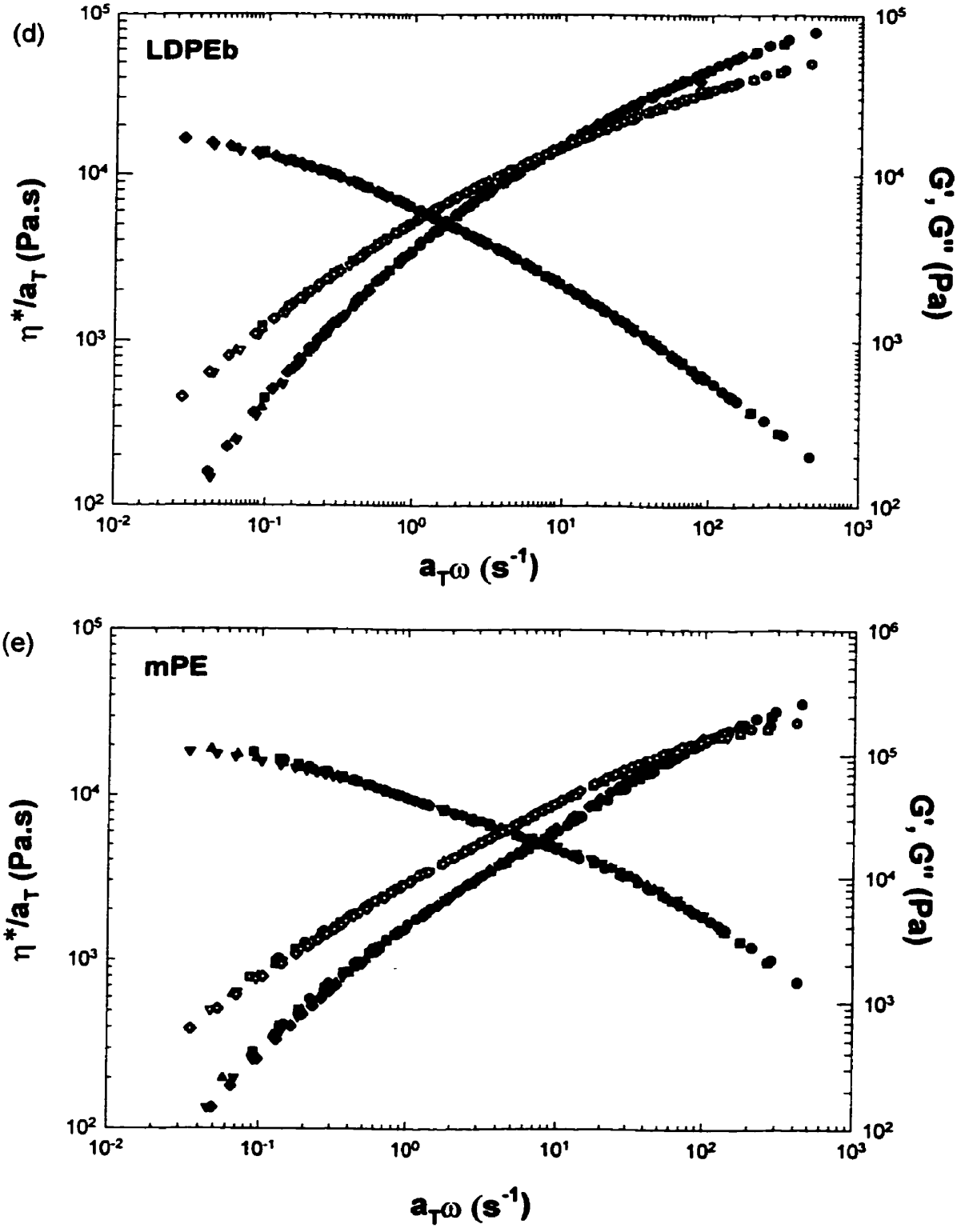

Figure 4.5. (continued)

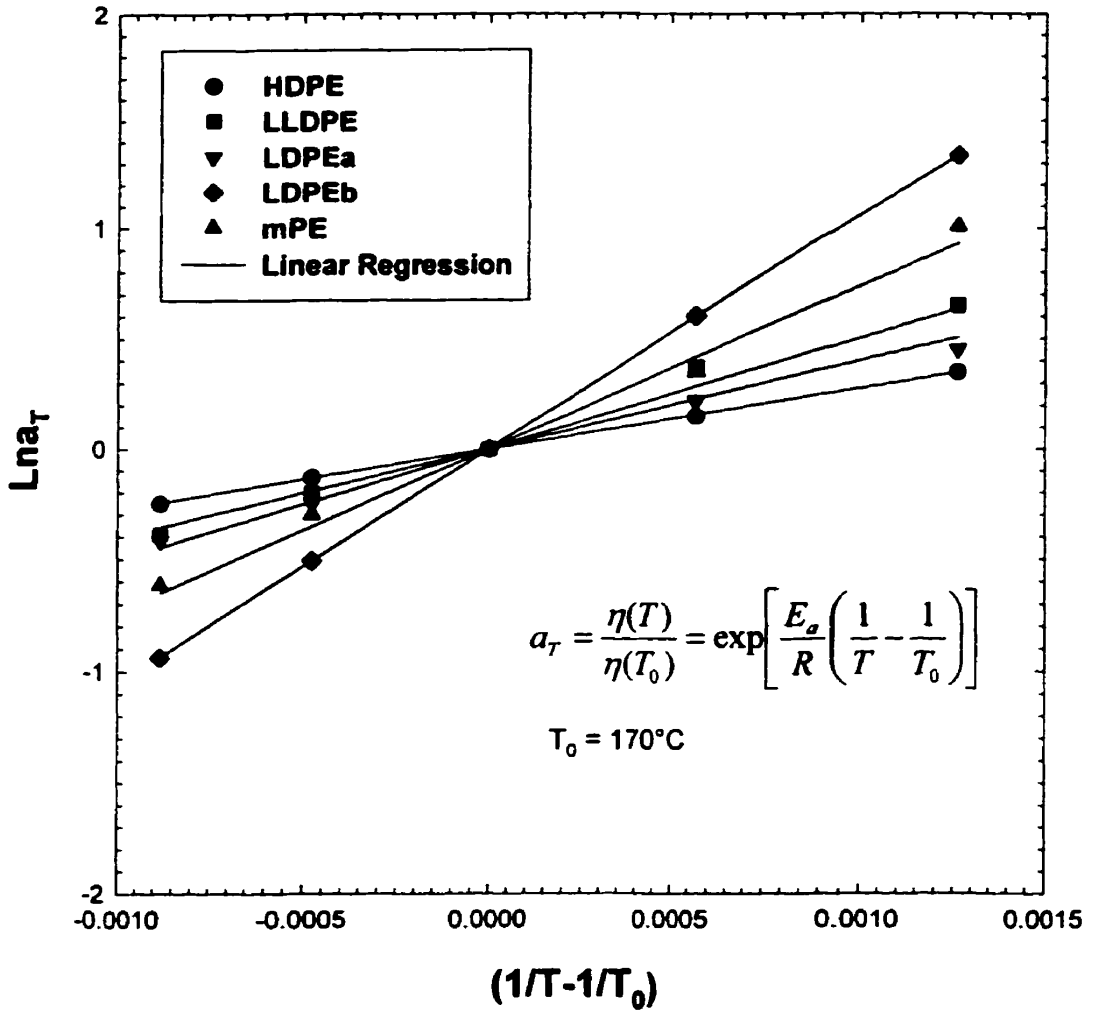

Figure 4. 6. Temperature shift factors by using Arrhenius equation at a reference temperature of 170°C.

4.1.3. Shear Viscosity

Figure 4.7 shows the complex and steady shear viscosities for the five resins at 200°C. Both piston-driven capillary rheometer and on-line capillary rheometer show fairly good agreement. The shear and complex viscosities of LLDPE and mPE match quite well at corresponding shear rate and frequency indicating that the Cox-Merz rule is fairly satisfied for both LLDPE and mPE within the error range of the experiment. However, for LDPEa, LDPEb, and HDPE, the shear viscosities are somewhat higher than the complex viscosities. For the branched resins, this is in agreement with the results of Shroff and Shida (1970), who showed that the differences between steady shear and dynamic viscosity increased with increasing bracnhing for PE resins. However, it is worth noting that some results in the literature (Utracki and Gendron (1984), Venkatraman et al. (1990)) reported that linear polyethylenes violate the Cox-Merz rule while branched polyethylenes exhibit a better agreement. The power-law parameters of the shear viscosity for five resins are listed in Table 4.3.

Table 4. 3. Power-law parameters in shear for five resins at 200°C.

Parameter-law parameter	HDPE	LLDPE	LDPEa	LDPEb	mPE
$m\ (Pa \cdot s^n)$	29740	15799	8754	5683	6943
n	0.45	0.456	0.45	0.49	0.65

Note that the shear viscosities encountered in practical extrusion operations are somewhere between 10-1000 s^{-1}, so it is very important to pay special attention to the shear viscosity at this area. Our experimental data show the following order from largest to smallest value: LDPEb > LDPEa > mPE > HDPE > LLDPE.

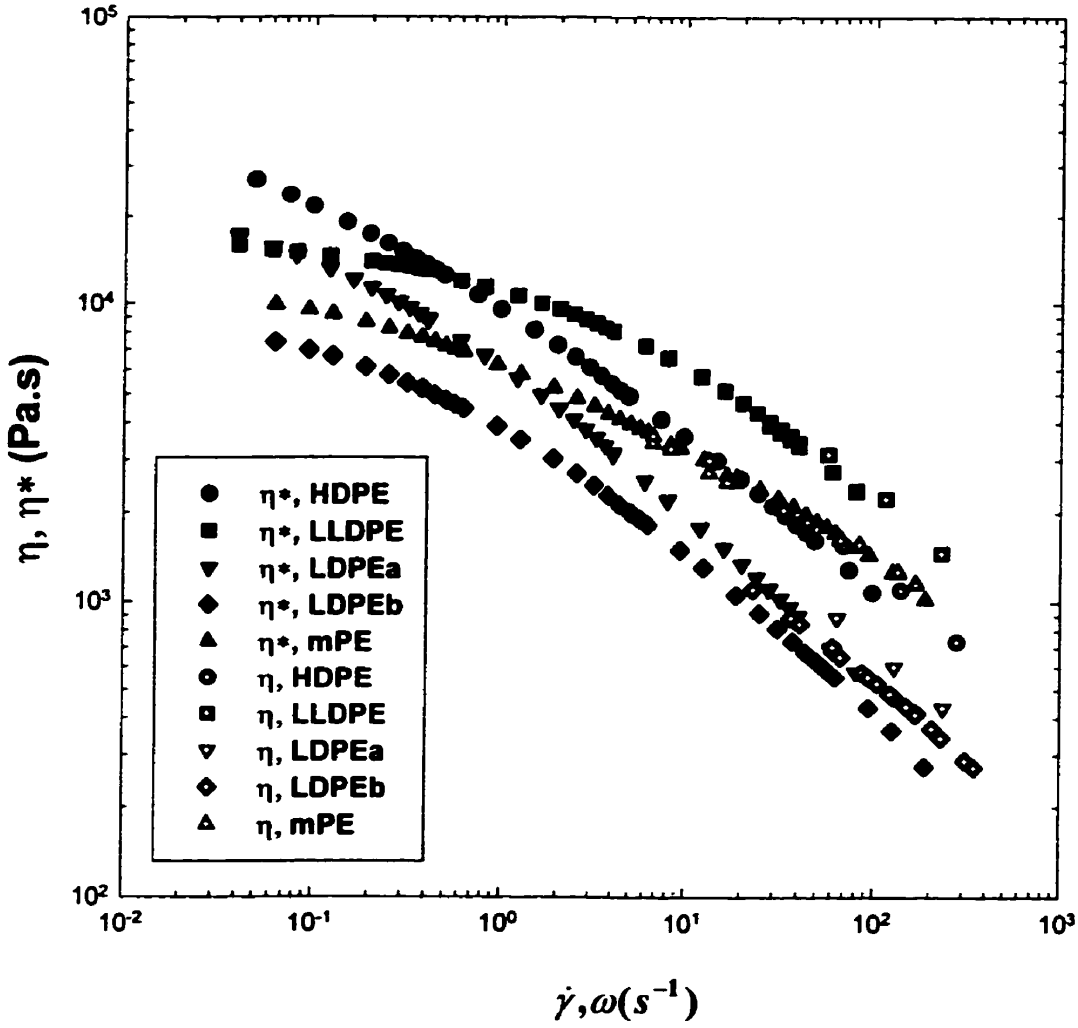

Figure 4. 7. Complex and steady shear viscosity data for five resins at 200°C.

4.1.4. Uniaxial Elongational Viscosity

Figure 4.8(a, b) gives the plots of the elongational viscosity versus the extensional rate obtained using the Cogswell and Binding analyses, for three resins, HDPE, LDPEb, mPE, investigated. We did not study the LLDPE here since the same type was not available. It can be seen that the elongational viscosity decreases with increasing the extensional rate over the range rates studied. That is to say, HDPE, LDPEb and mPE exhibit strain-thinning power-law behavior. The parameters L and t of elongational power-law model from the Binding analysis are reported in Table 4.4.

Table 4. 4. Power-law parameters in elongation from the Binding analysis.

Parameter	HDPE		LDPEb		MPE	
	D_1	D_2	D_1	D_2	D_1	D_2
$L(Pa \cdot s^t)$	113226	121914	58488	64394	50271	37331
t	0.33	0.33	0.43	0.36	0.53	0.71

Some observations are also worth noting: for all the polymers examined, the contribution of the shear components can not be neglected since it represents around 40% of the total pressure drop. Elongational viscosity calculated from the Binding method is lower than the one determined from the Cogswell. Small discrepancies are observed between the two sets of data from the dies D_1 and D_2 show that the viscosity data obtained from die D_1 are not in perfect agreement with those from die D_2. However, they are acceptable considering the difficulties of carrying meaningful measurements and accurately estimating the shear contribution to the pressure drop, mainly at low flow rates.

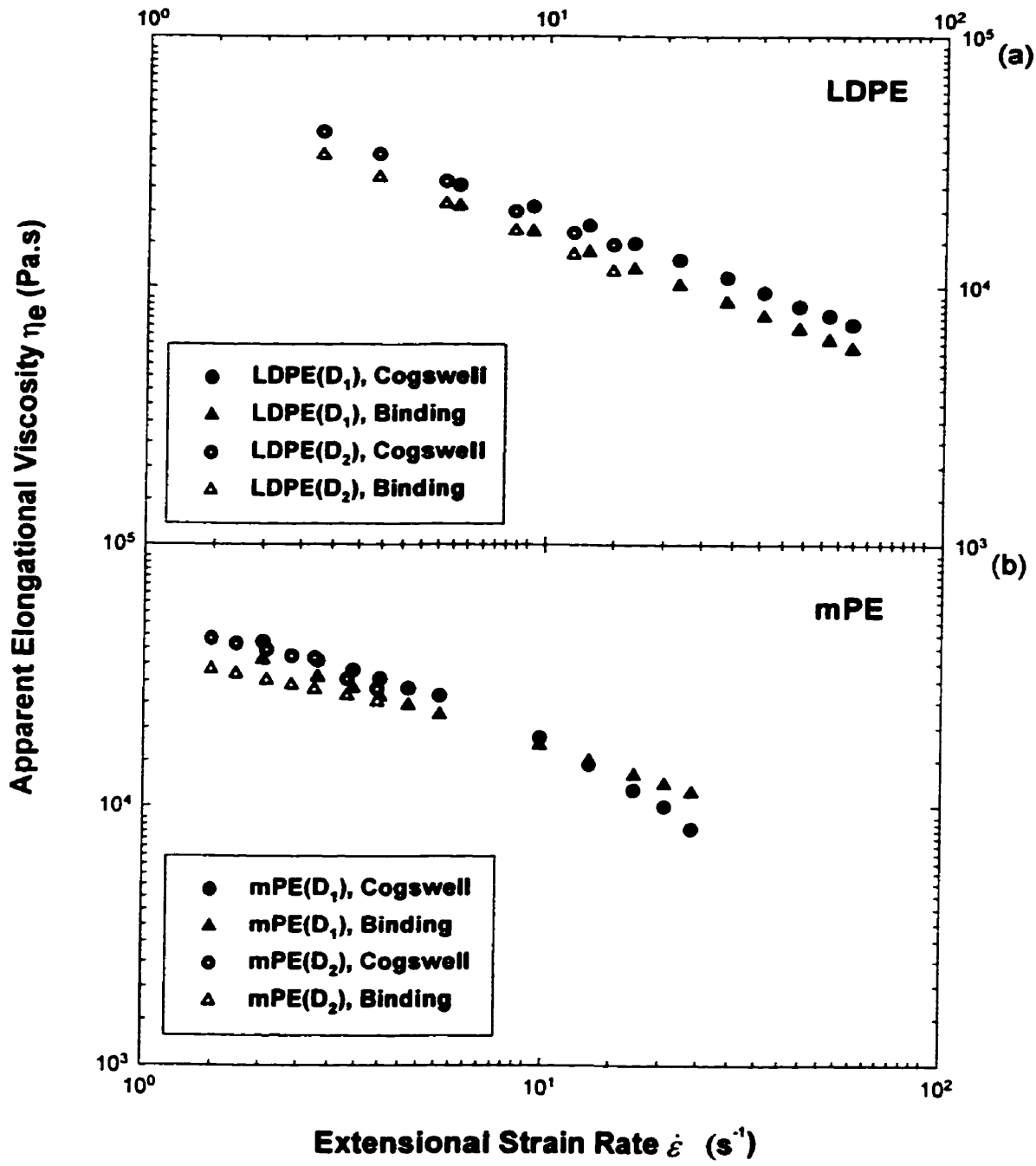

Figure 4. 8. Uniaxial Elongational Viscosity versus extensional rate for (a) LDPE and (b) mPE (c) HDPE at 200°C.

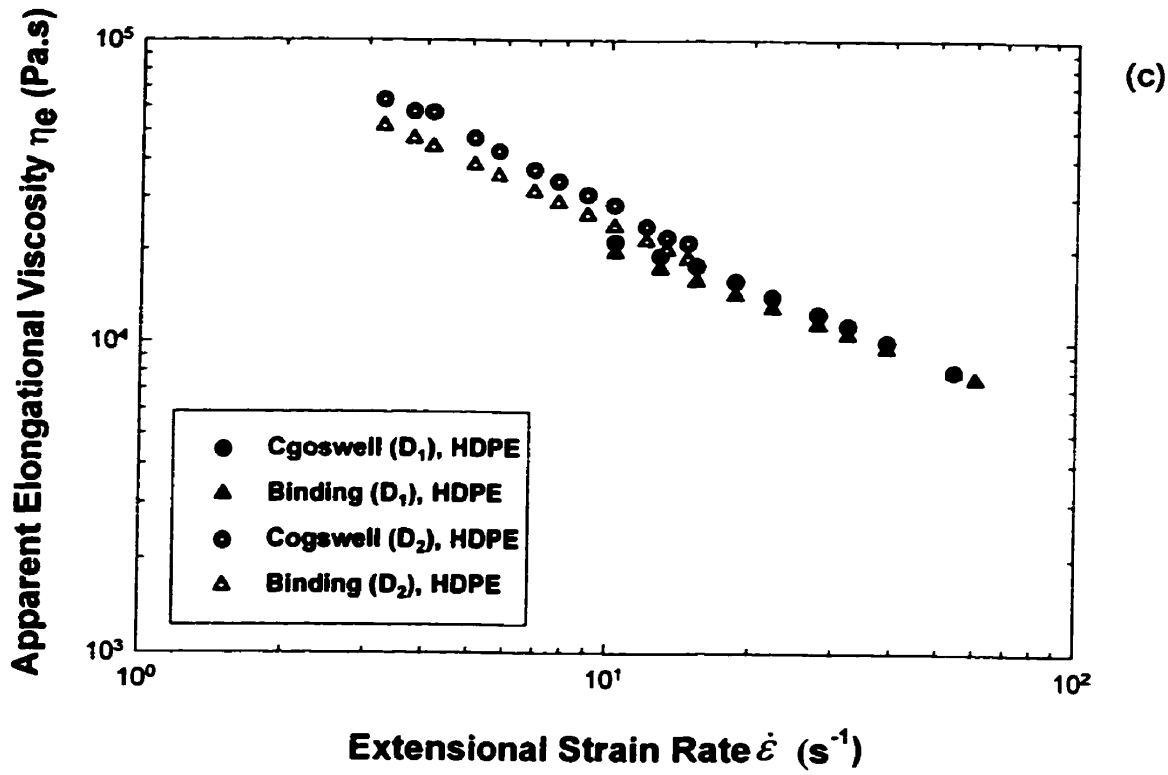

Figure 4.8. (continued)

The Trouton ratio, which is defined as the elongational viscosity to the shear viscosity, in terms of the effective rate of deformation $\bar{\dot{\gamma}}$ for the three polymers investigated, are presented in Figure 4.9. $\bar{\dot{\gamma}}$, which is defined as $\sqrt{\frac{1}{2}\mathrm{II}_{\dot{\gamma}}}$, is equal to $\dot{\gamma}$ for simple shear flow, and to $\sqrt{3}\dot{\varepsilon}$ for uniaxial elongational flow. For all the polymers studied, the Trouton ratio is always in excess of the value of 3, which is the case for inelastic Newtonian fluids or expected from the theory of linear viscoelasticity. The Trouton ratio for LDPEb far exceeds those for HDPE and mPE. This may be due to its relative strain-hardening behavior in elongational flow compared to shear flow. LDPEb shows strain-hardening behavior at high strain rates while mPE is more strain-thinning.

4.2. Results Temperature Profile

Temperature as a function of vertical distance from the die exit (z) is plotted for mPE and LDPEb in Figure 4.10. The temperature decays smoothly along the bubble length until it reaches a plateau. The results show the typical features found by other investigators: an initial cooling region leading up to a plateau followed by cooling of the solid. The plateau region is where the exothermic heat of crystallization is removed. However, we did not observed the region of solid cooling due the to the limit of experimental instrument.

It is worthy noting that the frost line height (FLH) we observed is defined as the line where the bubble becomes translucent. Morris (1998) refers to the onset of the plateau as the crystallization line height (CLH) and the end of the plateau as the freeze line (FZH). The frost line height (FLH) falls in between the CLH and FZH.

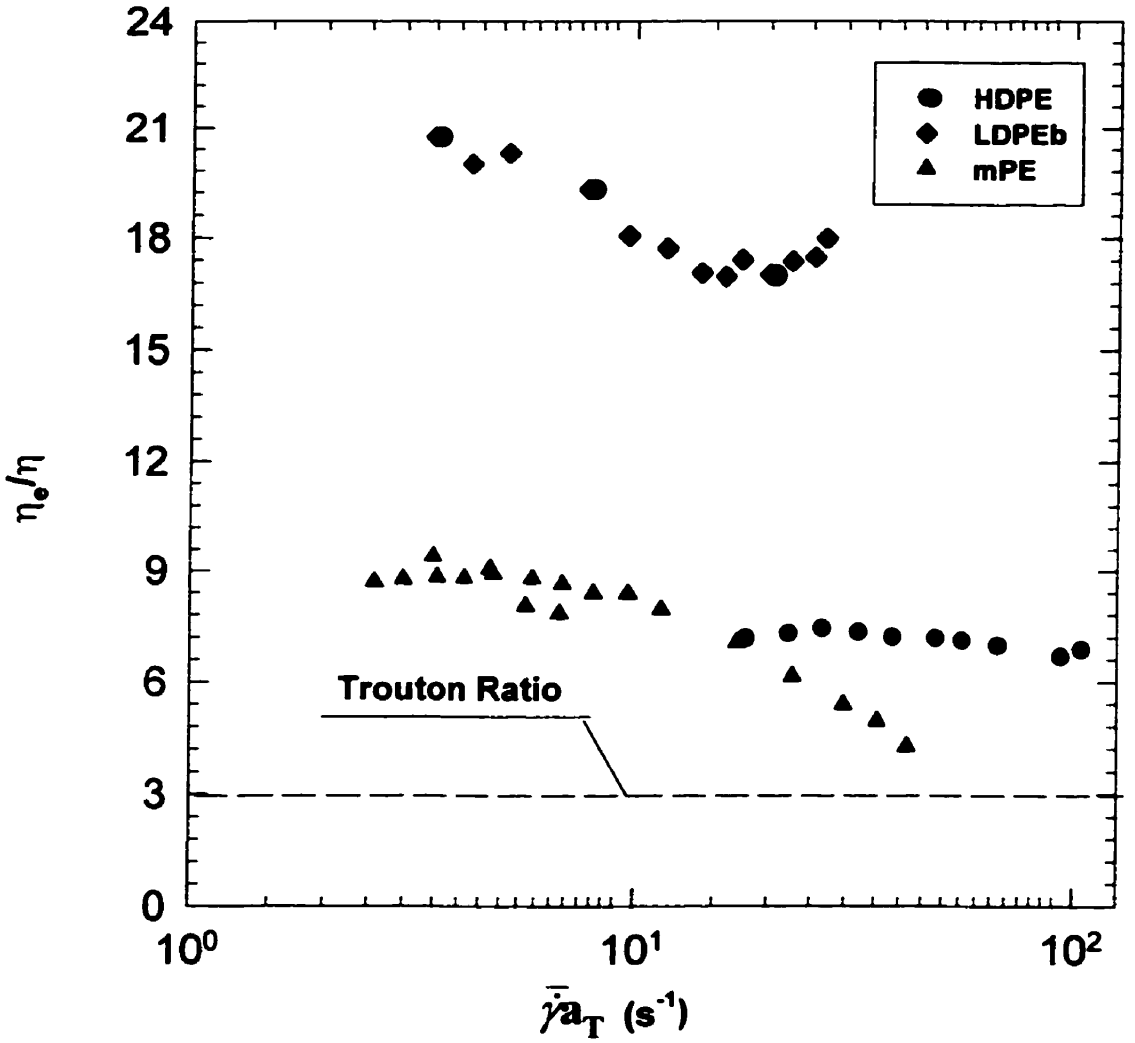

Figure 4. 9. Trouton Ratio for HDPE, LDPEb and mPE resins at the reference temperature as 170°C.

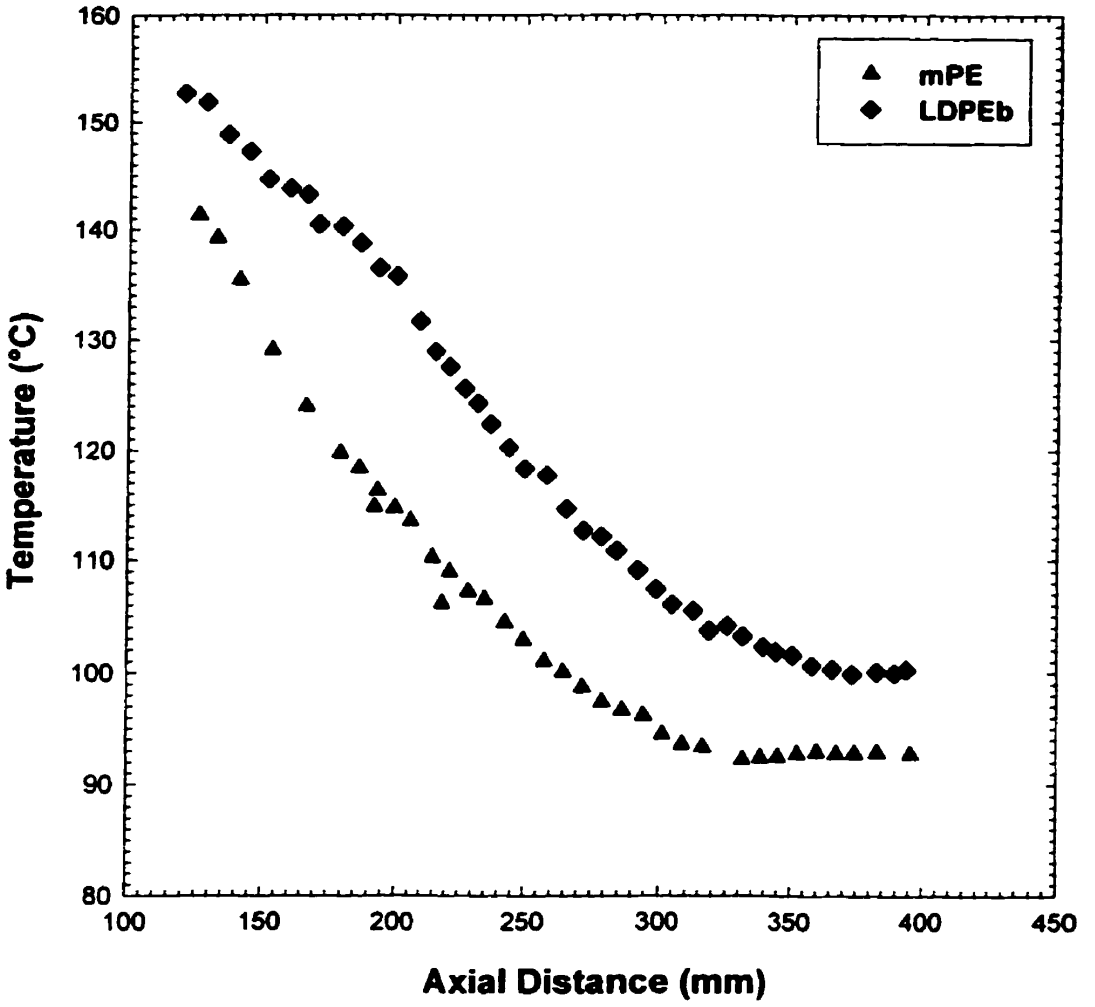

Figure 4. 10. Bubble Temperature along the axial distance for mPE and LDPEb. The Mass Flow Rate = 6.5 Kg/h, TUR = 6.0, BUR = 2.5, Temperature = 200 °C, FLH $\approx 300mm$

4.3. Results of Strain Rates

4.3.1. Calibration of LDV

Figure 4.11(a, b) shows the bubble velocity profiles measured by moving the laser upward then downward. The velocity profiles appear to be consitant in the range investigated for both mothod.

Figure 4.12 presents the comparison of the velocity measured by LDV and the real velocity. Both velocities show very good agreement at low take up speed (lower than 150 mm/s). The velocity profiles of the film to be measured should be in this range.

4.3.2. Velocity, Diameter and Thickness Profiles

Figure 4.13(a, b, c) shows the velocity, diameter and thickness profiles for LDPEb and mPE. Polynomials were used to fit the data. It may be seen that the bubble velocity of LDPEb increases monotonically along the length of the bubble. However, the bubble velocity of mPE shows a plateau in the velocity of the air ring. The diameter profiles of both LDPEb and mPE increase monotonically and plateauing beyond the frost line.

It should be mentioned here that the thickness profiles shown in the curve was calculated from equation (3.50). Moreover, we eliminate the influence of density since the error resulting from the constant density assumption in thickness should not be more than 3% according to our calculation. In comparison with the method of measuring the solidified bubble, it was observed that the thickness profiles, for both methods, make a good agreement above the frost line. However, below the FLH, the difference between these two profiles is very pronounced. This is due to the elastic recovery after the pulling

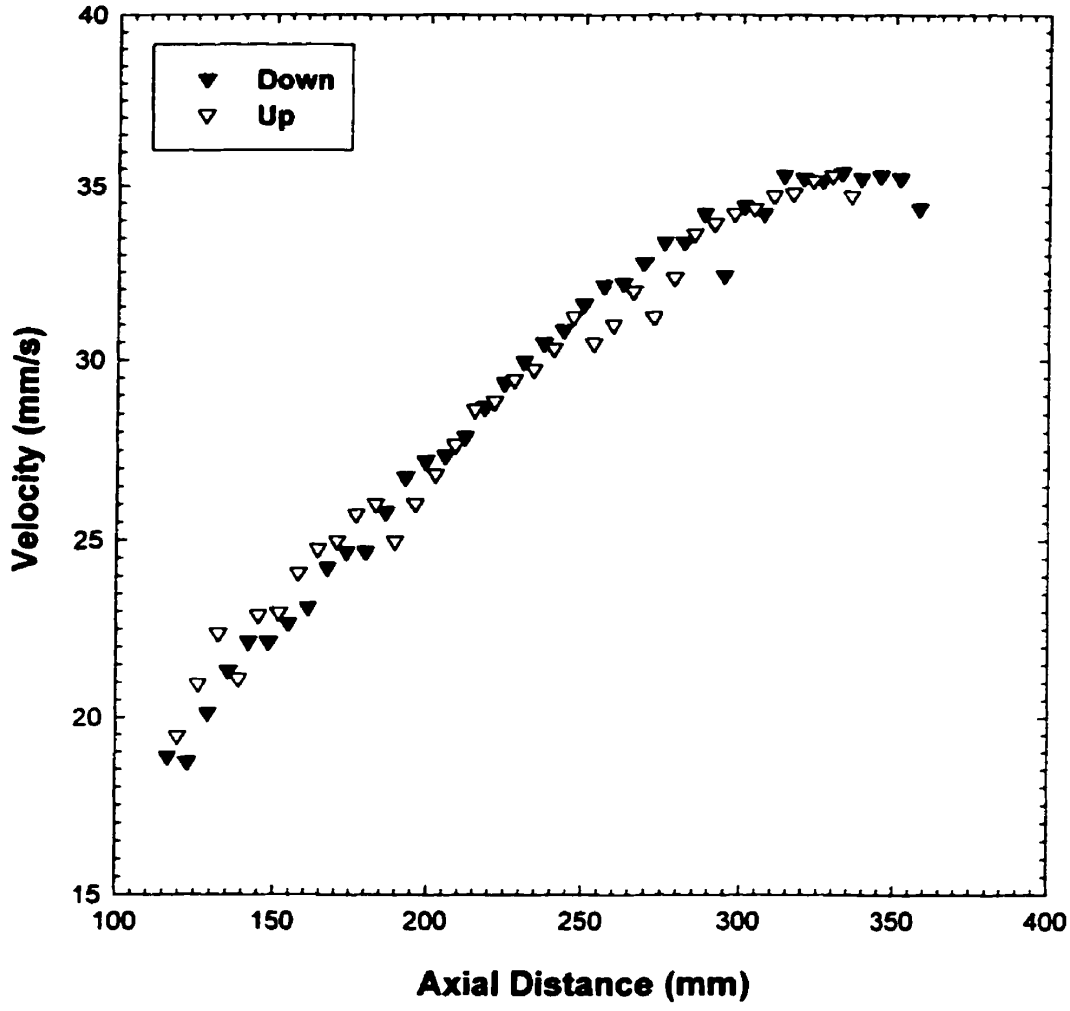

Figure 4. 11. Bubble velocity profiles along the length for LDPE. Polymer flow rate = 5.91 kg/h, extrusion temperature = 200oC, BUR = 1.73. FLH $\approx 300mm$. TUR = 3.80

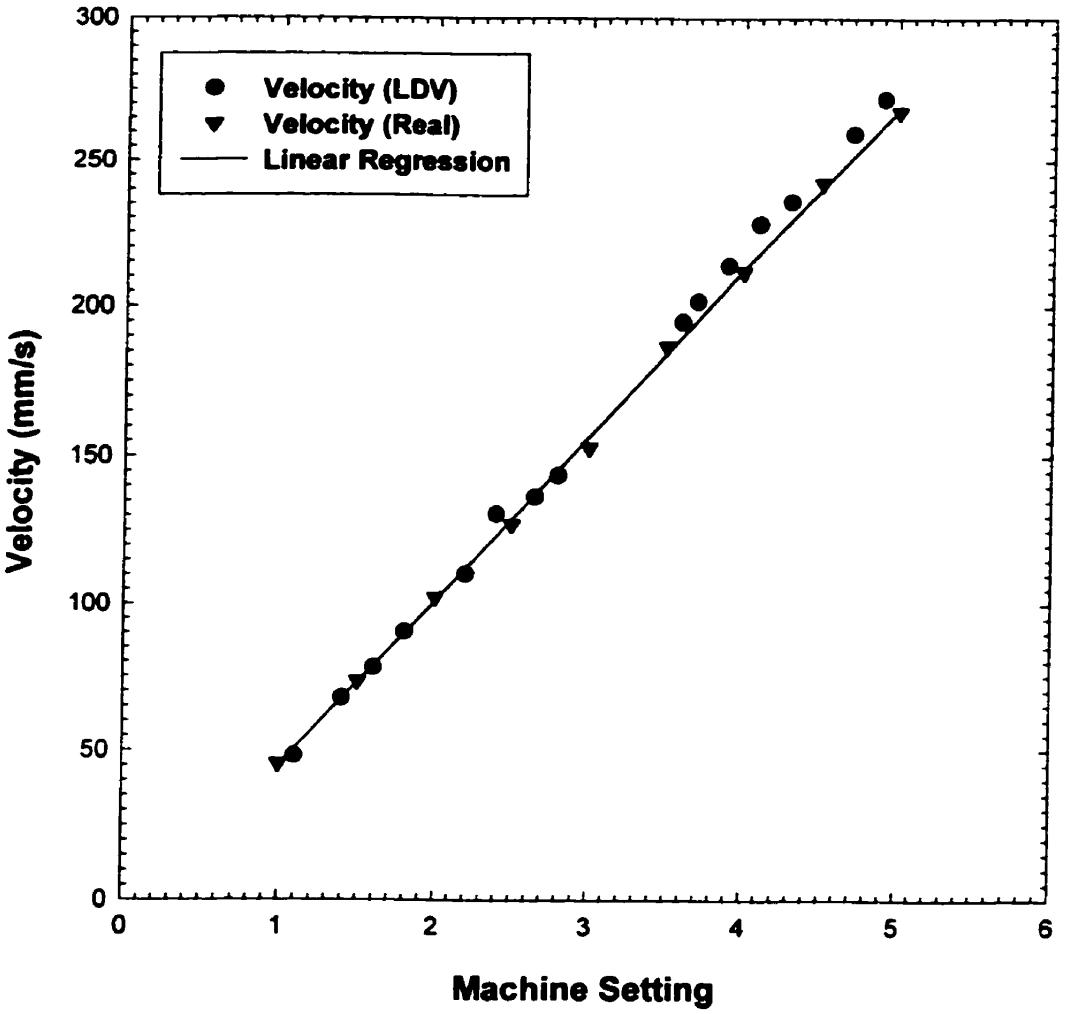

Figure 4. 12. Calibration of LVD.

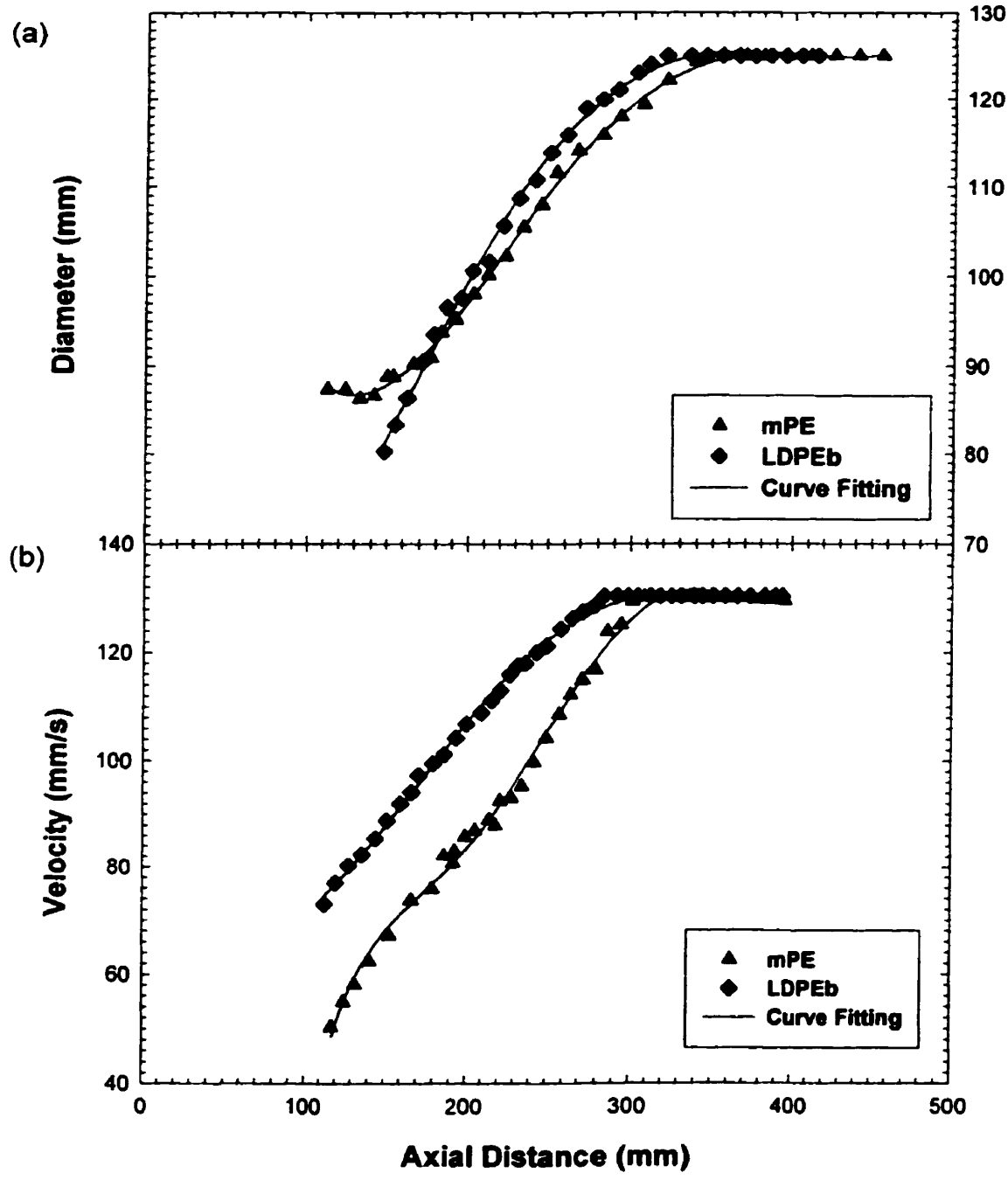

Figure 4. 13. Bubble diameter (a), velocity (b), and thickness (c) profiles along the axial distance for mPE and LDPEb. The film blowing conditions are the same as in Figure 4.10.

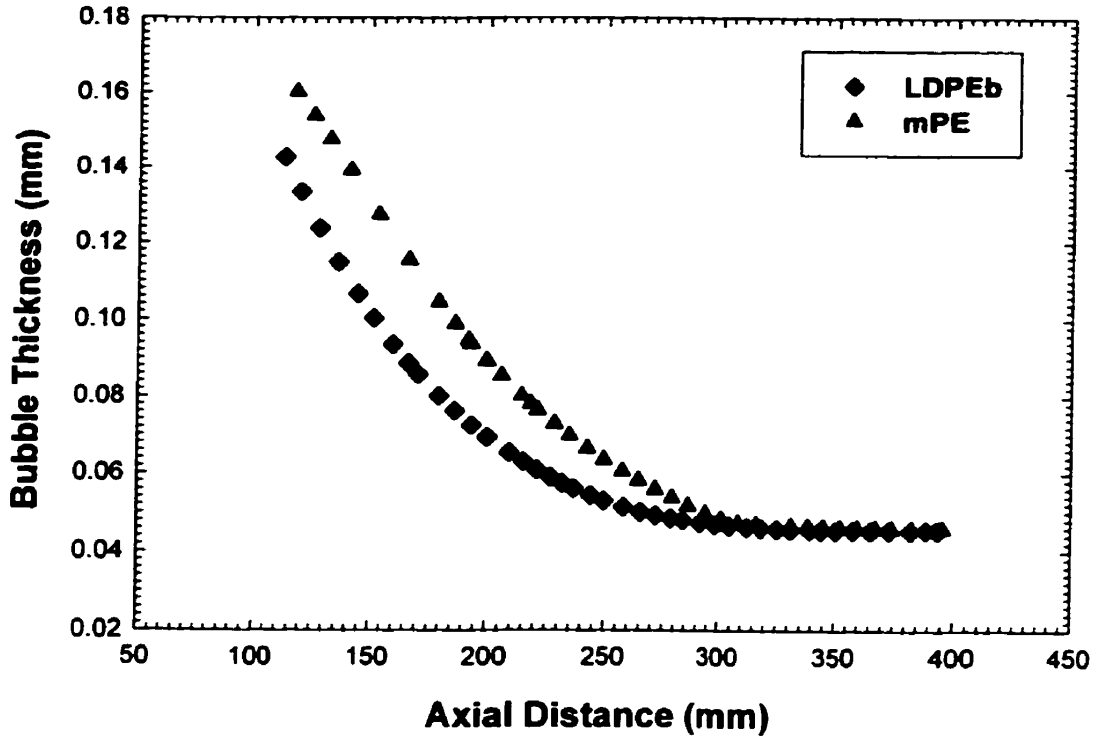

Figure 4.13. (continued).

of the bubble is stopped. Large differences were also reported by Huang and Campbell (1985) and Ghaneh-Fard et al. (1997b).

4.3.3. Strain Rates

The machine and transverse directions (MD and TD respectively) strain rates ($\dot{\gamma}_{11}, \dot{\gamma}_{33}$) were calculated from equations (3.53) and (3.54). Figure 4.12 compares the MD and TD strain rates of both mPE and LDPEb. For the LDPEb, the MD strain rate remains almost constant at first, then decreases smoothly until it becomes zero above the FLH; the TD strain rate is similar to that in MD except that it smoothly increases at first. For the mPE, the MD strain rate increases linearly and reaches a maximum and suddenly decreases to zero in the vicinity of FLH; however, the TD strain rate is quite different, it is first very small, then increases drastically and reaches a maximum and finally decreases to zero around FLH. Note that for LDPE, Farber and Dealy (1974) and Ghaneh-Fard et al. (1997a) observed that the strain rate in TD exceeds that in MD in the region of bubble expansion. Our data showed that such a result is not necessarily true.

4.4. Birefringence Results

Figure 4.13 presents the birefringence for both mPE and LDPEb. For all the range investigated, the birefringence values are always positive indicating that the orientation in MD is always greater than that in TD. Below the FLH, the birefringence values of both mPE and LDPEb show the same tendency, increasing slightly along with the bubble. This indicates that orientation in MD increases with axial tension. In the vicinity of FLH, the birefringence decreases slightly indicating that the orientation in MD increases slower than that in TD. This may be due to the relaxation of molecular orientation, which has

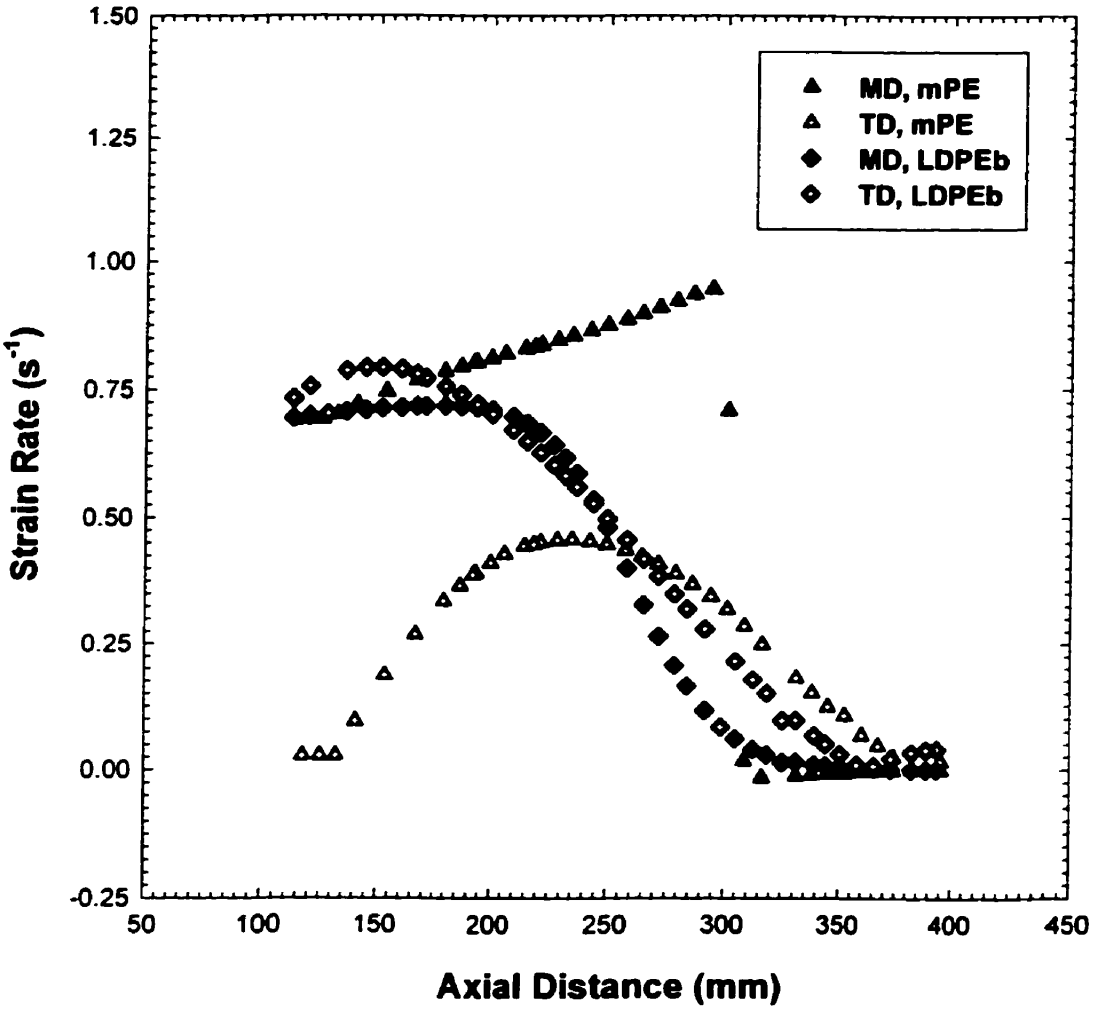

Figure 4. 14. Strain rates in MD and TD along the axial distance for mPE and LDPEb. The film blowing conditions are the same as in Figure 4.10.

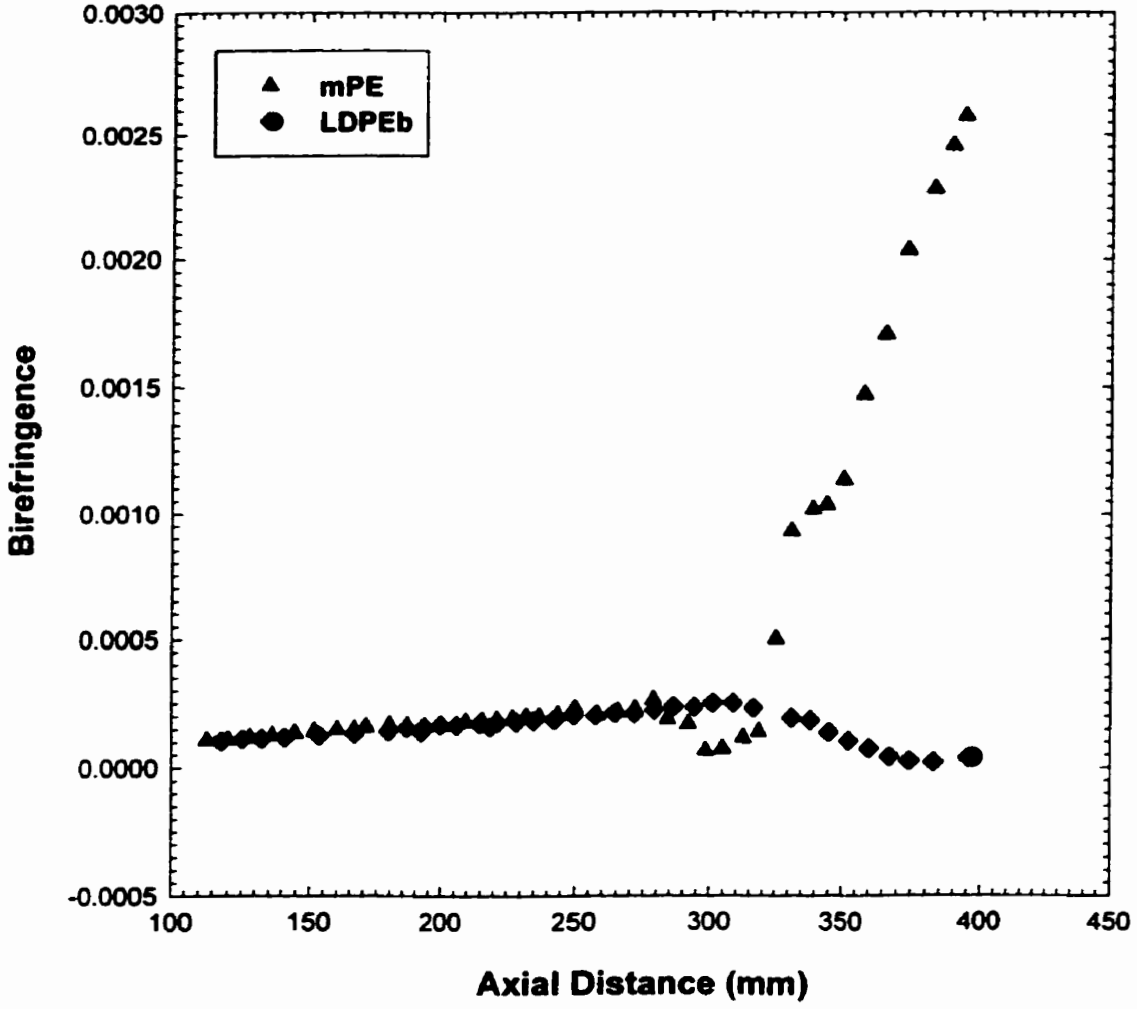

Figure 4. 15. Birefringence along the axial distance for mPE and LDPEb. The film blowing conditions are the same as in Figure 4.10.

been speculated by Maddams and Preedy (1978). However, they are quite different above the FLH. For mPE, the birefringence values increase drastically indicating the large increase in orientation during crystallization. This may be due to, as indicated by Choi et al (1982) and Shimomura et al. (1982), oriented nucleation and growth process. And for LDPEb, it decreases. This may be due to the bubble became translucent above the FLH and made the measurement of birefringence inaccurate. Our birefringence data show good agreement with those obtained by Ghaneh-Fard et al. (1997b) for LDPEa at low take-up ratio.

4.5. Machine and Transverse Stresses

As we mentioned in section 4.4, the birefringence measured may not be very accurate above the FLH due to the low transparency of the bubble. Moreover, what we are interested here is the section of the bubble between the die exit and the FLH. So we only present the stresses, shown in Figure 4.14, for mPE and LDPEb in MD and TD below the FLH. Comparing the stresses in MD with those in TD, both mPE and LDPEb show the same tendency: the stresses in MD are always higher than those in TD and the differences increase with the axial distance. However, by comparing the stresses for the mPE and for LDPEb, we can see pronounced differences. The stress curves for both mPE and LDPEb are almost overlapped in the region close to the die and increase slightly with the axial distance. At higher axial distance (around the inflation zone of the bubble), the stresses of LDPEb keep increasing up to the FLH. However, the stresses for the mPE increase drastically at same axial distance and change to smoothly increase again in the vicinity of FLH.

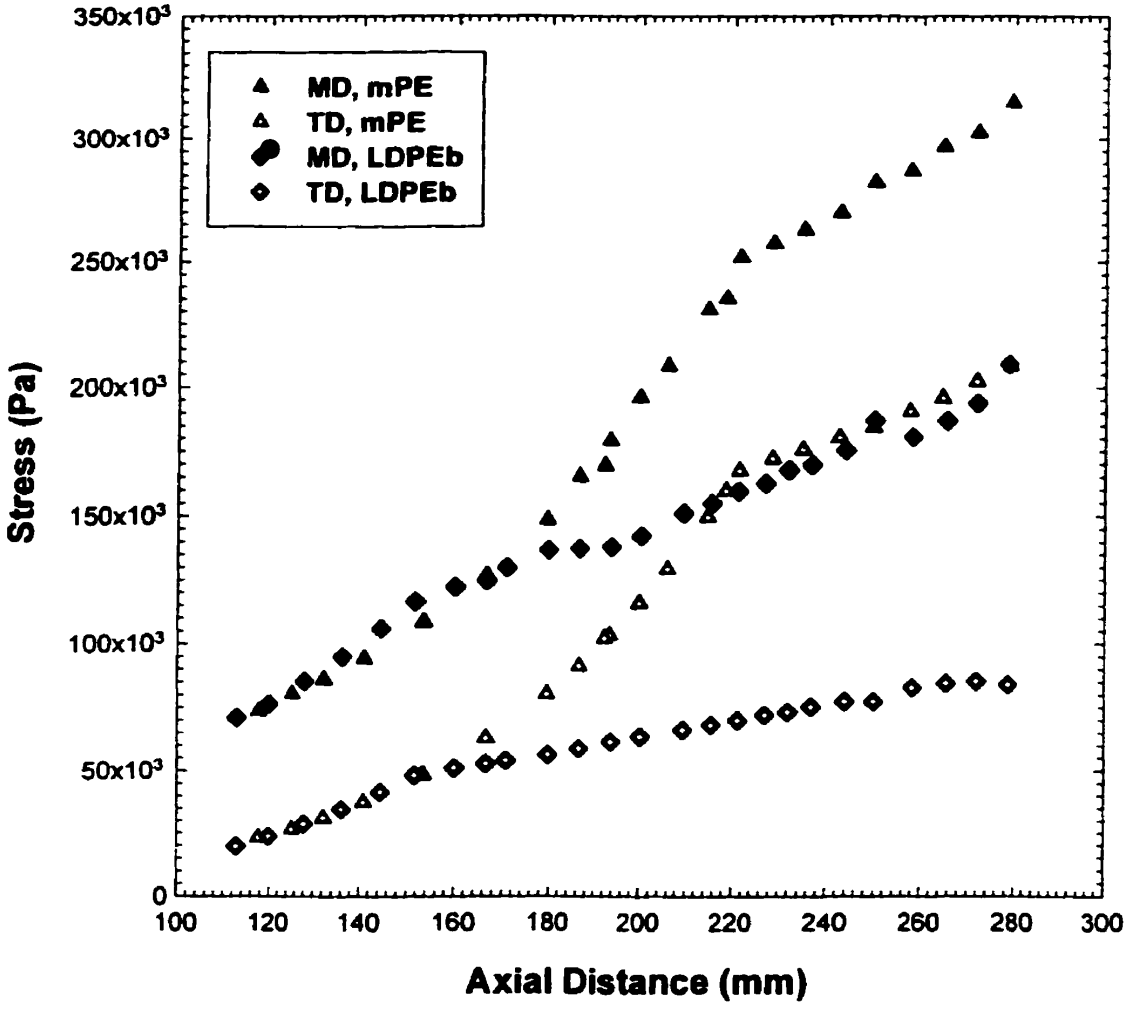

Figure 4.16. Stress profiles along the axial distance for mPE and LDPEb. The film blowing conditions are the same as in Figure 4.10.

4.6. Biaxial Elongational Viscosity

Figure 4.17a reports the apparent effective biaxial elongational viscosity, calculated form equation (3.75), along the axial distance. Not surprisingly, the biaxial elongational viscosities of both mPE and LDPEb increase monotonously with the axial distance due to the effect of temperature. The cooling of the tubular film by the flow of air past the bubble helps to generate such elongational viscosity profiles. However, the η_{fe} of LDPEb increases more rapidly than that of mPE in the vicinity of FLH.

Figure 4.17b shows the effective rate of deformation, $\bar{\dot{\gamma}}$, along the length of the bubble. The $\bar{\dot{\gamma}}$ for the LDPEb is very high and is almost constant at low axial distance, then decreases drastically at higher axial distance. However, the $\bar{\dot{\gamma}}$ for the mPE exhibits a reverse trend, increasing at first then staying almost constant in the vicinity of FLH.

4.7. Results of Bubble Stabilities

Since the stability of polyethylenes (LDPE, HDPE and LLDPE) had been extensively studied in details previously (Ghaneh-Fard et al, 1996a) in our laboratory, the purpose our study here is to complement the previous study with mPE stability data.

Following previous authors (Han and Park, 1975; Han and Shetty, 1977; Kanai and White, 1984; Minoshima et al., 1987; Ghaneh-Fard et al., 1996a), we defined three forms of instabilities and combination as follows: (1) Axisymmetric periodic variations of the bubble diameter. (2) Helical motions of the bubble and (3) variations in the positions position of the solidification line. We call the three forms of these instabilities bubble instabilities; helical instability and FLH instability.

The stability behavior of mPE is presented in Figure 4.18 (a, b, c) with the help of diagrams of the FLH versus the BUR for different TUR values studied.

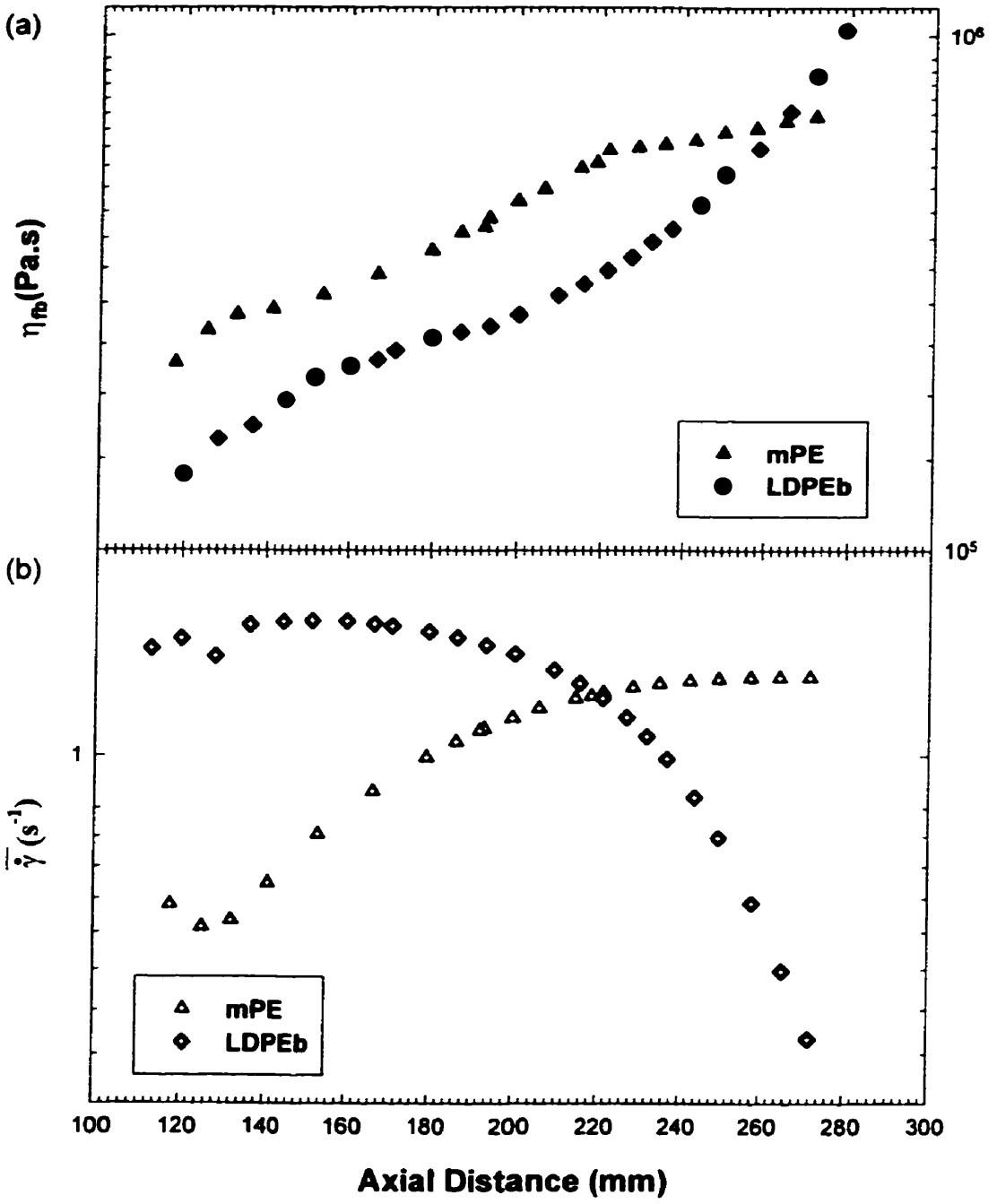

Figure 4.17. Apparent biaxial elongational viscosity (a) and the effective deformation rate (b) profiles along the axial distance for mPE and LDPEb. The film blowing conditions are the same as in Figure 4.10.

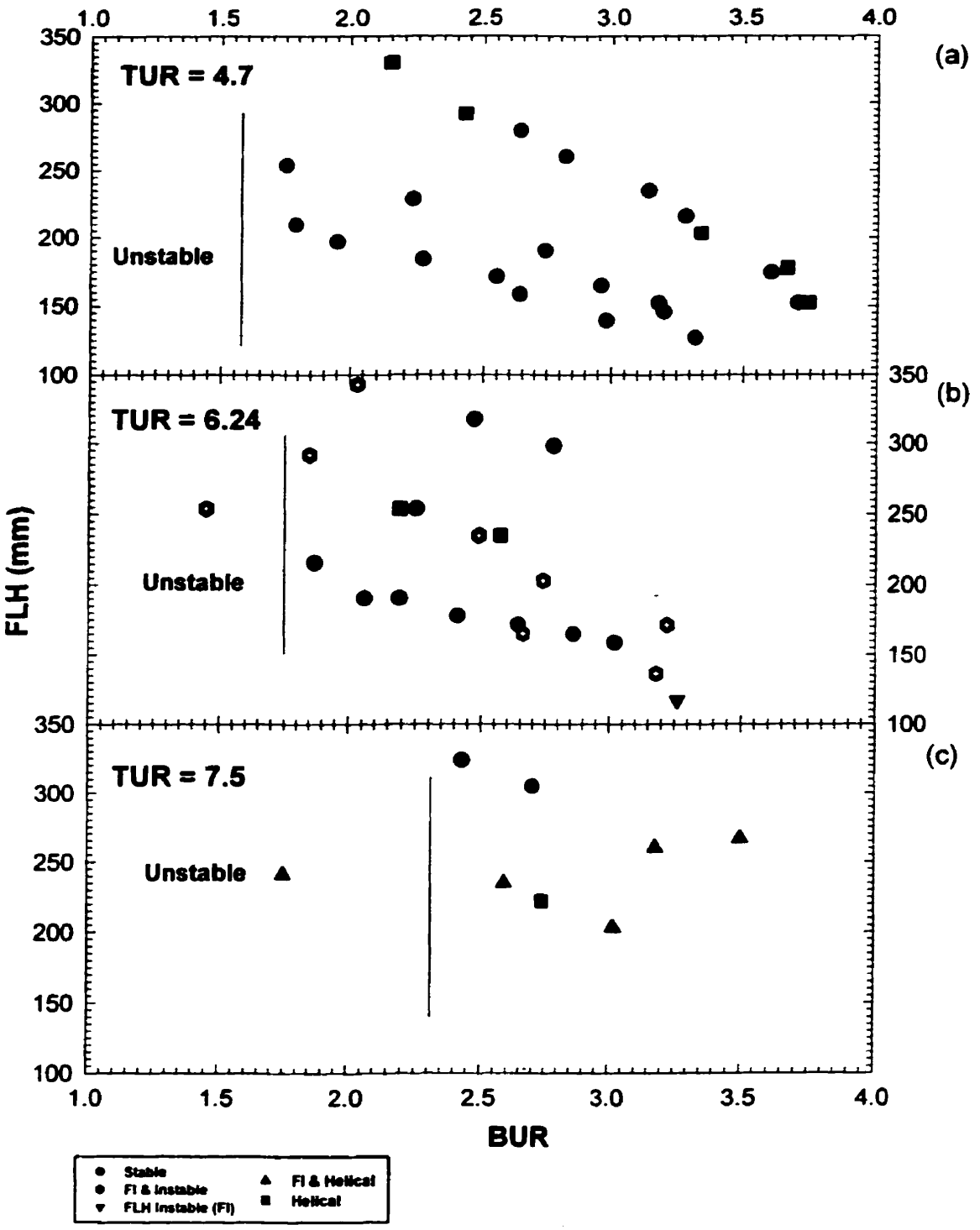

Figure 4.18. Bubble stability behavior of mPE under the extrusion temperature = 200°C, Flow rate = 5.4 Kg/h (a) TUR = 4.7, (b) TUR = 6.24, (c) TUR =7.5.

When the bubble was inflated by a small amount of air, that is to say, when BUR < 1.0, instability was observed. There was no distinct FLH. As the magnitude of the diameter fluctuations increased with time, the bubble finally broke. This phenomenon was also observed by Minoshima and White (1986); Ghaneh-Fard et al. (1996a).

At a low TUR value of 4.7, one can see that the bubble was almost stable under different FLHs when the value of BUR was between 1.65 to 3.5. With the increase of TUR, the stable operating space went narrower and only under a small value of BUR. It was impossible to a get stable bubble if the TUR was over 14.0.

Figure 4.19 (a, b) shows the stability of LLDPE at the same experimental conditions, extrusion temperature (mass flow rate) as mPE. When BUR < 1.0 or TUR > 14.0, LLDPE exhibited the similar behavior as mPE. It is very difficult to find which resin has the larger operation space between mPE and LLDPE.

Summarizing the previous study in our laboratory reported by Ghaneh-Fard et al (1996b), we may conclude that for LDPE and high molecular weight HDPE the tubular film process operates in a stable manner in a wide region of operation conditions. Instabilities occurring at higher take-up ratios have a similarity to the flow instability occurring in melt spinning process, where periodic variations in the cross-sectional area along the spin line appear as the take-up ratio is increased. We propose the following relative order of stability of five polymers studied:

LDPEa or LDPEb > HDPE > LLDPE or mPE

Stable operation is dependent on the processing conditions and on the peculiarities of the processing machinery and the deformational history in the die preceding the biaxially elongation process. However, stable operation is also a question of the used grade of raw material. A reasonable understanding of the observable

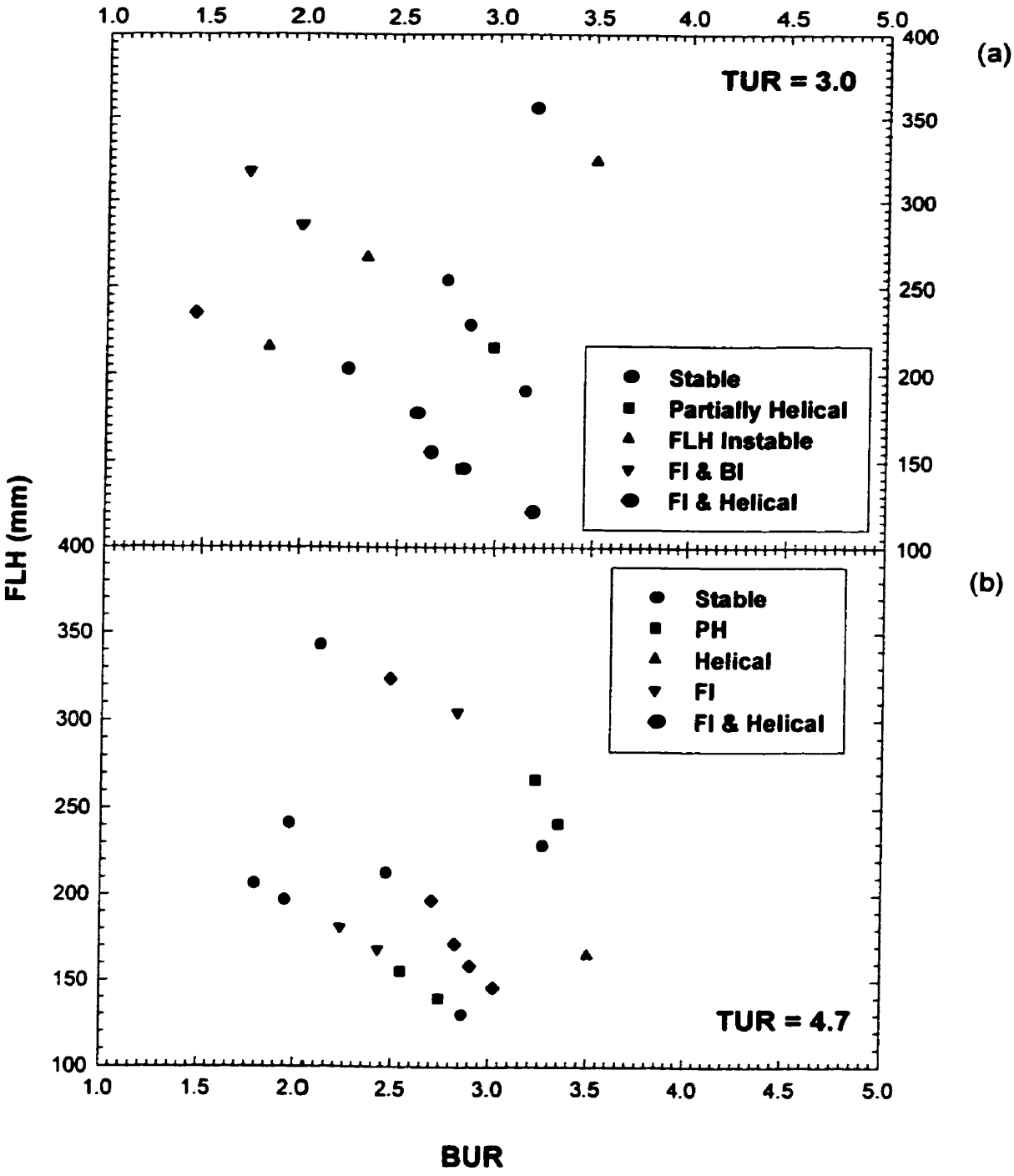

Figure 4.19. Bubble stability behavior of LLDPE under the temperature = 200°C, Flow rate = 5.4 Kg/h at (a) TUR = 3.0, (b) TUR = 4.7.

differences in terms of rheological properties (and by that on a molecular basis if sufficient measurements are available on model substances) is necessary in order to assist product development.

4.8. Relationship between Polymer Processability and Its Rheological Behavior

Rheological properties play an important role in film blowing. They govern the shape and stability of the bubble and the onset of sharkskin (surface roughness). Because of the complexity of the flows involved, it is not generally possible to establish simple quantitative correlations between these phenomena and easily measured rheological properties. However, an understanding of how variations in the rheological behavior of melts can affect the processing and properties of blown film is essential if one is to achieve optimum results from this process.

It should be pointed out that any discussion about processability must refer to particular polymer processing operations. Polymer processability in blown film extrusion is usually associated with three aspects of extrusion (Mavridis, 1998):

(a) Extrudability, i.e., ease of extrusion. Obviously, extrudability improves with lowering the viscosity at high shear rate, which in turn depends on molecular weight (often characterized by the Melt Index, or MI) and molecular weight distribution (MDW).

(b) Bubble Stability or Melt Strength. This relates to the ability of the resin/bubble to tolerate/dampen disturbances that tend to de-stabilize the bubble during blown film extrusion. Higher bubble stability allows extrusion at higher rates. The higher the melt strength of the resin the better the bubble stability. Melt strength, in turn, can be quantified (indirectly) by low shear-rate viscosity (Naitove and Schut., 1993).

(c) Sharkskin melt fracture. This is a rate-limiting onset of extrudate defects on the film. Generally, the higher the molecular and the narrower the MWD (or the less the Long Chain Branching, LCB), the earlier the onset of sharkskin melt fracture.

4.8.1. Complex and Shear Viscosity

It is evident that the LDPEa and LDPEb have the best extrudability, since they have lowest shear viscosities in the region of practical extrusion operations, where the shear rates is somewhere between 10-1000 s^{-1}, as mentioned in section 4.1.2. Conversely, the mPE and LLDPE have the worst processabilities. It is due to their narrow MWD and the absence of long chain branching, LCB.

As far as we aware, all the published papers reported that it was impossible to correlate bubble stabilities with the simple shear rheological data. However, in the region of practical extrusion operations investigated, namely, at high shear rate (10-1000 s^{-1}), our experimental data showed that the order of five resins in shear viscosities, from low to high, coincides with that in bubble stabilities, from stable to unstable. This phenomenon is very interesting. However, we should aware that the viscosity is temperature dependent. After die exit, polymer melt is under elongation with shear free. Also, different types of polymers give different temperature profiles even under the same processing conditions. Moreover, it is well accepted that polymer melt has a fading memory, especially at high temperature. All these facts give rise to the same conclusion that the bubble stabilities can not correlate with simple shear rheological data.

The wider molecular weight distribution (MWD) of LDPE compared with those of mPE and LLDPE is an indication not only of the presence of long macromolecules but also of long chain branched (LCB) macromolecules. The consequence of differences in

the molecular structure between these two polymers is much more prominent shear thinning characteristics of LDPE than those of mPE.

4.8.2. G', G'' and Their Relationship

From Figure 4.2, we may see that in the region of practical extrusion operations (10-1000 s^{-1}), the order of five resins in storage moduli, G', from low to high, coincides with that in bubble stabilities, from stable to unstable. From this point of view, we feel that the more elastic is the polymer, the less susceptible it is to expand uncontrollably in the radical direction and cause process instability. However, the picture is not complete since the loss moduli, G'', is in the same order in the same region examined.

It is well-accepted fact that the first normal stress difference N_1 in steady shear flow and the storage modulus G' in oscillatory shear flow may be considered as the amount of energy stored in a viscoelastic liquid. Also, the shear stress σ_{12} in steady shear flow and the loss modulus G'' in oscillatory shear flow may be considered as the amount of energy dissipated. Therefore, the N_1/σ_{12} ratio and G'/G'' ration may be interpreted as the ratio of the energy stored to the energy dissipated (Han, 1986).

As pointed out by Han and Lem (1983), in steady shear flow, one may consider the shear rate to be an input variable imposed on the fluid, whereas both σ_{12} and N_1 are output variables, i.e., responses of the fluid under test. In other words, the values of $\dot{\gamma}$ chosen during experiment have nothing to do with any molecular deformation that occurs, whereas σ_{12} represents the energy dissipated and N_1 represents the energy stored in the fluid. Similarly, in oscillatory shear flow, one may consider the oscillatory frequency (ω) to be an input variable and, G' and G'' are output variables (i.e., responses) of the fluid under text. With this interpretation of rheological responses, Han

and Lem (1983) have suggested that, in order to compare the elastic behavior of one fluid against others, logarithmic plots of N_1 versus σ_{12}, and of G' and G'', be used.

Following the suggestion of Han and Lem (1983)and using a simple dimentional analysis, the output variables G' and G'' in oscillatory shear flow can be represented in terms of the input variable ω by

$$G'_R = G'/G_0 = f_1(\omega\lambda) \tag{4.3}$$

$$G''_R = G''/G_0 = f_2(\omega\lambda) \tag{4.4}$$

In which λ is a relaxation time of the fluid G_0 is a quantity that has the dimensions of stress.

By eliminating $\omega\lambda$ from above two equations, we obtain

$$G'_R = f_1(\omega\lambda) = f_1\left[f_2^{-1}(G''_R)\right] = f(G''_R) \tag{4.5}$$

The above equation implies that the relationship between G'_R and G''_R is independent of the characteristic time of the fluid. Note, however, that plots of G' vs. G'' will depend on the physical parameters of the fluid via G_0. If G_0 is weakly dependent upon temperature and molecular weight, the relationship between G' and G'' will become virtually independent of temperature and molecular weight (Han, 1986).

Figure 4.20 presents the plot of $\log G'$ versus $\log G''$ for LDPEa at five different temperatures. As we expected, the five curves fall onto a single curve. The other four polymers, HDPE, LLDPE, LDPb, and mPE, also exhibit the same behaviors, as reported by Han and Jhon (1986) and Wong et al. (1998).

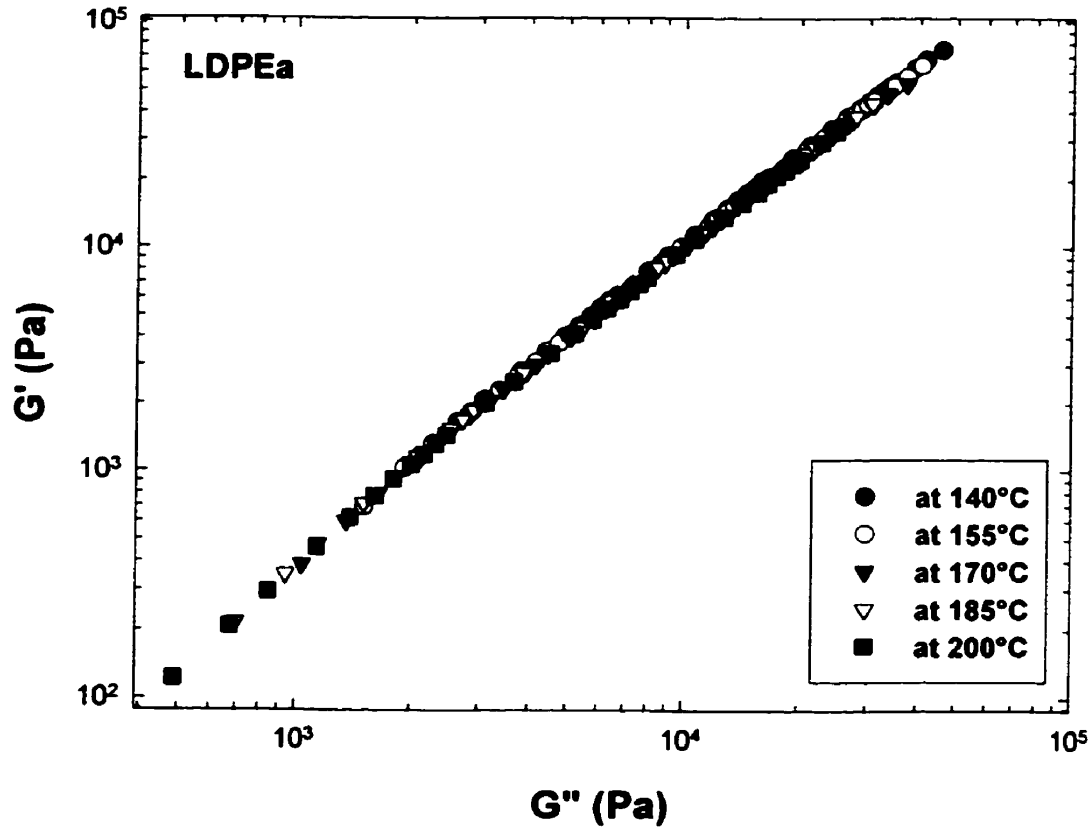

Figure 4.20. $\log G'$ versus $\log G''$ for LDPEa at five different temperatures.

Figure 4.21 shows the comprison of $\log G'$ versus $\log G''$ for five polymers. It can be seen that LDPEa and LDPEb are similar; LLDPE and mPE. At high G'', that is to say, when the values of loss modulus is large, the LDPEa and LDPEb exhibit the largest value of storage modulus (G'), where mPE and LLDPE lowest. Again, our experimental data showed that the order of five resins in G' values, from high to low, coincides with that in bubble stabilities, from stable to unstable. As we mentioned before, $\log G'$ - $\log G''$ plot does not show molecular weight and temperature dependence. However, it is strongly dependent on MWD and molecular structures such as long chain branches (Wong et al, 1998). The higher the MWD, the higher the G'. Han and John (1986) gave an extensive explanation with the aid of molecular theories.

4.8.3. Uniaxial Elongational Viscosity

It is well accepted that the restrictiveness of the type of shear data is their inability to provide direct relations with processing flows because the data only reflect the linear viscoelastic part of the material behavior. For this reason, uniaxial elongational rheology is complementary to the shear data as they capture the non-linear aspects of the melt flow. The observed shear rheology differences becomes even more explicit when examing the elongational viscosity at different constant elongational rates.

The film blowing process is a biaxial non-uniform elongational deformation where the uniaxial component predominates. If one seeks to correlate processing behavior with laboratory data, uniaxial extension experiments are not too far from the actual material deformation. The polymer non-linearity is thought to govern the performance of the bubble in the film blowing process. Therefore, the uniaxial elongational test is considered the most appropriate to show the range of non-linearity observable in a polymer melt.

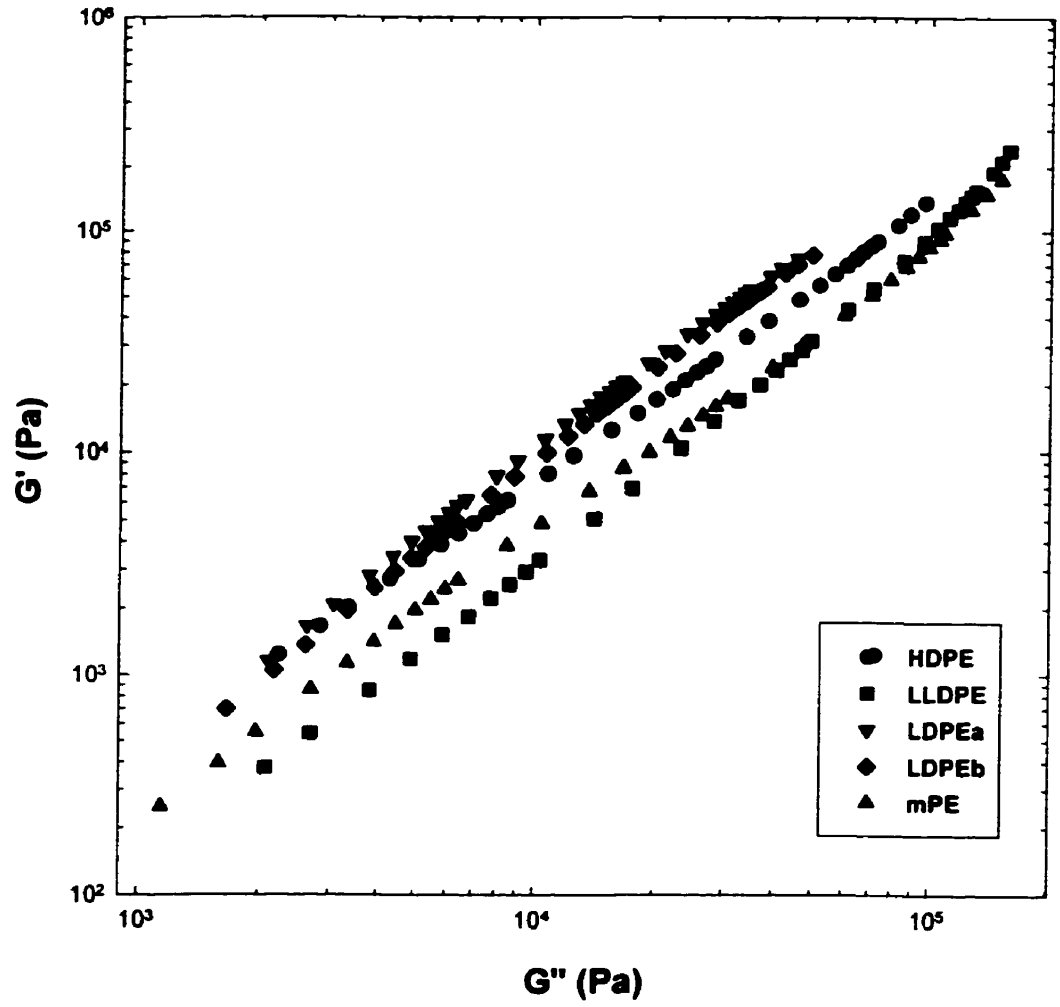

Figure 4.21. The comparison of $\log G'$ versus $\log G''$ for HDPE, LLDPE, LDPEa, LDPEb, and mPE.

It is well recognized that the material with the pronounced strain-hardening behavior always revealed superior stability. The importance of the high molecular weight fraction in the molecular structure on the strain hardening characteristics of linear polymers has been wildly recognized and well documented in the literature (Laun, 1989 and Munstedt, 1980).

Figure 4.22 shows the comparison of uniaxial elongational viscosity for HDPE, LDPEb, and mPE by using Binding analysis. Elongational viscosity curves for all materials investigated show a steady decrease in magnitude with increasing elongational rate. There are no strain-hardening behaviors observed in the region investigated. However, if we examine the Trouton ratio for all the polymers studied (see Figure 4.9), a relative strain-hardening behavior, which is the property that mostly determines the bubble stability and ease of processing, is shown for LDPEb. The mPE shows more strain-thinning than strain-hardening and exhibits the most unstable behavior during film blowing.

The elongational strain rates involved during film extrusion range from 0.01 to 1 s^{-1} depending on the take-up ratio and distance from the die to the freeze line (Ghaneh-Fard, 1997b). However, the lowest strain rates we can measure are beyond this range. Even though Covas and Carneiro (1990) have shown that the convergent flow analysis is able to correctly predict the relative behavior of the different materials but quantitatively shows considerable inaccuracy which may come from the assumptions made in the analysis, our data should be useful for comparing the relative elongational behavior of the polymers.

4.8.4. MD and TD Stresses

In comparison with LDPEb, mPE exhibits lower extensional stresses in the molten blown bubble and this renders the mPE bubble more prone to instabilities. This

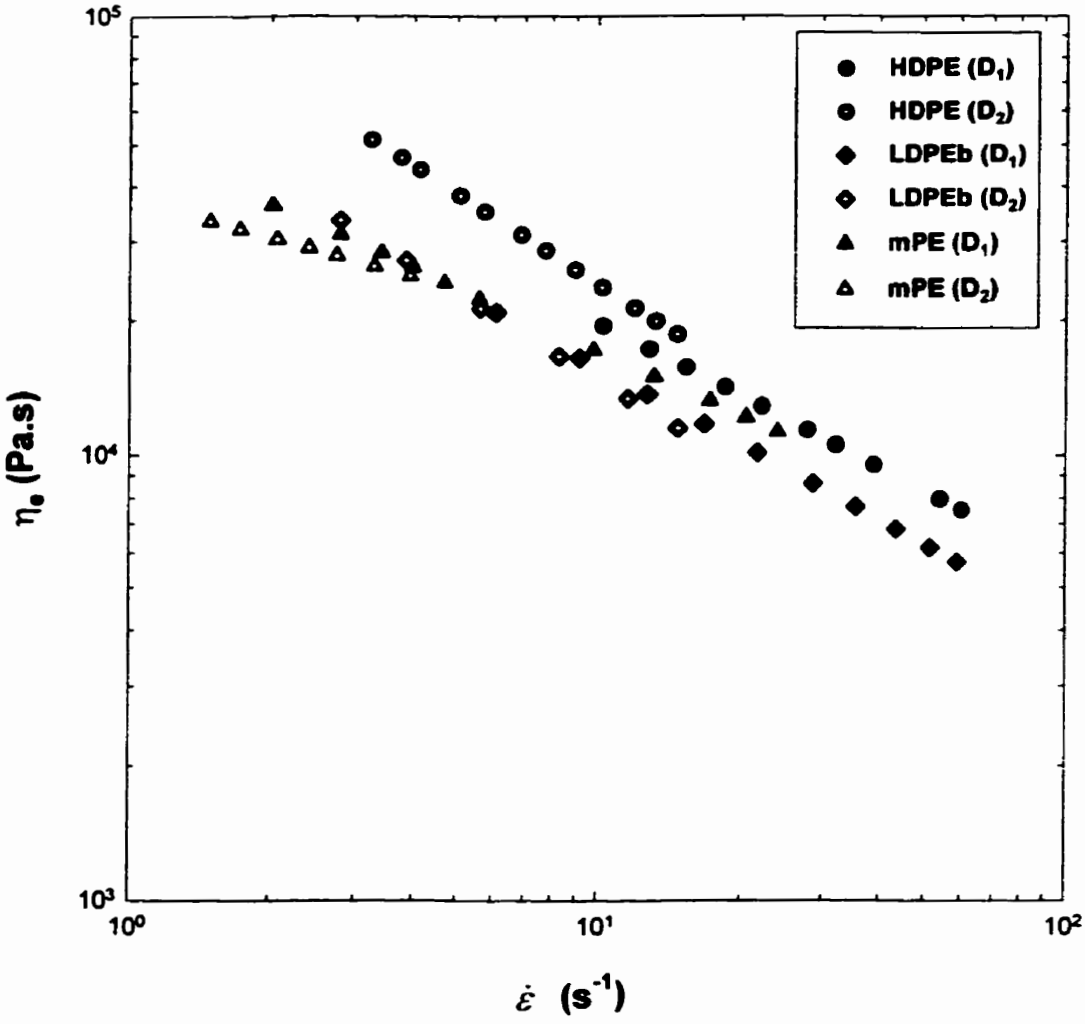

Figure 4.22. Comparison of elongational viscosity of HDPE, LDPEb, and mPE by using Binding analysis at the temperature of 200°C.

phenomenon, which was also observed by Dealy and Wissbrun (1990) for LLDPE, is due to the strain softening behavior.

4.8.5. Biaxial Elongational Viscosity

In tubular film blowing the melt emerging from an annular die is stretched both in axial and tangential directions. This is a non-isothermal, non-homogeneous, biaxial deformation. Biaxial and uniaxial material responses are very similar but not equal. In film blowing uniaxial elongation dominates, especially in the bubble neck where the pulsations are initiated. The same low elongation rates as in uniaxial elongational flow can not be reached temporarily with our laboratory instrument. Comparing basic material properties in elongation with processing behavior may perhaps enlighten the observed variations in stability.

Note that we are dealing with a non-isothermal process. Therefore, it is necessary to compare the rheological parameters under the same processing conditions, temperature, i.e.. We randomly choose a temperature of 170°C as our reference temperature. The plot of biaxial elongational viscosity versus deformation rate for mPE and LDPEb was created by using shift factors at the reference temperature and is shown in Figure 4.23. LDPEb exhibits strain hardening at low deformation rate. It is well accepted that the strain-hardening behavior makes LDPE more stable than other polyethylenes in uniaxial extensional flow.

Figure 4.24 shows the biaxial elongational viscosity versus deformation rate for HDPE, LLDPE and LDPEb, based on the data of the previous study in our laboratory (Ghaneh-Fard, 1997). Compared with LLDPE, LDPEa exhibits a lower elongational viscosity.

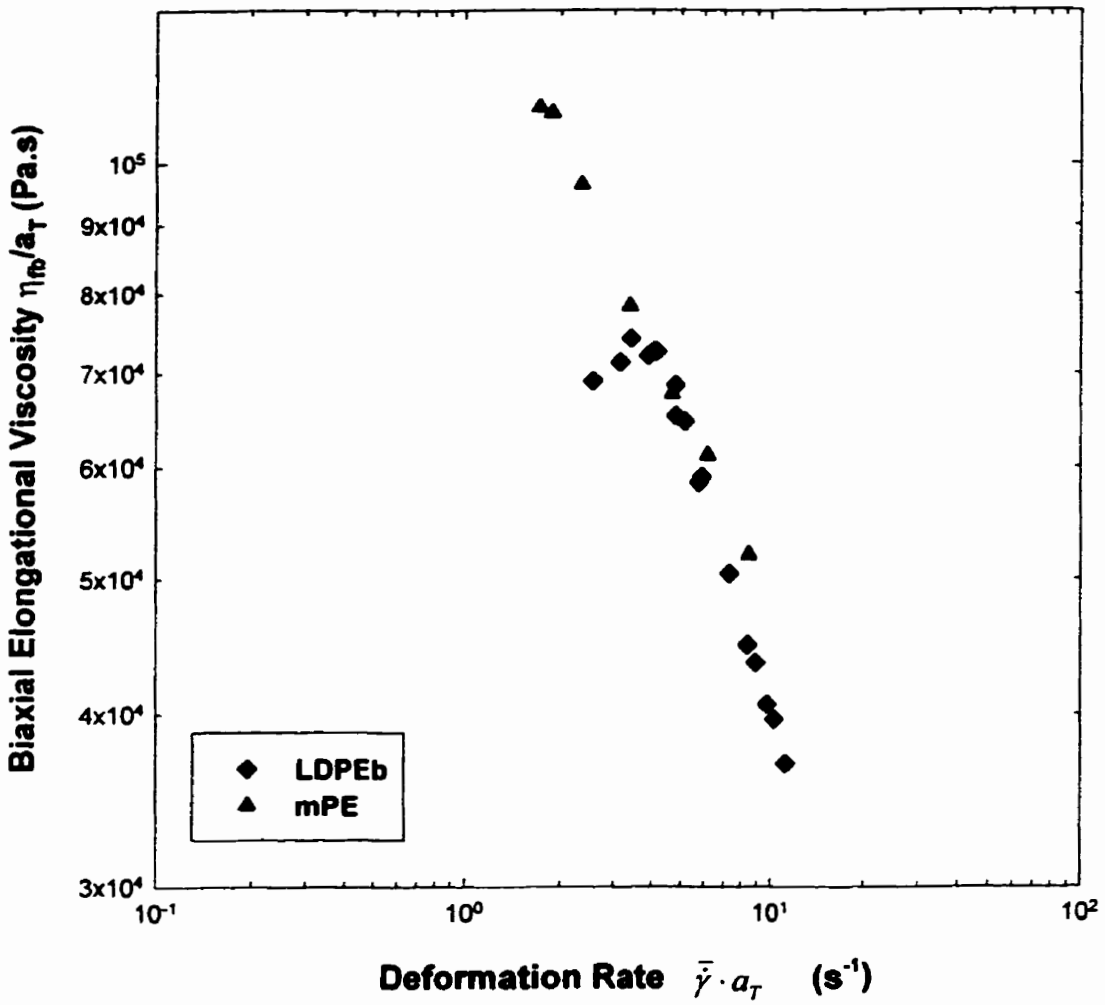

Figure 4.23. Biaxial elongational viscosity versus deformation rate at the reference temperature of 170°C for LDPEb and mPE during film blowing. The film blowing conditions are the same as in Figure 4.10.

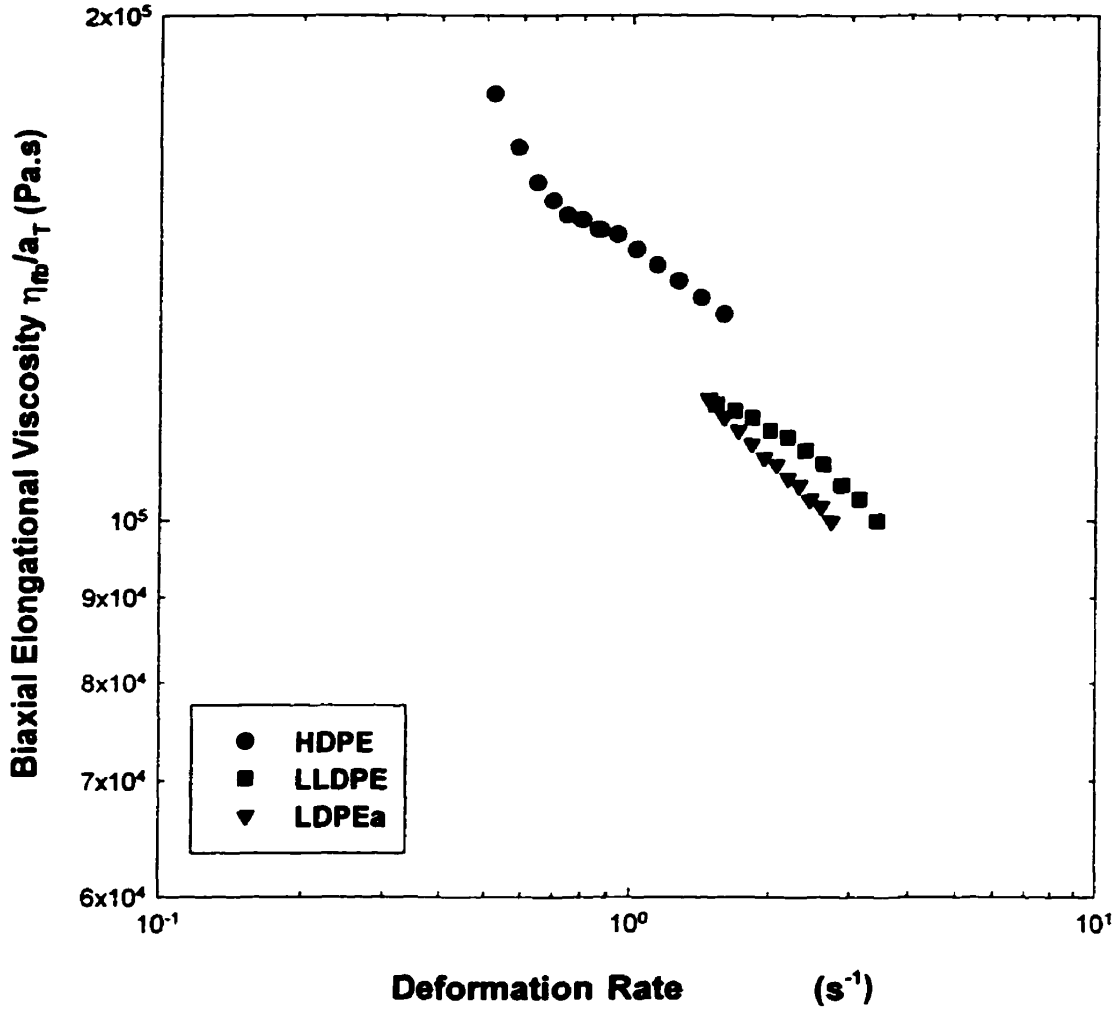

Figure 4.24. Biaxial elongational viscosity versus deformation rate at the reference temperature of 170°C for HDPE, LLDPE and LDPEa during film blowing. The flow rate = 4.05 kg/h, extrusion temperature = 220°C, TUR = 9.5. BUR = 2.0, FLH ≈ 250 mm (Calculated from experimental data of Ghaneh-Fard et al. 1997b)

Considering the polymer melts as Newtonian fluids and the bubble as uniform biaxial stretching, then one may get the following relationship:

$$\eta_{fb} = 2\eta_e = 6\eta \tag{4.6}$$

We name η_{fb}/η as biaxial Trouton ratio (BTR). Figure 4.25 (a, b) shows TRB versus $\bar{\dot{\gamma}}$, the effective rate of deformation defined in equation (3.74). For all the polymers investigated, the values of BTR are always in excess of the value of 6. Figure 4.25a presents the data calculated from the experimental data of the previous authors (Ghaneh-Fard et al. 1997b) in our laboratory. The LDPEa far exceeds 6 in the BTR and shows relative strain-hardening behavior. The HDPE shows relative strain-thinning behavior at first then relative a strain-hardening behavior. The LLDPE is near to 6 in BTR and shows slightly relative strain-hardening behavior. Figure 25b presents the data based on our experimental data. Also, the BTR of the LDPEb far exceeds the value of 6. However, similar to the HDPE, LDPEb shows relative strain-hardening at first then strain-hardening behavior. mPE shows relative strain-thinning behavior and has a lower BTR than LDPEb.

In order to summarize, we present the Trouton ratio and BTR ratio versus $a_T\bar{\dot{\gamma}}$, for the resins investigated, at the same reference temperature of 170°C. The LDPEa and LDPEb far exceed 6 in BTR and show a very pronounced relative strain-hardening behavior. HDPE and mPE have the lower values of BTR than those of LDPEa and LDPEb. HDPE shows both relative strain-thinning and hardening behavior while mPE shows only strain-thinning behavior. LLDPE is near to the value of 6 in BTR and shows slightly strain-hardening behavior. The LDPEb has a very high Trouton ratio and shows relative strain-hardening behavior at high deformation rate while HDPE and mPE have the lower value in Trouton ratio. HDPE shows slightly relative strain-hardening behavior

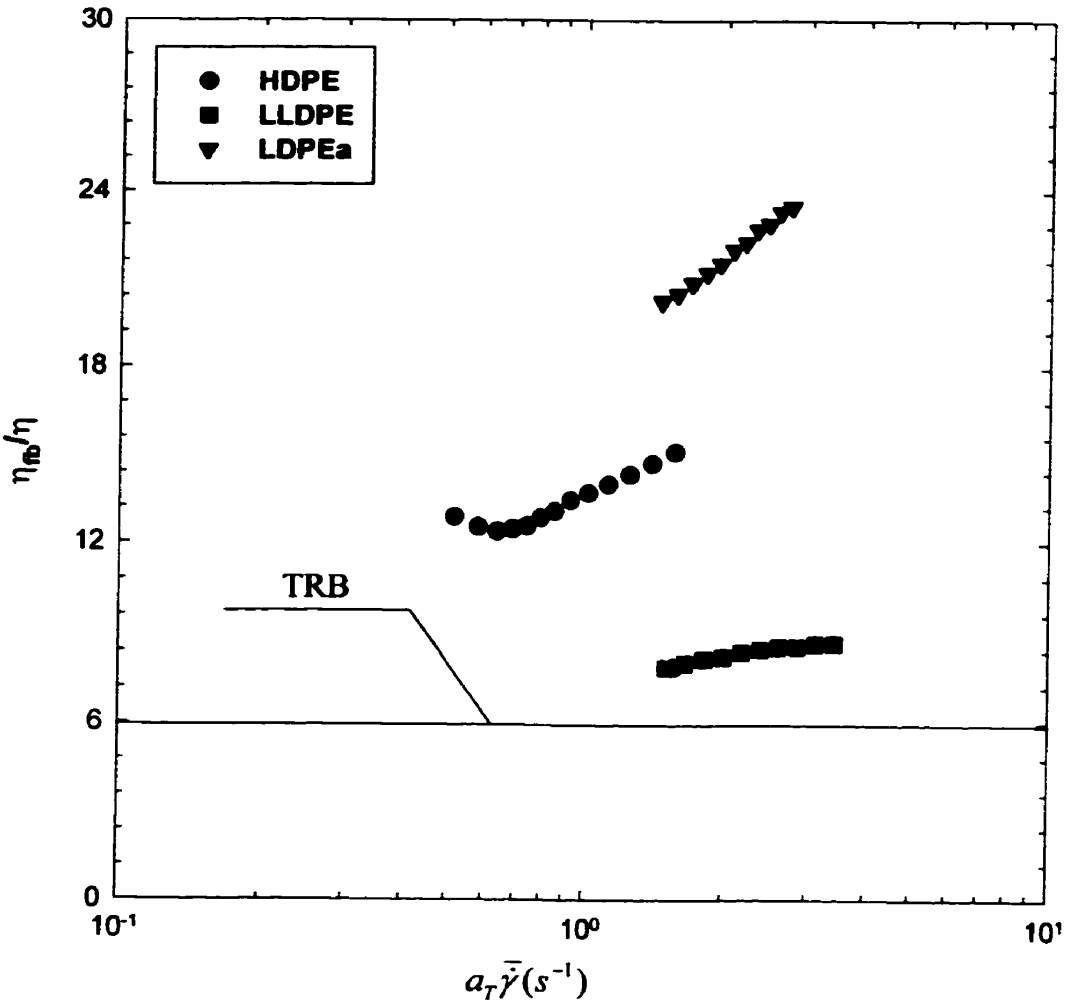

Figure 4.25a. η_{fb}/η versus $a_T\bar{\dot{\gamma}}$ at the reference temperature of 170°C for HDPE, LLDPE and LDPEa during the film blowing. The film blowing conditions are the same as in Figure 4.24.

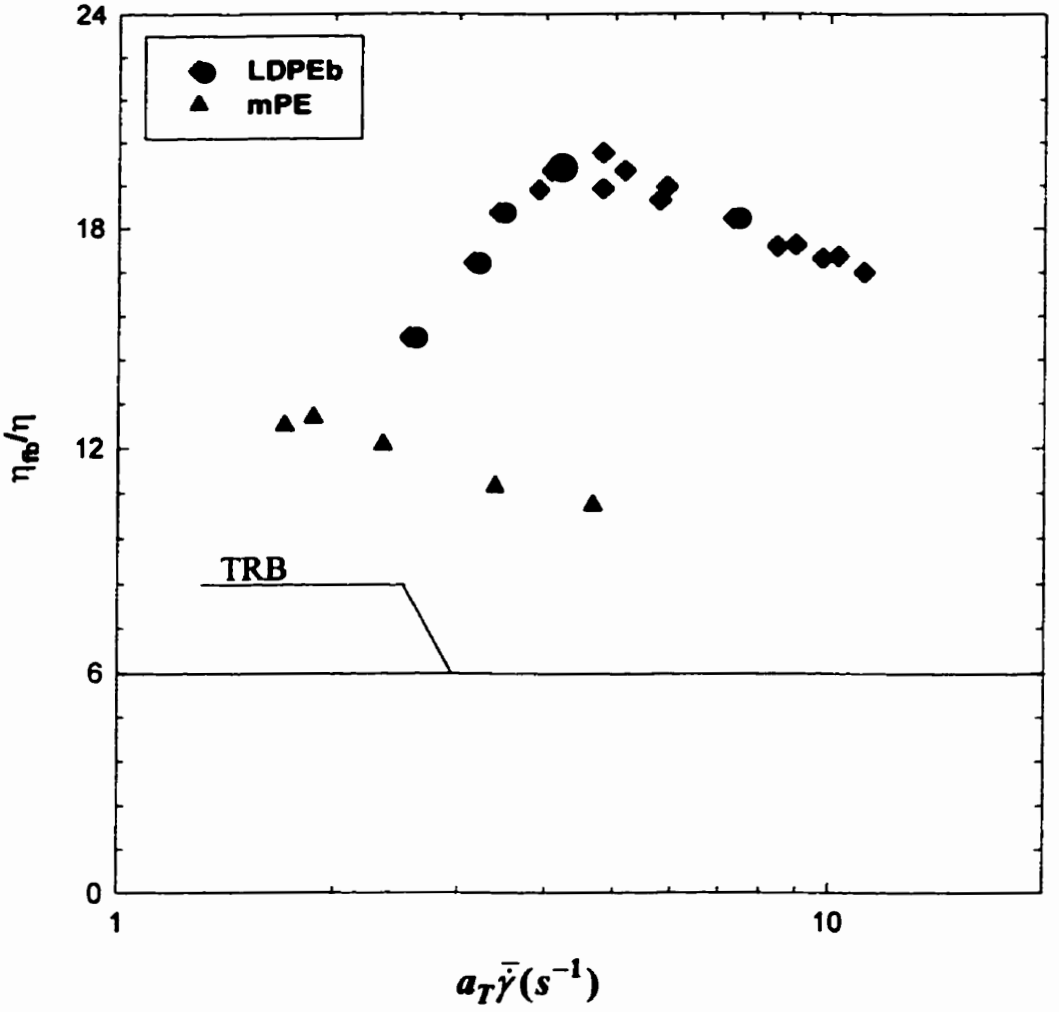

Figure 4.25b. η_{be}/η versus $a_T\bar{\dot{\gamma}}$ at the reference temperature of 170°C for LDPEa and mPE during the film blowing. The film blowing conditions are the same as in Figure 4.10.

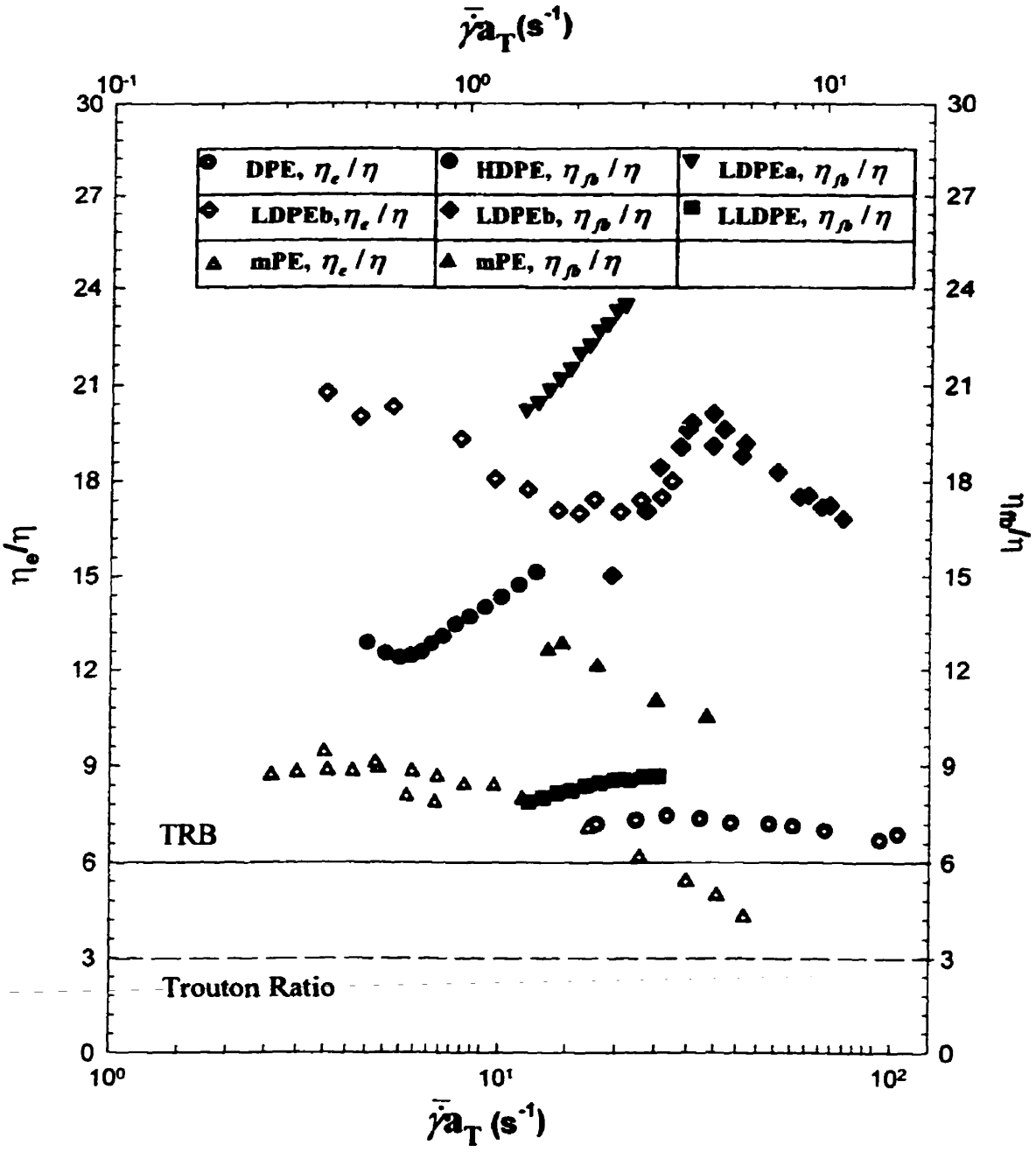

Figure 4.26. Comparison of Trouton ratio and TRB for five polyethylenes at a reference temperature 170°C.

while mPE shows more strain- thinning. The Trouton ratio and BTR for all the resins investigated are summarized in Table 4.5.

Table 4. 5. Summary Trouton ratio and BTR for five polyethylenes.

Biaxial Trouton Ratio	Relative strain-hardening → Relative strain-thinning				
	LDPEa	LDPEb	HDPE	LLDPE	mPE
	Magnitude: large → Small				
	LDPEa	LDPEb	HDPE	mPE	LLDPE
Trouton Ratio	Relative strain-hardening → Relative strain-thinning				
	LDPEb		HDPE		mPE
	Magnitude: large → Small				
	LDPEb			HDPE/mPE	

Experimental trials showed that the materials with the pronounced strain-hardening behavior always revealed superior stability. The more relative strain-hardening the polymer melt, the more stable bubble during the film blowing process. An often still more pronounced strain-hardening behavior can be found for LDPE, which is well known for its high bubble stability.

The poor performances of LLDPE and mPE in processes where the elongational deformation prevails over shear is thought to be related to their low elongational viscosities of LLDPE and mPE mostly because of the linear structure of their macromolecules. On the other hand, LDPE performs well in such processes due to its high elongational viscosity related to the presence of long chain branched macromolecules in its structure (Micic et al., 1998).

Finally, we re-plot all four kinds of viscosities – complex viscosity, shear viscosity, uniaxial elongational viscosity, and biaxial elongational viscosity versus

frequency, shear rate, elongational rate, and deformation effective rate respectively at the reference temperature 170°C with the aid of shift factors for all the polymers investigated and present the plots in Figure 4.27. The apparent non-uniform effective biaxial viscosity was compared to simple shear and uniaxial elongational viscosities but also can not be correlated through any simple constitutive equation.

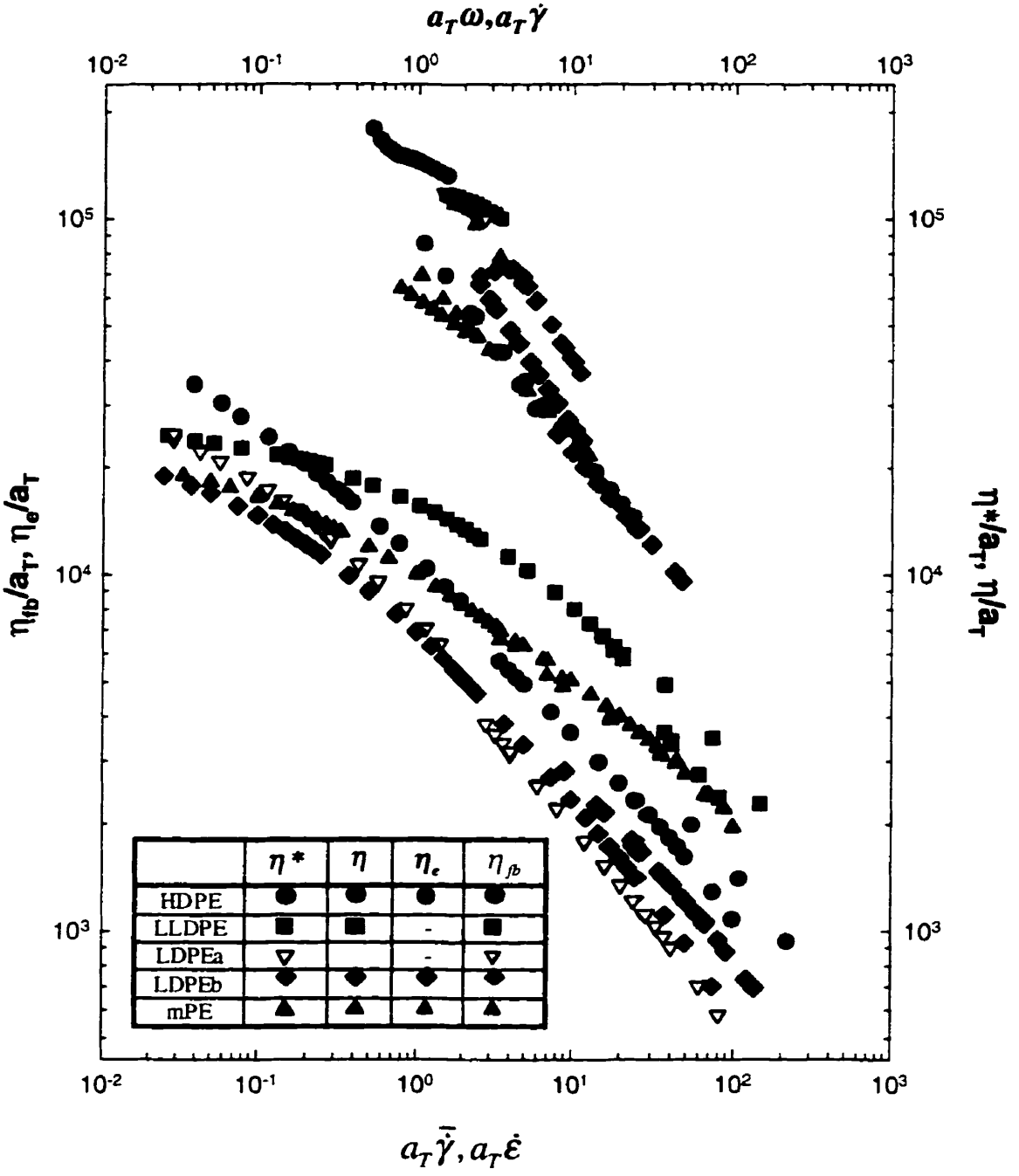

Figure 4.27. Complex, shear, uniaxial elongational, biaxial elongational viscosities versus frequency, shear rate, elongational rate, deformation rate respectively under the same reference temperature of 170°C for five resins.

CHAPTER V CONCLUDING REMARKS

5.1. Conclusions

In order to get a better understanding of the effects of rheoligical properties on the pprocessing performance in film blowing, different techniques were used to measure the rheoligical properties of five polyethylenes: HDPE, LLDPE, LDPEa, LDPEb, mPE.

The Cox-Merz rule works fairly well for mPE and LLDPE, but still shows some deviations for the other three resins over the range studied.

In comparison with the experimental data of previous author in our laboratory, mPE, a new member of polyethylene families, exhibits similar bubble stability behavior as LLDPE, who has smaller operating space and has bubble instability at low BUR. The relative order of stability for polymers studied is as follows:

LDPEa > HDPE > LLDPE > mPE

In the region of practical extrusion operations (10-1000 s^{-1}) for all the polymers investigated, the order of bubble stabilities for coincides with the orders of simple shear viscosity, complex viscosity at the same reference temperature, namely, the higher complex viscosities, shear viscosities and storage moduli the resins have, the less bubble stabilities during film blowing.

$\log G'$ versus G'' plot is virtually independent of temperature for all the polymers investigated. The higher the MWD, the higher the G', the more stable the bubble during film blowing. It is shown that the order of five resins in G' values, from high to low, coincides with that in bubble stabilities, from stable to unstable.

The apparent unaxial extensional flow properties for three polymers, HDPE, LDPEb and mPE, have been studied using convergent dies of two different geometries, where the flow is mostly extensional, in constant elongational rate. The uniaxial elongational viscosities have been calculated from the mass flow rate and entrance drop via two techniques, Cogswell and Binding analyses. The two methods lead to the elongational viscosity in the same order of magnitude. The elongational viscosity calculated by the Cogswell analysis is slightly lower than that calculated by Binding analysis. The viscosity data obtained from die D_1 are not in perfect agreement with those from die D_2, but the differences are acceptable. In the range of experiments investigated, the elongational viscosities of all three polymers showing strain-thinning behavior and no strain-hardening behavior was observed. The strain rate dependency of elongational viscosity can not be correlated to the bubble stability of resins during film blowing.

The master curves were obtained using time-temperature superposition principle. At five different temperatures, all the five polymers show "thermo-rheologically simple" behavior with the aid of a shift factor, unique feature of the temperature.

The mPE and LDPEb display different bubble diameter and axial film velocity profiles which lead to quite different strain rate profiles. The strain rate of mPE in MD is always higher than that in TD in the region from die exit to the FLH while strain rate of LDPEb TD was not consistently lower than that in MD except in the vicinity of FLH. In contrast to the experimental data obtained by Ghaheh-Fard et al (1997b), our data show pronounced difference.

The birefringence values of both mPE and LDPEb are shown to be almost the same and to be very small in the molten zone. For mPE, the birefringence value increases rapidly in the crystallization zone indicating the oriented nucleation and groowth process. By using stress-optical law, both MD and TD normal stresses can be calculated via birefringence, bubble diameter and velocity, and the pressure inside the bubble. For both

mPE and LDPEb, the stresses in MD are always higher than those in TD. There is no obvious relation between strain rates and stresses.

The apparent non-uniform biaxial elongational viscosity of both mPE and LDPEb was calculated along the length of the bubble by using the stress and strain data. The mPE shows a higher biaxial elongational viscosity and a lower deformation rate than those of LDPEb at the die exit while LDPEb exhibits a higher viscosity and lower deformation rate than those of mPE in the vicinity of FLH.

The apparent biaxial elongational viscosity versus deformation rate for five polymers investigated at a reference temperature as 170°C were also calculated using the shift factor. All the polymers except LDPEb exhibit strain-thinning behaviors, whereas LDPEb exhibited strain-hardening behavior at low deformation rate. The LDPEa shows a lower elongational viscosity than HDPE and LLDPE. It is wildly recognized that elongational viscosity of a polymer plays an important role in controlling the bubble stability during the film blowing process. We feel that the bubble stability is a function of both the magnitude of the elongational viscosity and the strain hardening characteristics of polymer.

The Trouton ratio, for HDPE, LDPEb and mPE, versus deformation rate have been studied. In all cases, the ratio exceed the limiting case of Newtonian fluids for which the ratio equal to 3. The Trouton ratio of the LDPEb is much larger than those of HDPE and mPE, and increase with elongational rate (relative strain-hardening behavior). This is the property that mostly determines the bubble stability (and ease of processing).

The biaxia Trouton ratio (BTR), η_{fb}/η, for five polymers, versus deformational rate have also been studied. Similar to the Trouton ratio, BTRs of five polymers exceed the 6, which is the case for Newtonian fluids. The BTRs of LDPEa and LDPEb far exceed those of LLDPE and HDPE and show very pronounced realtive strain-hardening

behavior. We feel that the more relative strain-hardening the polymer melt, the higher the BTR of the polymer melt, the more stable bubble during the film blowing process.

It appears that, in the molecular process involved with stretching, information on elongational viscosity is at least as important as information on shear flow properties, in understanding the bubble stabilities of polymeric materials.

5.2. Future Work

The results of the present study are very encouraging, but a broad spectrum of questions have to be examined in the future. We recommend the following objects for future work:

- Complement uniaxial elongational viscosity data by improving the equipment, in order to get the lower elongational rates, and by improving the technique, in order to get more reliable data.
- The technique of birefringence measurement used in our study is monochromatic polarized light retardation. This technique is suitable for biaxial orientation measurements in polymers with low degrees of orientation (Takahashi and Fuller, 1996). In film blowing process, it is recommeded to develop an improved apparatus which is suitable for highly oriented film.
- In order to improve the performance of mPE, it is desirable to blend it with LDPE. Then examine bubble dynamics in relation to rheological data of various blends.
- The rheological properties of the polymer melt should be correlated to the mechanical and optical properties of the final product film.

REFERENCES

Agassant, J.-F., Avenas, P., Sergent, J.-Ph. and Carreau, P. J. Polymer Processing: Principles and Modeling New York, Hanser Publishers, (1991)

Ajji, A. Guèvremont, J. Mattews, R. G. and Dumoulin, M. M. "Orientation Determination Using Birefringence and Spectroscopic Techniques" SPE ANTEC'99 2361 (1999)

Ajji, A. Cole. K. C. and Ben Dali, H. "Measurements of Absolute Birefringence of Biaxially Orientation Films and Sheets On-line or Off-line" SPE ANTEC'98 1534 (1998)

Alaie, S. M. and Papanastasiou "Modeling of Non-isothermal Film Blowing with Integral Constitutive Equations" Int. Polym. Process. **8,** 51 (1993)

Alfrey, T. "Plastics Processing and Fabrication Problems Involving Membranes and Ratational Symmetry" SPW Transactions **5**, 68 (1965)

Ashok, B. K. and Campbell, G. A. "Two-phase Simulation of Tubular Film Blwoing of Crystalline Polymers" Int. Polym. Process. **7**, 240 (1992)

Ast, W. "Air Cooling on Blown Film Lines" Kunstoffe **64**, 146 (1974)

Babel, A. K. and Campbell, G. A. "Correlating the Plastic Strain with the Properties of the Low Density Polyethylene Blown Film" J. Plastic Film & Sheeting **9**, 246 (1993a)

Babel, A. K. and Campbell, G. A. "Metallocene Catalysed Polyethylene in Blown Film Applications – A Comparision Between Monoextruded Blended Films and Coextruded Films" SPE ANTEC'93 444 (1993b)

Babel, A. K. and Campbell, G. A. "A Model Linking Process Variables to the Strength of Blown Films Produced from LDPE and LLDPE" Tappi J. **78**, 199 (1995)

Beagan, C. M., Mc Nallyy G. M. and Murphy, W. R. "Metallocene Catalysed Polyethylene in Blown Film Application Between Monoextruded Blended Films and Coextruded Films" SPE ANTEC'98 511, (1998)

Bernabeu, E. and Boix J. M. "Optical Properties of Extruded Polyethylene Thin Films Related to Anisotropy and Inhomogeneous Microstructure" Polym. Eng. Sci. **26**, 1203 (1996)

Binding, D. M. "An Approximate Analysis for Contraction and Converging Flows" J. of Non-Newt. Fluid Mech. **27**, 173 (1988)

Bin Wadud, S. E. and Baird, D. G. "Rheology of Metallocene-catalyzed Polyethylenes – The effect of Branching" SPE ANTEC'99 1200 (1999)

Cain, J. J. and Denn, M. M. "Multiplicities and Instabilities in Film Blowing" Polym. Eng. Sci. **28**, 1527 (1988)

Campbell, G. A. and Cao, B. J. Plastic Film and Sheeting **3**, 158 (1987)

Cambell, G. A. and Huang, T. A. "Deformational History of LLDPE/LDPE blends on Blown Film Equipment" Advances in Polymer Technology **5(3)**, 181 (1985)

Cao, B., Sweeney, P., Campbell, G. A. "Viscoplastic-Elastic Modeling of Tubular Blown Film Processing" AICHE J. **36**, 420 (1990)

Cao, B., Sweeney, P., Campbell, G. A. "Simultaneous Surface and Bulk Temperature Measurement of Polyethylene During Film Blowing" J. Plastic Film and Sheeting **6**, 117 (1990)

Carreau, P. J., De Kee, D. and Chhabra, R. P. Rheology of Polymeric Systems: Principle and Application New York, Hanser (1997)

Chai, C. K. "Melt Rheology and Processability of Conventional and Metallocene Polyethylenes" SPE ANTEC'99 1210 (1999)

Choi, K., Spruiell, J. E. and White, J. L. "Orientation and Morphology of High Density Polyethylene Film Produced by the Tubular Blowing Method and Its Relationship to Process Conditions" J. Polym. Sci.: Polymer Physics Edition **20**, 27 (1982)

Cogswell, F. N. "Converging Flow of Polymer Melts in Extrusion Dies" Polym. Eng. Sci. **12**, 64 (1972)

Cogswell, F. N. Polymer Melt Rheology George Dodwin Limited, Abington, Cambridge (1994)

Collyer, A. A. and Utracki, L. A. Polymer Rheology and Processing England, Elsevier Science Publishers (1990)

Covas, J. A. and Carneiro, O. S. "Assessing the Convergent Flow Analysis as a Technique for Characterizing the Extensional Flow of Polymer Melts" Polymer Testing 9, 181 (1990)

Dealy, J. M. and Wissbrun, K. F. Melt Rheology and Its Role in Plastics Processing: Theory and Applications New York, Van Nostrand Reinhold (1990)

Debbaut, B., Goublomme, A., Homerin, O., Koopmans, R., Lieman, D., Meissner, J., Schroeter, B., Reckmann, B., Daponte. T., Verschaeren, P., Agassant, J.-F., Vergnes, B. and Venet, C. "Development of High Quality LLDPE and Optimised Processing for Film Blowing" Int. Polym. Process. **13(3)**, 262 (1998)

Dowd, L. E. "What Happens When You Cool and Draw Blown Films" SPE J. **28**, 22 (1972)

Farber, R. and Dealy, J. "Strain History of Melt in Film Blowing" Polym. Eng. Sci. **14**, 435 (1974)

Fleissner, M. "Elongational Flow of HDPE Samples and Bubble Instability in Film Blowing" Int. Polym. Process. **2**, 229 (1988)

Flory, P. J. "Statistical Mechanics of Chain Molecules" Interscience New York (1969)

Furumiya, A., Akana, Y., Ushida, Y., Masuda, T. and Nakajima, A. "Relationship between Molecular Characteristics and Physical Properties of Linear Low Density Polyethylenes" Pure & Appl. Chem **57(6)**, 823 (1985)

Fuller, G. G. "Optical Theometry" J. Rheol. **23**, 457 (1990)

Ghijsels, A., Ente, J.J.S.M. and Raadsen, J. "Melt Strength Behavior of PE and its Relation to Bubble Stability in Film Blowing" Int. Polym. Process. **4**, 284 (1990)

Ghaneh-Fard, A., Carreau, P. J. and Lafleur, P. G. "Application of Birefringence to Film Blowing" J. Plastic Film and Sheeting **12**, 68 (1996a)

Ghaneh-Fard, A., Carreau, P. J. and Lafleur, P. G. "Study of Instabilities in Film Blowing" AICHE J. **42**, 1388 (1996b)

Ghaneh-Fard, A., Carreau, P. J. and Lafleur, P. G. "On-Line Birefringence Measurement in Film Blowing of a Linear Low Density Polyethylene" Int. Polym. Process. **2**, 136 (1997a)

Ghaneh-Fard, A., Carreau, P. J. and Lafleur, P. G. "Study of Kinematics and Dynamics of Film Blowing of Different Polyethylenes" Polym. Eng. Sci. **37**, 1856 (1997b)

Ghaneh-Fard, A. "Study of the Film Blowing Process and On-line Measurements of Birefringence" Ph.D Dissertation Dept. Chem, Eng., École Polytechnique de Montréal (1997c)

Gibert, M. Liu, Z. and Hitt, D. J. "Biaxial Orientation of Poly(Vinyl Chloride) Compounds: Interaction Between Drawing, Structure, and Properties" Polym. Eng. Sci. 37, 1858 (1997)

Graessley, W. W. "Viscoelasticity and Flow of Polymer Melts and Concentrated Solutions" in Physical Principles of Polymers Edited by Mark, J. E., Amerr. Chem. Soc., Wash. D. C., (1984)

Greener, J. and Evans, J. R. G. "Uniaxial Elongational Flow of Particle-Filled Polymer Melts" J. Rheol. **42**, 697 (1998)

Gupta, R. K., Metzner, A. B. and Wissbrun, K. F. "Modeling of Polymeric Film-Blowing Processes" Polym. Eng. Sci. **22**, 172 (1982)

Han, C.D. and John, M. S. "Correlations of the First Normal Stress Difference with Shear Stress and of the Storage Modulus with Loss Modulus for Homopolymers" J. Appl. Polym. Sci. **32**, 3809 (1986)

Han, C.D., Kim, Y. J., Chuang, H.-K. and Kwack, H. "Rheological Properties of Branched Low-Density Polyethylene" J. Appl. Polym. Sci. **28**, 3435 (1983)

Han, C.D. and Kim, Y. W. "Studies on Melt Spinning. V. Elongational Viscosity and Spinnability of Two-Phase System" J. Appl. Polym. Sci. **18**, 2589 (1974)

Han, C.D. and Kwack, H. "Rheology-Processing-Property Relationships in Tubular Blown Film Extrusion. I. High-Pressure Low-Density Polyethylene" J. Appl. Polym. Sci. **28**, 3399 (1983)

Han, C.D. and Lem. K. W. Polym. Eng. Rev. **2**, 135 (1983)

Han, C.D. and Park, J.Y. "Studies on Blown Film Extrusion. I Experimental Determination of Elongational Viscosity" J. Appl. Polym. Sci. **19**, 3257 (1975a)

Han, C.D. and Park, J.Y. "Studies on Blown Film Extrusion. II. Analysis of the Deformation and Heat Transfer Process" J. Appl. Polym. Sci. **19**, 3277, (1975b)

Han, C.D. and Park, J.Y "Studies on Blown Film Extrusion. III. Bubble Instability" J. Appl. Polym. Sci. **19**, 3291 (1975c)

Han, C.D and Shetty, R. "Flow Instability in Tubular Film Blowing. I. Experimental Study" IEC Fundam. **16**, 49 (1977)

Hoppler, H. U., Dinkel, A. and Tomka, I. Pilymer **36**, 3809 (1995)

Huang, T. A. and Campbell, G. A. "Deformational History of LLDPE/LDPE blends on Blown Film Equipment" Advances in Polymer Technology **5**, 181 (1985)

Huang, T. A. and Campbell, G. A. "Deformational and Temperature History Comparison for LLDPE and LDPE Elements in the bubble Expansion Region of Blown Films" J. Plastic Film and Sheeting **2**, 30 (1986)

Ide, Y. and White, J. L. "Experimental Study of Elongational Flow and Failure of Polymer Melts" J. Appl. Polym. Sci. 1978, **22**, 1061

Janeschitz-Kriegl, K. "Polymer Melt Rheology and Flow Birefringence" Berlin, Springer-Verlag (1983)

Kang, H.J., White, J. L. and Cakmak, M. "Single and Double Bubble Tubular Film Extrusion of Polyethylene Terephthalate" Int. Polym. Process. **5**, 62 (1990)

Kanai, T., Kimura, M., and Asano, Y. "Studies on Scale-Up of Tubular Film Extrusion" SPE ANTEC'86 912, (1986)

Kanai, T., White, J. L. "Kinematics, Dynamics and Stability of Tubular Film Extrusion of Various Polyethylenes" Polym. Eng. Sci. **24**, 1185 (1984)

Kanai, T. and White, J. L. "Dynamics, Heat Transfer and Structure Development in Tubular Film Extrusion of Polymer Melts" J. Polym. Eng. **5**, 135 (1985)

Kim, H. C., Pendse, A. and Collier, J. R. "Polymer melt Lubricated Elongational Flow" J. Rheol. **38(4)**, 831 (1994)

Kimura, S. Osaki, K. and Kurata, M. "Stress Relaxation of Polybutadiene at Large Deformation. Measurement of Stress and Birefringence in Shear and Elongation" J. Polym. Sci. **19**, 151 (1981)

Kitano, T., Kataoka, T. "The Effect of the Mixing Methods on Viscous Properties of Polyethylene Melts with Fiber" Rheol. Acta **19(6)**, 753 (1980)

Koyama, K. and Ishizuka, O. "Birefringence of Polyethylene Melt in Transient Elongational Flow at Constant Strain Rate" J. Polym. Sci. **27**, 297 (1989)

Kuijk, E. W. Tas, P. P., and Neuteboom, P. "A Rheological Model for the Prediction of Polyethylene Blown Film Properties" SPE ANTEC'98 3001, (1998)

Kurtz, S. J. "Relationship of Stress in Blown-film Process" Int. Polym. Process. **10,** 148 (1995)

Kwack, T. H. and Han, C. D. "Rheology-Processing-Property Relationships in Tubular Blown Film Extrusion. II. Low-Pressure Low-Density Polyethylene" J. Appl. Polym. Sci. **28**, 3419 (1983)

Kwack, T. H. and Han, C. D. "Development of Crystalline Structure during Tubular Film Blowing of Low-Density Polyethylene" J. Appl. Polym. Sci. **35**, 363 (1988)

Lacroix. C., Grmela, M. and Careau, P. J. "Morphological Evolution of Immiscible Polymer Blends in Simple Shear and Elongational Flows" J. of Non-Newt. Fluid Mech. **80**, 183 (1999)

La Mantia, F. P. and Acierno, D. "Influence of the Molecular Structure on the Melt Strength and Extensibility of Polyethylenes" Polym. Eng. Sci. **25**, 279 (1985)

Laun H. M. and Schuch, H. "Transient Elongational Viscosity and Drawability of Polymer Melts" J. Rheol. **33**, 119 (1989)

Lawler, J. V., Muller, S. J., Brown, R. A. and Armstrong, R. C "LaserDoppler Velocimetry of Velocity Fields and Transitions in Viscoelastic Fluids" J. Non-Newt Fl, Mech. **20**, 51 (1986)

Lee, K. Y. and Han, C. D Polym. Eng. Sci. **30**, 665 (1990)

Legros, N., Ghaneh-Fard, A., Cole, K. C., Ajji, A., and Dumoulin, M.M "Tensile Properties and Orientation Evolution with Processing Conditions in Polyethylene Blown Films" SPE ANTEC'98 729 (1998)

Liu, C.-C., Bogue, D. C. and Spruiell, J. E. "Tubular Film Blowing: Part 1, On-line Experimental Studies" Int. Polym. Process. **10**, 226 (1995a)

Liu, C.-C., Bogue, D. C. and Spruiell, J. E. "Tubular Film Blowing: Part 2, Theoretical Modeling" Int. Polym. Process. **10**, 230 (1995b)

Luo, X-L. and Tanner, R. I. "A Computer Study of Film Blowing" J. Polym. Sci. **25**, 621 (1985)

Mackay, M. E. and Astarita, G. "Analysis of Entry Flow to Determine Elongational Properties Revisited" J. of Non-Newt. Fluid Mech. **70**, 219 (1997)

Maddams, W. F. and Preddy, J. E. "X-Ray Diffraction Orientation Studies on Blown Polyethylene Films. II. Measurements on Films from a Commercial Blowing Unit" J. Appl. Polym. Sci. **22**, 2739, (1978)

Marsh, R. D. L., Duncan, J. C. and Brister, S. J. Thermal Analysis **45**, 891 (1995)

Mavridis, H. "A New High-Performance LLDPE for Blown Film Applications" SPE ANTEC'98 1006 (1998)

Meissner J. "Basic Parameters, Melt Rheology, Processing and End-use Properties of Three Similar Low Density Polyethylene Samples" Pure Appl. Chem **42**, 553 (1975)

Michaeli, W and Schmitz, G. "Investigation of Blown Film Extrusion Using the Laser Doppler Velocimetry" SPE ANTEC'95 181 (1995)

Micic, P., Bhattacharya, S.N. and Field, G. "Transient Elongational Viscosity of LLDPE/LDPE Blends and Its Relevance to Bubble Stability in the Film Blowing Process" Polym. Eng. Sci. **38**, 1685 (1998)

Minoshima, W. and White, J. L. "Instability Phenomena in Tubular Film, and Melt Spinning of Rheological Characterized High Density, Low Density and Linear Low Density Polyethylenes" J. of Non-Newt. Fluid Mech. **19**, 275 (1986)

Morris, B. A. "The Effect of Coextrusion on Bubble Kinematics, Temperature Distribution and Property Development in the Blown Film Process" SPE ANTEC'98 1006 (1998)

Munstedt, H. and Laun, H. M. "Elongational Behavior of a Low Density Polyethylene Melt II. Transient Behavior on Constant Stretching Rate and Tensile Creep Experiments. Comparison with Shear Data. Temperature Dependence of the Elongational Properties" Rheol. Acta. **18**, 492 (1979)

Naotove, H. H. and Schut, J. H. Plastics Technology **41**, 10 (1993)

Okamoto, M. Kojima, A. and Kotaka, T. "Elongational Flow and Birefringence of Low Density Polyethylene and its Blends with Ultrahigh Molecular Weight Polyethylene" Polym. **39**, 2149 (1998)

Osaki, K. and Bessho, N., Kojimoto, T. and Kurata, M. "Flow Birefringence of Polymer Solutions in Time-Dependent Field" J. Rheol. **23**, 457 (1979)

Pearson, J. R. A and Pettrie, C. J. S. "The Flow of a Tubular Film Part 1. Formal Mathematical Representation" J. of Fluid Mech. **40**, 1 (1970a)

Pearson, J. R. A and Pettrie, C. J. S. "The Flow of a Tubular Film Part 2. Interpretation of the Model and Discussion of Solutions" J. of Fluid Mech. **42**, 609 (1970b)

Pearson, J. R. A and Pettrie, C. J. S. Plast. Polym. **38**, 85 (1970c)

Petrie, C. J. S. Rheol. Acta "Memory Effects in a Non-Uniform Flow: A Study of the Behavior of a Tubular Film of Viscoelastic Fluid" **12**, 8 (1973a)

Petrie, C. J. S. "Memory Effects on a Non-uniform Flow: A Study of the Behavior of a Tubular Film of Viscoelastic Fluid" Rheol. Acta **12**, 92 (1973b)

Petrie, C. J. S. "A Comparison of Theoretical Predictions with Published Experimental Measurements on the Blown Film Process" AICHE J. **21**, 275 (1975)

Ramesh, N. S. and Malwitz, N. "Innovative Approach to Understand Metallocene Based Polyolefins and Thermoplastic Resins for Film Applications" SPE ANTEC'97 1954 (1997)

Redner, A. S. "On-line Birefringence Measurements in Production of Biaxially Oriented Polymers" SPE ANTEC'98 1598 (1998)

Ryu, D. S., Inoue, T., and Osaki, K. "A birefringence study of polymer crystallization in the process of elongation of films" Polymer **39**, 2515 (1998)

Seo, Y. and Wissler, E. H. "The Effect of Extrude Swell on Modeling the Film Blowing Process" Polym. Eng. Sci. **29**, 722 (1989)

Shimomura, Y., Spruiell, J. E., and White, J. L. "Orientation Development in the Tubular Film Extrusion of Polypropylene" J. Appl. Polym. Sci. **27**, 2663 (1982)

Shroff, R. N. and Shida, M. "Effect of Long-Chain Branching on the Relation between Steady –Flow and Dynamic Viscosity of Polyethylene Melts" J. Polym. Sci. Part A-2, **2**, 1917 (1970)

Simpson, D. M. and Harrison, I. R. "The use of Deformation Rates in the Scale-Up of Polyehtylene Blown Film" SPE ANTEC'91 203 (1991)

Sweeney, P. A. and Campbell, G. A. "Real Time Video Techniques in the Analysis of Blown Film Instability" Int. Polym. Process. **7**, 229 (1992)

Takahashi, T. and Fuller, G. "Stress Tensor Measurement Using Birefringence in Oblique Transmission" Rheol. Acta **35**, 97 (1996)

Tas, P. P. "Film Blowing: from Polymer to Product" Ph.D Dissertation Dept. Mech, Eng., Eindhoven University of Technology, The Netherlands (1993)

Terry, B. W. and Yang, K. "A New Method for Determine Melt Density as a Function of Pressure and Temperature" SPE J. **20**, 540 (1964)

Utracki, L. A. and Gendron, R. "Pressure Oscillation During Extrusion of Polyethylenes. II" J. Rheol. **28**, 601 (1984)

Van Aken, J. A. and Janeschitz-kriegl H. "New Apparatus for the Simultaneous of Stresses and Flow Birefringence in Biaxial Extension of Polymer Melts" Rheol. Acta **19**, 744 (1980)

Venkatraman, S., Okano, M. and Nixon, A. "A Comparison of Torsional and Copillary Rheometry for Polymer Melts: the Cox-Merz Rule Revised" Polym. Eng. Sci. **30**, 308 (1990)

White, J. L. and Yamane, H. "A collaborative Study of the Stability of Extrusion, Melt Spinning and Tubular Film Extrusion of Three high Density, Two Low Density and a Linear Denity Polyehtylene Samples" Pure Appl. Chem. **59**, 193 (1987)

Wild, L., Ryle, T. and Knobeloch, D. Am. Chem. Soc.:Polym. Prepr. **47**, 133 (1982)

Wong, C. M., Shih, H. H. and Huang, C. J. "Effect of Various Polyethylene Structure on Film Extrusion" J. Rein. Plast. Comp. **17**, 945 (1998)

Wu, M. "Effects of Dispersion on Rheological Properties of Filled Polypropylene" Master Thesis Dept. Chem, Eng., École Polytechnique de Montréal (1999)

Yamane, H., and J. L. White "Simulation of Tubular Film Extrusion of Polymer Melts" Int. Polym. Process. **2**, 107 (1987)

Yeow, Y. L. "Stability of Tubular Film Blow: A Model of the Film-Blowing Process" J. of Fluid Mech. **75**, 577 (1976)